Energy & Environmental Science

Accepted Manuscript

ROYAL SOCIETY OF CHEMISTRY

www.rsc.org/ees

RECENT PROGRESS ON NITROGEN/CARBON STRUCTURES DESIGNED FOR USE IN ENERGY AND SUSTAINABILITY APPLICATIONS

Journal:	*Energy & Environmental Science*
Manuscript ID:	EE-REV-12-2013-044078.R1
Article Type:	Review Article
Date Submitted by the Author:	21-Jan-2014
Complete List of Authors:	Wood, Kevin; Colorado School of Mines, Metallurgy and Material Science O'Hayre, Ryan; Colorado School of Mines, Materials and Metallurgical Engineering; Colorado School of Mines, Dept of Metallurgical and Materials Engineering Pylypenko, Svitlana; Colorado School of Mines, Materials and Metallurgical Engineering

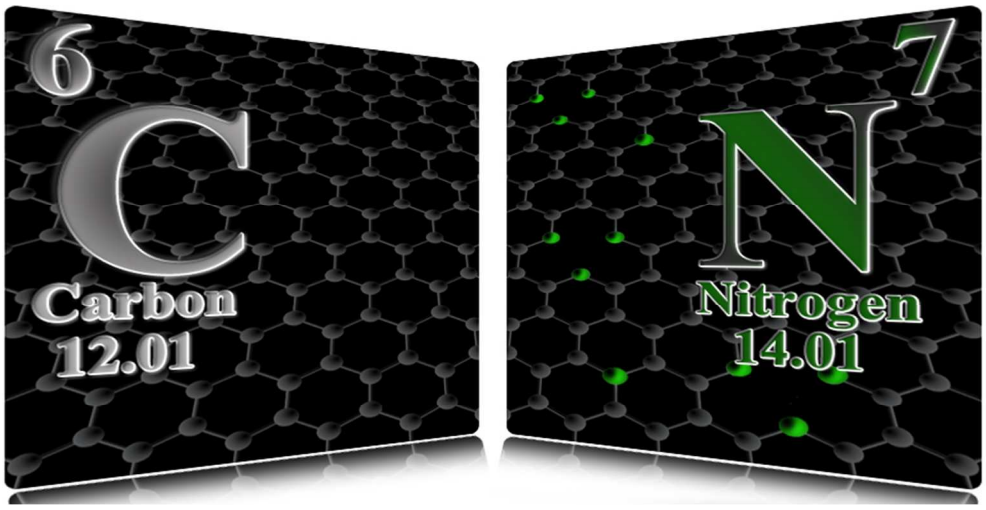

Nitrogen modification of carbon structures is making a vast impact across the scientific community, specifically in the realms of energy and sustainability.
80x39mm (300 x 300 DPI)

RECENT PROGRESS ON NITROGEN/CARBON STRUCTURES DESIGNED FOR USE IN ENERGY AND SUSTAINABILITY APPLICATIONS

Kevin N. Wood [a], Ryan O'Hayre [a], and Svitlana Pylypenko [a,*]

[a] *Department of Metallurgical & Materials Engineering, Colorado School of Mines, 1500 Illinois Street, Golden, Colorado 80401, United States*

Abstract

Heteroatom modification represents one of the largest studied areas of research related to nanostructured carbon materials, with integrated applications stretching from energy production and storage to sustainability and medical uses. While a wide variety of dopants (boron, phosphorus, iodine, fluorine, etc.) have been studied, doping carbon structures with nitrogen ad-atoms has arguably experienced the greatest progress and brought the most attention over the last several years. Research in this field has conclusively demonstrated that nitrogen doping is an effective way to tailor the properties of carbon and tune the material for various applications of interest. This review provides a comprehensive overview of advances in the last 5 years on state-of-the-art carbon modification with nitrogen heteroatoms. Improvements in well-established fabrication/modification processes are discussed as well as novel strategies. Additionally, recent theoretical and experimental findings related to the benefits and effects of nitrogen medication for specific applications in the energy and environmental fields are reviewed.

Table of Contents

1. Introduction **2**

2. Materials **3**
- **2.1. Graphene** **4**
  - 2.1.1. Direct synthesis 4
  - 2.1.2. Post-treatment 6
- **2.2. Carbon nanotubes** **7**
- **2.3. Activated commercial carbon blacks** **9**
- **2.4. Highly porous and mesoporous carbon** **10**
  - 2.4.1. Ionic liquids 12
  - 2.4.2. Hydrothermal carbonization 13
- **2.5. Carbon nitride** **14**
- **2.6. Other carbon structures and synthesis methods** **15**

3. Theoretical Studies **16**
- **3.1 Electronic Effects** **17**
- **3.1 Applications** **18**
  - 3.2.1. Fuel Cells 18
  - 3.2.2. Batteries 21
  - 3.2.3. Hydrogen Storage 21

4. Applications **22**
- **4.1. Fuel Cells** **22**
  - 4.1.1. Precious metal N-containing catalyst systems for methanol electrooxidation 22
  - 4.1.2. Precious metal N-modified catalyst systems for oxygen electrooxidation 26
  - 4.1.3. Non-precious metal N-modified catalyst systems for oxygen electroreduction 27
  - 4.1.4. Metal-free N-containing catalyst systems for oxygen electroreduction 30
- **4.3. Batteries** **34**
- **4.4. Supercapacitors** **37**
- **4.5. Hydrogen Storage** **40**
- **4.6. CO_2 Capture** **42**
- **4.7. Other Applications** **45**
  - 4.7.1. Chemical Production (H_2O_2, butyronitile, oxidized-cyclohexane) 45
  - 4.7.2. Photocatalysis 46
  - 4.7.3. Biosensing 47

5. Outlook and Conclusions **48**

Boarder Context

The race is on to find efficient, sustainable, and renewable methods of energy production. Intriguingly, two of the cheapest and most abundant elements in the universe, carbon and nitrogen, may hold part of the solution. Researchers are exploring how many forms of carbon, from graphene to pyrolized egg shells, can be modified with nitrogen to to enhance their performance and durability as key elements in many promising energy and sustainability applications. The potential applications of nitrogen-modified carbon materials range from fuel cells to batteries, molecular sorption to bio-sensing, and catalysis to medicine. This review provides an update on the vigorous current activity in this field, enabling researchers to identify new and creative uses and breakthroughs for nitrogen-modified carbon materials that may drive solutions to our future energy and environmental needs.

1. Introduction

Carbon remains one of the most attractive and well-studied materials systems in the scientific community due to its amazing variety and versatility in combination with low cost, availability, and wide ranging properties[1–5]. The physical, chemical, optical and electronic properties of carbon, varies according to its allotropic form and also greatly depends on its structure, morphology and surface composition. High surface area carbon materials have been extensively used for sorption, sensing, photovoltaic, catalysis and storage applications. In many catalytic and hydrogen-storage applications, carbon materials are also used as supports to facilitate dispersion of noble and non-noble catalysts. Among the various carbon materials, carbon blacks and activated carbons are the most traditional, with various nanostructured carbons such as graphene, fibers, nanotubes, and mesoporous morphologies emerging in recent decades. Functionalization of carbon-based materials can modify their surface, interfacial, and electronic properties, thereby further increasing their utility across a wide range of applications.

Among possible chemical choices for carbon modification, nitrogen functionalization has long been a natural and widely studied option. Nitrogen-containing carbon structures have attracted great attention in large part because of their abundance, accessibility, and low health risk. As far back as the early 1800's nitrided carbon structures in various polymorphs were extensively examined for their thermal conductivity, low compressibility, and high strength[6–8]. In more recent years, the study of carbon and nitrogen has expanded into the sub-stoichiometric regime of nitrogen-modified carbons. This modification allows for the beneficial properties of the carbon to be utilized while finely tuning the final electrical, morphological, and chemical properties of the functionalized carbon network.

Nitrogen is the natural choice for efficient and beneficial modification due to three specific reasons. Firstly, N is one neighbor away from C on the periodic table and by replacing one C with N in the carbon network the total number electrons in the system can be tailored one electron at a time. Secondly, N has an atomic radius similar to that of C, thereby preventing significant lattice mismatch. Thirdly, N-doping can induce an n-type electronic modification to the carbon structure, in analogy to typical semiconducting materials, which enables the potential use of these C-N structures in multiple important nanoelectronic applications.

Due to the width and breadth of this field, it is almost impossible to fully review and cover all aspects of study. As such, in this review we try focusing on the work done within the last 5 years (2009-2013). Starting from a foundational review of recent findings on the synthesis, characterization, and theory of nitrogen modified carbon materials; we then focus primarily on the use of these materials in energy conversion, storage, and sustainability applications.

2. Materials

Increasingly sophisticated requirements for sustainability and energy applications drive the need for new inexpensive and environmentally friendly materials. To this end, researchers have increasingly pursued nitrogen modification of many types of well-studied carbon nanostructures in addition to "from-scratch" fabrication of entirely new types of C-N structures. In this section, we review the recent work on N-modification of graphene, carbon nanotubes (CNT's), porous carbon structures, and carbon nitride as well as novel covalent-triazine frameworks, carbon nanospheres, and onion-like C-N structures. To start the discussion, Figure 1 shows the various functionalities referred to throughout this manuscript.

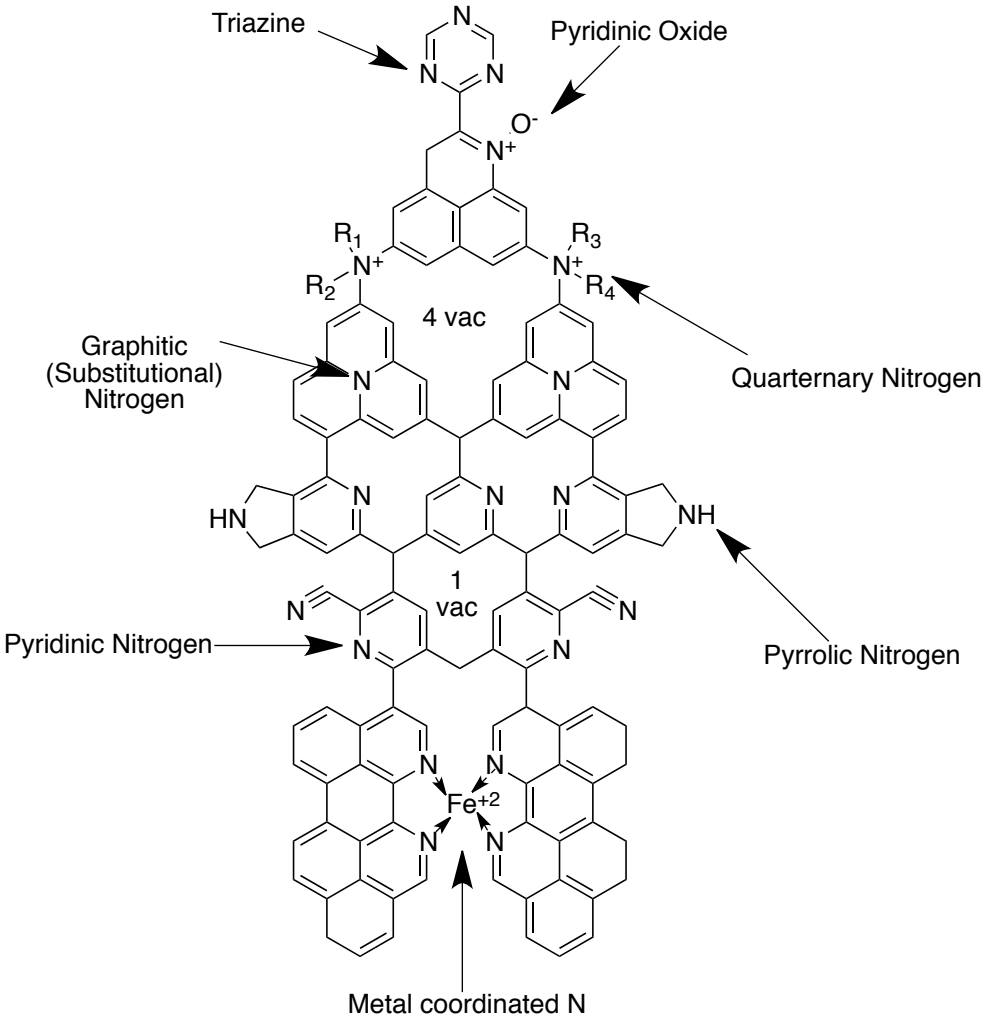

Figure 1: *Structures of the various types of nitrogen functionalities commonly observed in the N-doped materials discussed throughout this review. The three most common types are pyridinic, pyrrolic and graphitic. Among the other functionalities discussed are quaternary, triazine, pyridinic oxide and metal coordinated nitrogen. The figure also shows the different vacancy possibilities. This figure is your guide to the functionalities discussed throughout this review.*

2.1. Graphene

Graphene is a single sheet of carbon atoms arranged in a hexagonal lattice. Due to its many unique physical and electronic properties, it has been dubbed by many as a 'dream material'. Since the first report of its synthesis via the "Scotch tape"[9] method in 2004, the field of graphene research has witnessed extraordinary activity. While pure graphene by itself has many intrinsic benefits, chemical doping provides an important route to further tailor its properties for specific applications. Typically, there are two main approaches to chemically dope graphene: 1) the adsorption of gas, metal, or organic molecules onto the graphene surface and/or 2) substitutional doping, which introduces heteroatoms into the graphene lattice. In the context of nitrogen modification, both of these methods can modulate the electronic properties of graphene and they typically result in the combination of three *common* bonding configurations within the carbon lattice; graphitic N, pyridinic N, and pyrrolic N[10] (Figure 1).

N-modified graphene shows different properties compared with pristine graphene. For instance, the spin density and charge distribution of the carbon atoms will be influenced by neighboring nitrogen dopants[11]. This charge localization can help participate in catalytic reactions directly, as in the ORR, or can help tether metal nanoparticles to the graphene support[12]. Furthermore, monolayer DFT studies reveal that nitrogen doping suppresses the density of states near the Fermi level and shifts the Fermi level above the Dirac point[13,14]. This increases the band gap of graphene making it feasible for n-type semiconducting applications. Additionally, N-graphene also has beneficial properties for use in batteries, sensors, and supercapacitors, furthering its appeal across research disciplines[10].

Graphene can be nitrogen modified through two primary methods: 1) direct synthesis or 2) post-treatment. In principle, direct synthesis strategies have the potential to induce homogeneous modification throughout the entirety of the material, however current efforts have not conclusively demonstrated this potential. The major direct N-graphene synthesis routes include chemical vapor deposition, solvothermal fabrication, layer separation growth, and arc-discharge. While these direct synthesis methods have shown success (particularly direct CVD synthesized N-graphene), post-treatment nitrogen modification methods, which include bombardment, thermal annealing, or solution treatment are more widely used. In comparison to direct synthesis methods, post treatment methods generally lead only to surface doping, leaving the interior (bulk) of the treated carbon material unchanged.

2.1.1. Direct Synthesis

Chemical vapor deposition (CVD) has been used for decades to synthesize a variety of carbon structures[11,15–18]. Recently, a number of CVD variations have been explored to prepare N-graphene. In several instances, liquid organic molecules have been used as graphene precursors, however this process requires careful choice of the precursor structure. Even if nitrogen moieties are included in the liquid, only double bonded C=N species lead to the formation of N-graphene. Because of this issue, liquid pyridine has proven to be the most favorable liquid organic for creating nitrogen functionalized

graphene. Alternatively, gas mixtures can also be used to create both pristine and N-modified graphene. In these processes, a simple hydrocarbon (i.e. CH_4) is used as the carbon source, while ammonia is typically used as the nitrogen source. Importantly, the graphene doping level can be controlled through flow rate adjustments and gas precursor ratios. Using this technique N concentration levels can be controlled between 1-9 at% (See Figure 2a).[16,18,19,11,20,21] However, CVD processes can be relatively expensive and difficult to scale. The wide range of potential applications has therefore motivated the exploration of more facile techniques that have the ability to scale easily and create large volumes of material.

Solvothermal processing is potentially one such approach. Although it has been less extensively investigated, it has several attractive advantages including a simple operation method, mild synthesis conditions, and the capability to deliver relatively large quantities of N-graphene[22]. Deng et al. demonstrated this novel technique based on the reaction of tetrachloromethane with lithium nitride below 350^{0}C. This reaction allows for gram-scale production and synthesis can be easily scaled for commercial use. Their results suggest that nitrogen moieties can be successfully incorporated into the graphene structure using this approach with contents ranging from 4.5-16.4% nitrogen[23].

Most N-graphene fabrication techniques create multi-layer (6+ layers) rather than monolayer or few-layer graphene. However, in certain applications it may be beneficial to synthesize graphene in monolayer or 2-3 layer form[24]. This is hard to accomplish because reducing the number of layers tends to increase the thermodynamic driving force for transformation to other carbon allotropes such as carbon nanotubes (CNT's). Recently, however, Panchakarla et al. demonstrated that an arc discharge between two carbon electrodes in a hydrogen environment creates 2-3 layers of graphene without forming CNT's[24]. Furthermore, this process can be exploited to create N-modified graphene if the arc is deployed in a hydrogen atmosphere containing either ammonia or pyridine[24,25]. Materials fabricated from this method contain less than 1.5 % nitrogen, but XPS results indicate the formation of graphitic and pyridinic nitrogen functionalities directly incorporated into the graphene structure.

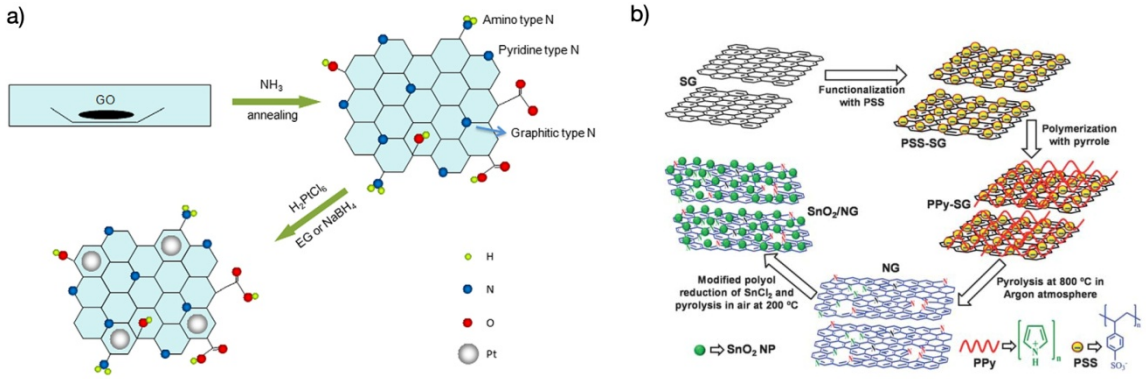

Figure 2*: (a) Direct synthesis route: Illustration of the treatment of graphene oxide by NH_3 for simultaneous reduction and N-doping, followed by the loading of Pt nanoparticles (nanoparticles not-to-scale) Reprinted (adapted) with permission from Citation[21]. Copyright (2013) Elsevier. (b) Post-modification route: Schematic illustration of synthesis of N-doped graphene using the pyrolysis of polypyrrole coated functionalized graphene, with subsequent*

deposition of SnO_2 nanoparticles. Reprinted (adapted) with permission from Citation[26]. Copyright (2013) Royal Society of Chemistry.

2.1.2. Post-treatment

While there are advantages to creating N-graphene through direct synthesis, post-treatment methods maybe more feasible for certain applications and are likely closer to commercialization. By far the most extensively studied method for post-modification is thermal annealing. Commonly, this is conducted in an ammonia atmosphere[27–32,21,33], but other environments have been studied as well[34,35]. The ammonia thermal process results in low doping levels below 3%, typically attained by annealing between 800-900^{0}C. Results suggest that the resulting N-functionalities are mostly pyridinic and pyrrolic. This is ascribed to the nature of thermal treatment, where dopant incorporation most readily occurs at the plane edges and on defect sites[29]. The low nitrogen level is understood because the pristine nanostructure of graphene yields a relatively small concentration of the edge and defects sites that are needed for dopant incorporation. In order to increase nitrogen content, some researchers have instead started with graphene oxide (GO) and employed nitrogen precursors such as melamine, in combination with an ammonia heat treatment to simultaneously reduce the GO and modify it with nitrogen. Such procedures can create N levels as high as 10 at%[34]. Li et al.[31] showed that the N content achieved in this process depends strongly on temperature (decreasing N as temperature increases), likely due to reduction of the graphene oxide during the treatment. The reduction of graphene oxide (GO) in an ammonia/hydrazine environment has also been used to create nitrogen moieties[36,37]. This is an interesting *pseudo in-situ* N-graphene fabrication process because hydrazine is frequently used to reduce GO to pristine graphene.

Higher dosage levels can also be achieved by physically inducing chemical defects into the graphene. This can be accomplished through energetic post-synthesis bombardment techniques like plasma treatment or ion implantation. Historically, nitrogen plasma treatments have focused on the modification of CNT's. However, graphene has recently been functionalized in this matter as well[38–43]. Nitrogen plasma treatment is attractive as a facile modification method because the plasma strength and/or exposure time can be tuned to control the level of N-doping.[40] Nitrogen contents as high as 8% have been reported; however, bombardment techniques generally lead to oxygen functionalization as well[44]. At least in one report, oxygen was incorporated to concentration levels as high as 28%[39]. Intriguingly, this unplanned oxygen co-functionalization has also proven to be beneficial for some applications. In plasma treatment, ammonia is typically the nitrogen source, but recently it has been shown that N_2 gas can also be used during ion implantation to reach dosage levels as high as ~10%[45]. Using plasma modification, a wide range of functionalities can be achieved. Interestingly, a survey of the literature suggests that pyrrolic nitrogen is the dominant species created by plasma modification. In contrast, nitrogen ion-beam implantation appears to produce a more balanced mix of nitrogen functionalities, although further studies are needed to clarify these issues[46].

A number of other techniques have also led to the successful incorporation of nitrogen into the graphene nanostructure. Very recently, Vinayan et al. demonstrated a novel nitrogen doping process carried out by the pyrolysis of polypyrrole (PPy) coated poly(sodium 4-styrenesulfonate) (PSS) functionalized graphene[26]. The anionic polyelectrolyte PSS introduces negatively charged SO^{3-} surface groups that interact with the N^+ groups present in the PPy and gives rise to a uniform coating of the polymer on the graphene surface. The pyrolysis of the PPy/graphene, completed at 800 ^{0}C, removes the PPy, leaving behind

nitrogen atoms incorporated into the graphene structure (Figure 2b). This process leads to a nitrogen incorporation of around 7.5% with a relatively large quantity of graphitic nitrogen as well as some pyridinic nitrogen species.

2.2. Carbon nanotubes

After Iijima's pioneering work in the early 1990s, carbon nanotubes (CNT's) triggered significant interest in nanotechnology as well as a renaissance in the fundamental condensed matter physics of carbon. CNT's continue to captivate researchers after a quarter century of study due to their attractive mechanical and chemical stability as well their high thermal and electrical conductivities. Due to the fact that the application of CNT's relies strongly on their surface properties, surface chemistry has been a major focus of CNT research in recent years. While oxygen functionalization has been the most intensively studied, in the last decade investigations have shifted to species like nitrogen due to promising results for a variety of applications.

Previous research has shown that the addition of nitrogen into CNT's increases the edge plane structure, creating more active sites and increasing electrochemical activity. Similarly, a combination of functionalization and CNT width can tune the electrical properties for use as an n-type semiconductor. Combining the intrinsic properties of CNT's with the significant electrical modification provided by nitrogen functionalization, N-CNT's have significant research appeal[3].

As with graphene, different CNT synthesis or post-treatment modification techniques can lead to variations in the concentration and range of functional species. For CNT's, CVD and pyrolysis are the most extensively studied nitrogen incorporation methods. In 1997, Sen et al. first prepared CNT's that contained small amounts of nitrogen by pyrolizing aza-aromatics over metal nanoparticles[47]. Then in 2002, N-CNT's were grown onto substrates through a microwave plasma enhanced chemical vapor deposition (MWPECVD) process[48]. In the last 5 years, derivatives of these techniques have remained the focus of attention, with the three major functionalization approaches being CVD[49–57], thermal heat treatment[58–60], and pyrolysis[61–64].

Wiggins et al. used a floating catalyst CVD approach in 2009 that allowed for selective nitrogen doping and the controlled growth of CNT structures by using precursors consisting of ferrocene and either xylene or pyridine to directly control the nitrogen content. XPS analysis revealed nitrogen concentrations as high as 7.4% and Fe levels below 0.2%[53]. Chen et al also employed floating catalyst CVD using melamine precursor to synthesize the CNT's with bamboo-like structure shown in Figure 3. Using this method, higher nitrogen concentrations result in CNT's with larger diameter and altered structure. Recently, it has been shown that metal catalysts are not required for the formation of CNT's and by utilizing the proper anisotropic carbon structures; self-catalyzed CNT's can be formed. In 2011, Wang et al. attempted to directly synthesize metal-free N-CNT's via a carbon self-catalysis process exploiting the use of a detonation-assisted CVD technique. Their results showed that nitrogen strongly promotes nanotube formation, without the need for metal atoms, and displays the ability to promote the self-assembly of tubular carbon nanostructures[54]. Their approach yielded nitrogen concentration as high as 20 at% by using melamine as a precursor. In 2012, the synthesis of large quantities of vertically aligned N-CNT's with modulated nitrogen content was reported using a spray pyrolysis CVD technique[65]. A 2009 report found that vertically aligned nitrogen carbon nanotubes (VA-NCNT's) could be fabricated through pyrolysis of a nitrogen containing metal heterocyclic molecule in either the presence or absence of additional NH_3 vapor. Analysis revealed nitrogen in pyridinic

and pyrrolic forms at concentrations as high as 6%, as well as the complete removal of the metal seed[61] . Another study reported that aligned NCNT's could also be prepared by ultrasonic spray pyrolysis from mixtures of imidazole and acetonitrile[66]. SEM and TEM images revealed that increasing the concentration of imidazole decreased the nanotube diameter and increased the nanotube length as well as the density of the bamboo-like C-N structures.

In the last few years, several groups have demonstrated heat treatment in the presence of ammonia (as well as other precursors [67]) as a route to introduce nitrogen functionalities in prefabricated CNT's. In one study, thermally treated MWCNT's were oxidized in a HNO_3 gas environment at 200^{0}C for 2 days. After drying, the oxidized carbon nanotubes were heated under an ammonia environment at varying temperatures for 6 hours[59]. This process has been repeated[59,60] and analysis indicates that as the ammonia treatment temperature increases, the oxygen and nitrogen contents decrease. However, at higher temperatures the ratio of N:O is much larger.

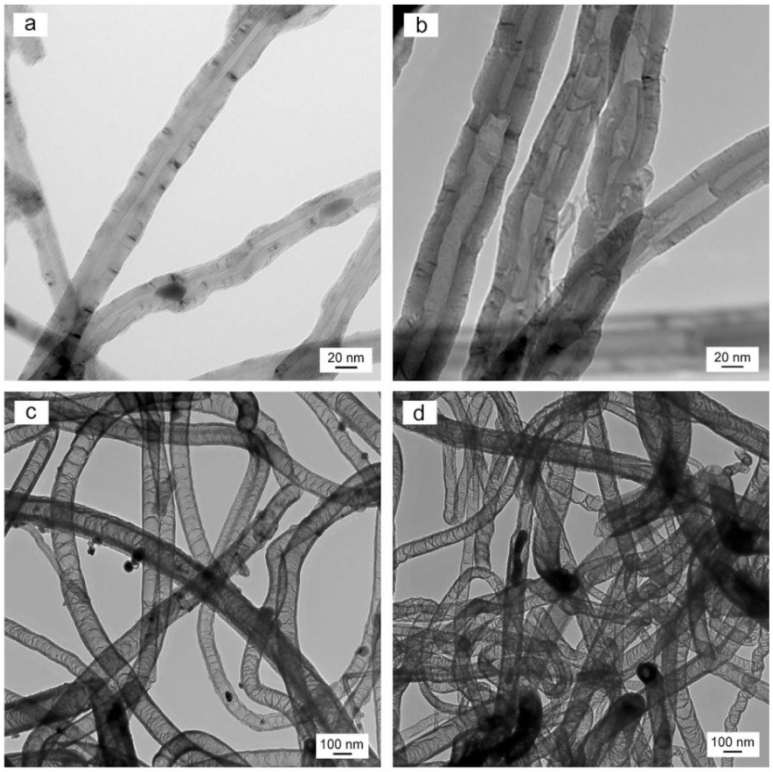

Figure 3: *TEM images of (a) CNT's, (b) CN_x (1.5 at.% N), (c) CN_x (5.4 at.% N), and (d) CN_x (8.4 at.% N) showing the effect of nitrogen on the structure of CNT's. Reprinted (adapted) with permission from Citation*[68]*. Copyright (2009)* Elsevier

Hsu et al. used aniline to form polyaniline, which was then coated and pyrolyzed around CNT's to form a nitrogen-doped porous carbon layer that was used to stabilize precious metal sites during the reduction and pyrolysis process. Similarly, polymerization of nitrogen containing organics has been shown to have a promising future for CNT post modification carbonization. An et al. showed that carbonization of polypyrrole created N-CNT's with nitrogen contents as high as 8.6 at%. In this system, BET testing showed that these

nanotubes had higher specific surface areas and a pore structure consisting of micropores, mesopores and macropores[69].

Ionic liquids have been established as precursors for a variety of compounds, but just recently they have been applied as precursors for N-modification of prefabricated CNT's. Nitrogen contents as high as 10 wt% have been achieved. However, due to the expense of the ionic liquid precursor materials, only thin CNT coatings have been studied. Recently, Tuaev et al. showed that homogeneous coatings of nitrogen-doped carbon on carbon nanotubes could be achieved using ionic liquids. Their results showed modest nitrogen incorporation. The 10 wt% N-C coating on the CNT's leads to a total N concentration of ~1%, which in this case was sufficient for its intended application[62]. These findings could lead to after-the-fact tuning of CNT's for various industries, a prospect that has already been demonstrated for pharmaceutical applications[60,49]. However, throughout all these processes it should be appreciated that high nitrogen content is not the main metric of NCNT quality. Rather, intelligent design and targeted functional group control is most desired in order to optimize behavior for specific applications.

2.3. Activated Commercial Carbon Blacks

Commercial carbon blacks, which are the most widely used carbon nanomaterials, are produced by subjecting heavy residual oil feedstock to extremely high temperatures in a carefully controlled combustion reactor. These carbons can be made in various commercial grades with differing carbon structures and pore sizes, each produced through minute reactor adjustments. Researchers have used these carbon materials as inks, coatings and even in plastics for numerous applications. A large body of work has been focused on modifying commercial carbons with nitrogen through pyrolysis, annealing, bombardment or other after-the-fact techniques. Different techniques can lead to different quantities and varieties of nitrogen functional groups. There is great attraction in the potential to nitrogen-modify industry-leading carbon blacks for specific applications in order to tune the electronic structure and enhance their relative performance.

As an example, Biddinger et al. created C-N nanostructures by pyrolysis of acetonitrile over Vulcan XC-72[70]. XPS results showed overall nitrogen concentrations as high as 8.6%, which the researchers deconvoluted into pyridine, quaternary, and oxygenated pyridine functionalities. Additionally, other precursors, using nonprecious metals, were used to modify carbon blacks, such as polyaniline [71]. Jaouen et al. used an iron-based precursor and heat-treatment with ammonia to incorporate iron atoms coordinated to pyridinic nitrogen functional groups into black pearl 2000—a well-known commercial carbon black material. This method yielded nitrogen content as high as 3.2 at %. Interestingly, the group observed some nitrogen incorporation even when the ammonia treatment was neglected[72]. Plaza et al. also used ammonia treatment to modified activated carbon materials, without metal addition. Their studies showed nitrogen incorporation up to 5 wt% and provided promising results for CO_2 capture applications[73,74].

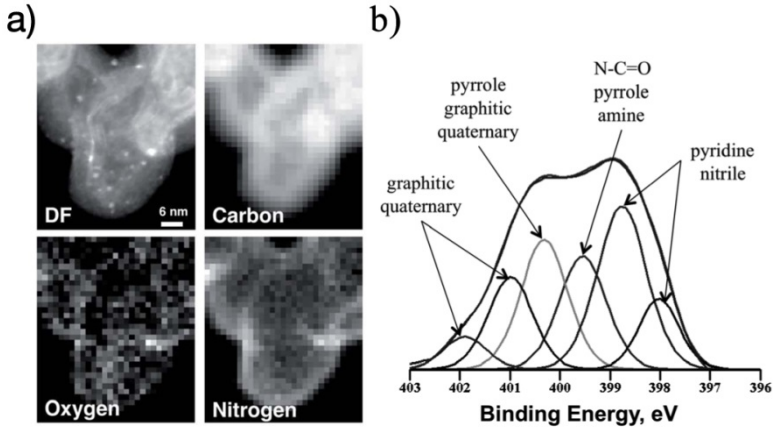

Figure 4: *(a) HAADF-STEM image and corresponding EELS oxygen, carbon, and nitrogen maps obtained from Graphitic Vulcan doped with nitrogen and decorated with Pt nanoparticles showing enrichment of the support surface with doped nitrogen. (b) XPS N1s spectrum of N-doped Graphitic Vulcan. Reprinted (adapted) with permission from Citation* [75]*. Copyright (2013) Royal Society of Chemistry.*

Commercial carbon blacks have also been modified with ion bombardment. This technique decreases the order of the graphitic structure of the carbon black and incorporates nitrogen groups into only the top ~1 to 2 nm layers (Figure 4a) [75]. In their study, Vulcan black was ion implanted with N_2 gas in a custom implantation/sputter chamber. The material was used as a PtRu catalyst support and showed nitrogen incorporation at nearly 2 at.% after bombardment for 1hr with a nitrogen ion beam current of 14mA. Increasing the ion implantation dosage by increasing the beam current up to 45-50 mA allowed the nitrogen concentration to reach ~5 at% [75]. XPS analysis showed a range of nitrogen functionalities that were similar to those observed on N-doped HOPG (Figure 4b). A similar approach was used for post modification of a commercial Johnson Matthey PtRu catalyst supported on carbon black. The authors compared samples implanted for 1hr at 12mA and 45mA and found that the higher beam-current dosage led to a relative increase in the concentration of low binding energy nitrogen species such as pyridine[76]. This result suggests that it may be possible to tune the specific types of nitrogen functional groups that are created by ion implantation in order to optimize the functionalization process for specific applications.

2.4. Highly Porous and Mesoporous Carbon

Nitrogen-modified ordered mesoporous and highly porous carbon materials have seen considerable research because of their potential applications in areas such as adsorbents, supports, gas storage hosts, and electrode materials. Based on the size of pore diameters, carbon materials can be classified as microporous (diameter<2 nm), mesoporous (2 nm < diameter < 50 nm), and/or macroporous (diameter >50 nm). The properties of porous carbon materials largely depend on the surface area and porosity of the carbon as well as on any heteroatom modifiers built into porous structure. Research on nitrogen incorporation into porous carbons has led to a wide variety of functionalities including amides, imides, lactames, pyrrolic and pyridinic groups. Researchers have shown that N-modification can enhance the anion adsorption capacity of meso-carbons as well as modify their pore structure and surface area. In addition, nitrogen modification has been shown to improve thermodynamic stability when meso-carbons are used as supports structures, specifically for electrocatalysis and charge collection[77].

The traditional method of obtaining ordered mesoporous carbons by nanocasting from silica is a complicated and high-cost procedure. However, the recent advent of a direct synthesis strategy using organic–organic self-assembly offers potentially lower cost and more scalable manufacturing of these materials. Although N-functionalization of ordered mesoporous carbons from the organic-organic direct strategy is still lacking, much effort has been placed on improving and understanding nitrogen modification through ionic liquid hard templating, in situ polymerization, and post-modification treatment.[77] Combining the understanding of nitrogen-containing mesoporous carbons with the creation of a facile/inexpensive, direct synthesis technique could lead to major breakthroughs in the energy harvesting and conversion fields.

Post-synthesis modification of porous carbon materials has also been widely investigated. In the typical process, an organic nitrogen-containing precursor (most frequently ammonia) is used to introduce nitrogen into the porous carbons structure. Either gaseous or aqueous environments can be employed, depending on the precursor. The carbon can be directly modified in a single step method, or oxidized prior to nitrogenation. Different precursors will yield variations in the obtained surface chemistry and porosity of the modified carbon. Porous carbon materials treated at high temperatures with ammonia show increased porosity and form surface groups such as $-NH_2$, –CN, pyrrolic and graphitic nitrogen due to free radicals formed during the heating process. Nitrogen content and speciation is affected by the treatment temperature[78–80]. At high temperatures, pyridinic and graphitic (401.2eV) carbon become more prevalent[80]. This result is consistent with the ammonia heat treatment of other carbon structures as well. Ammonia-treated porous carbon produces nitrogen contents as high as ~4 wt.% at treatment temperatures of 973 K.

To date, porous carbon materials prepared by post-synthetic amine modification or ammonia treatment have led to materials lacking in stability and having poor performance for many applications[81,82]. Therefore, recent efforts have been placed on direct 'one pot' synthesis of nitrogen functionalized porous carbon structures. Hao et al. described the fabrication of a new type of nitrogen-containing carbon monolith prepared through a direct pyrolysis technique using a copolymer of resorcinol, formaldehyde, and lysine[83]. Their results showed higher nitrogen content in the bulk rather than on the surface. They also saw that as the pyrolysis temperature was increased beyond 500°C, the total obtained nitrogen levels decreased and shifted toward higher XPS binding energies. While these results were similar to those obtained from post modification processes, their as-prepared carbon monolith was nearly crack-free. Su et al. fabricated a series of polypyrrole-derived N-containing microporous carbon spheres and demonstrated an important trend that increasing temperature leads to beneficial increase in the surface area, but results in lower nitrogen concentrations (Figure 5) [84].

Direct polymerization of polyaniline using a template is also a well-studied method of direct synthesis[85–89]. Silva et al. have demonstrated mesoporous oxygen- and nitrogen-doped carbons synthesized from in-situ polymerized polyaniline (PANI) through carbonization in a silica SBA-15 template. The mesoporous silica template was then etched away from the structure leaving behind the PANI-derived mesoporous carbon. The obtained material exhibited remarkably active performance for oxygen reduction, challenging conventional paradigms. Moreover, it is worth emphasizing that nitrogen speciation in the PANI-derived mesoporous carbon was dominated by pyrrolic nitrogen, chemically resembling the N groups in porphyrin-like structures which have also shown good catalytic activity for oxygen reduction[88].

Recently, Ma et al. pioneered a one-step evaporation-induced self-assembly strategy focused on creating N-doped porous carbon nanostructures with large surface area. The materials were obtained through in-situ copolymerization of resorcinol and formaldehyde where HNO_3 was used as both the catalyst and the nitrogen source without involving the use of halogenides[90]. The nitrogen content and surface area could be tuned by adjusting the synthesis parameters. This one-pot method is particularly attractive because HNO_3 is inexpensive and easily accessible.

2.4.1. Ionic liquids

An extensive body of work has examined the use of ionic liquids (ILs) in combination with hard template structures to create controlled, porous carbon materials[91–94,79,95,96,81]. IL's are molten salts possessing melting temperatures generally below 100 C; in the last few decades they have attracted attention due to their low vapor pressure, high electrical conductivity, and excellent thermal stability. Due to their low vapor pressures, ILs can been used to complete the carbonization process without evaporation[81]. Unfortunately, this process leaves behind disordered structures, which have wide pores and poor surface areas if left unconfined. In addition, some reports indicate that the carbonization yield can be low[92] and the cost of these materials can be prohibitive unless small amounts are utilized effectively. Multiple recent studies have explored the possibility of using IL's without templating, some of which have resulted in materials with very poor surface areas[97,98]. However, a 2009 report[92] demonstrated a phase separation process induced by an inorganic salt that acts as a porogen, leading to high surface area materials after water washing[99,100,101].

While interest in template-free synthesis continues to grow, the use of hard templating provides a beneficial avenue for expanding current knowledge and application based on improved control and understanding offered by these materials. Qui et al. demonstrated porous carbons with nitrogen contents ranging from 8-20% using a mixture of SBA-15 and a nitrogen containing IL by first heating the mixture to 100°C and then carbonizing at a range of higher temperatures. As the carbonization temperature increases, the nitrogen content decreases. However, BET surface area and pore size increase, showing that the proper fabrication procedure is strongly application dependent.

As discussed in the CNT section, carbonization of IL's has recently been explored using CNT's as the structural host, due to their defined morphology that allows for a good control of the homogeneity of the coating. This is attractive because allows the elimination of the template material, thus potentially decreasing costs. While this novel coating idea has only led to nitrogen contents near 1 at%, it could provide a future pathway for reducing the cost and re-engineering the current templating strategy.

To this end, other creative template strategies have been explored. One such approach reported by Qui et al. explored the fabrication of nitrogen-doped carbon nanofiber webs (CNFWs) prepared by carbonization-activation of polypyrrole with KOH. The nanofiber webs were created using a reactive template solution of dissolved cetrimonium bromide and ammonium persulfate. The final materials exhibited nitrogen contents as high as 16 wt% (mostly pyrrolic N, with some pyridinic species) and BET values above 2300m^2/g[102]. Results showed that the pyrolysis time affected the nitrogen content and speciation of the final structure.

2.4.2. Hydrothermal Carbonization

The use of plant biomass to produce carbonaceous materials is garnering interest commensurate with increased emphasis on sustainability. While biomass has been used to create carbon structures for centuries (e.g. charcoal), the recent reinvigoration of this field has led to re-exploration of a process called hydrothermal carbonization (HTC). HTC has a number of distinct advantages as it is inexpensive and can create a variety of sustainable carbonaceous materials with attractive, "built-in" functionalization possibilities and unique nanostructure that can be used in various applications. HTC can be used to create C-N structures from sustainable nitrogen sources with appropriate co-reactivity, where the final structure is tuned using principles from colloid and polymer science. Recently, researchers have used HTC to fabricate nitrogen functionalized materials for applications such as CO_2 sequestration, and electrochemical catalyst supports for supercapacitors, fuel cells and batteries[103–108].

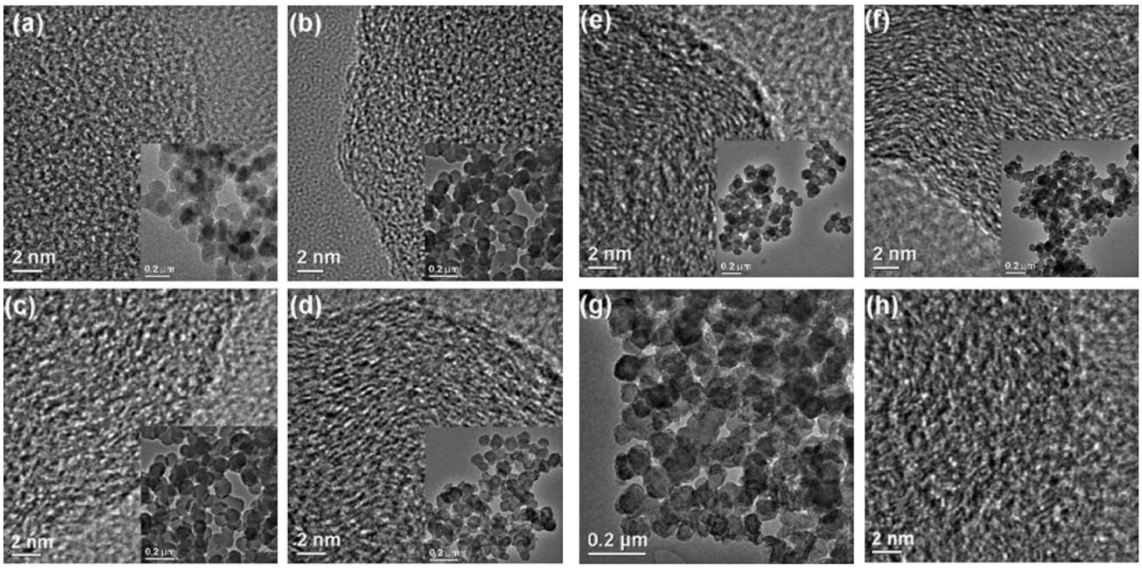

Figure 5*: TEM images (a) polypyrrole nanospheres, 14.3 at% N, and carbon nanospheres carbonized at BET 45 m^2/g (b) 300°C, 14.1 at% N, BET 23 m^2/g(c) 600°C, 12.5 at% N, BET 36 m^2/g (d) 900°C, 7 at% N, BET 89 m^2/g (e) 1100°C, 5.9 at% N, BET 20 m^2/g (f) 1300°C, 4.3 at% N, BET 12 m^2/g and microporous carbon nanospheres (g) and (h) 2.2 at% N BET 1080 m^2/g. Reprinted (adapted) with permission from Citation[84]. Copyright (2011) Royal Society of Chemistry.*

Natural nitrogen containing molecules such as, proteins, glucosamine or aminated saccharides can be used to fabricate carbonaceous materials with 8-10% nitrogen via HTC (Figure 5). These types of natural molecules typically form materials with higher aromatic character, which have the ability to retain greater levels of nitrogen after high temperature carbonization and achieve BET values as high as 3012 m^2/g[109]. NMR used after carbonization reveals similar overall ending structures no matter the complexity of the starting molecule used, however the nitrogen functionalities may vary. In one interesting example, the sustainable preparation of a porous, nitrogen-doped high surface area carbon has been demonstrated using prawn shells as a natural nanostructured inorganic/organic composite[106].

2.5. Carbon nitride

For years, carbon nitride investigations have centered on understanding graphitic carbon nitride (g-C_3N_4) as a single crystal with high strength properties. However recently, polymer-derived carbon nitrides have opened up new horizons. Since 2006, when the first use of g-C_3N_4 as a metal-free heterogeneous catalyst emerged, the number of studies on polymer derived carbon nitride has steadily increased. While this branch of research is just emerging, modified carbon nitrides have already exhibited promising catalytic activity for certain reactions[110]. It has been shown that g-C_3N_4 and related allotropes have the necessary properties to catalyze oxidation and hydrogenation reactions as well as photochemical water splitting. Furthermore, it has been shown that carbon nitride is a medium-bandgap semiconductor with the HOMO and LUMO orbital's positioned in a range were it can act as a mild electron transfer agent with powerful chemical potential[111]. Since carbon nitride is metal-free, it also tolerates functional groups and is therefore suited for multipurpose applications in biomass conversion and sustainable chemistry.

For these catalytic and energy storage applications, carbon nitride materials should possess relatively high surface areas. Unfortunately, g-C_3N_4 materials are typically made through self-condensation of organic precursors, which creates bulk materials with surface areas below ~10 m^2/g[110]. For the practical applications of these materials, the introduction of controlled porosity at the nanoscale must be realized—essentially the goal is to create carbon-nitride analogs of mesoporous carbon structures. Mesoporous g-C_3N_4 was first obtained through nanocasting with mesoporous silica templates[104]. Analogous to the silica-based templating of mesoporous carbons, an organic precursor is infiltrated in the silica template, and after water extraction, is heated for several hours to ensure the condensation of the precursor into polymeric C_3N_4. Utilizing this "hard template" approach provides morphological control of the mesoporous carbon nitride, giving rise to surface areas between 86m^2/g and 439m^2/g, depending on the type of silica template used[112,113]. However, these surface areas are still less than optimal due to the weak binding affinities of the basic precursors in neutral silica templates, which make it kinetically difficult to diffuse the precursors into the nanopores of the templates[114]. Recently, a SBA-15 meso-zeolite template was used in conjunction with liquid cyanamide to form a carbon nitride structure with a better 2D mesoporous hexagonal framework, resulting in a final mesoporous carbon nitride with surface area nearly identical to that of the silica template (Figure 6)[115]. Applying the knowledge obtained from recent mesoporous carbon research could greatly impact the development of mesoporous carbon nitrides. In particular, the advent of a facile, inexpensive nanocasting strategy for mesoporous carbon nitride would provide a major impetus for the use of these materials in energy storage and capture.

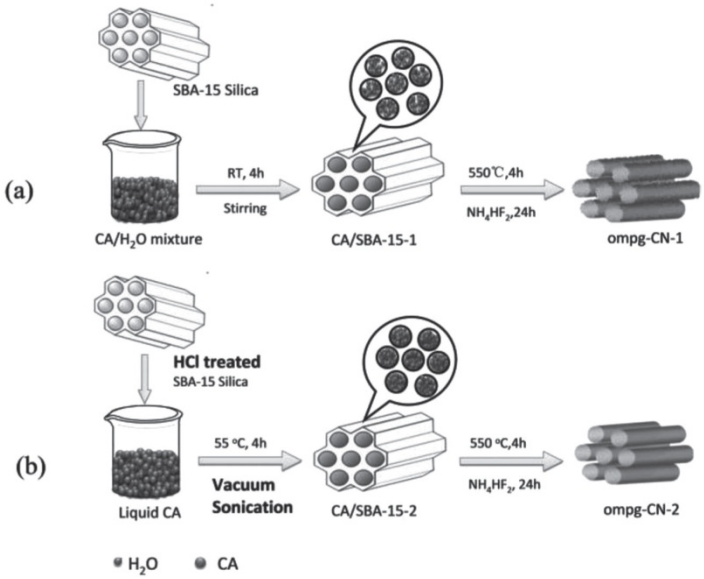

Figure 6*: Illustration for the synthesis process of ordered mesoporous-CN using (a) traditional method and (b) new method. Reprinted (adapted) with permission from Citation*[115]*. Copyright (2013)Wiley-VCH.*

As an alternative pathway, core-shell structures containing carbon nitride have been investigated as they can yield higher surface area and lower cost[116]. In these systems, metal carbon nitride materials act as the shell and are supported on electronically conductive graphite nanoparticles, the core. Both hybrid inorganic–organic polymer networks and zeolitic inorganic–organic polymer electrolyte materials were used to impregnate an electronically conductive support (e.g. a high surface area graphite), and after a suitable pyrolysis processes, core–shell carbon nitride electrocatalysts were formed with a good dispersion of active sites for catalytic applications. Results showed that carbon nitride shells formed out of hybrid polymer networks led to higher overall nitrogen content (as high as 18%). Similar carbon nitride contents were obtained using carbon tetrachloride and ethylenediamine and a silica template. These structures contained no metal and showed promising results for Hydrogen storage[82,114]. Continued exploration of these types of core-shell structures could lead to inexpensive high surface area materials with high concentrations of surface carbon nitride sites [116].

Finally, the formation of highly crystalline graphitic carbon nitride has been demonstrated using a simple self-condensation of dicyandiamide in a salt melt of lithium chloride and potassium chloride[117]. This synthesis route has given rise to a new type of structure, verified as poly(triazine imides), that consists of triazine structures bridged together with imide functional groups[118] (see Figure 1). Beneficially, it appears this type of carbon nitride material is stable in aqueous solution, allowing for potential use in applications requiring thin film coatings[119].

2.6. Other Carbon Structures and Synthesis Methods

A wide range of other carbon structures have been investigated, including highly ordered pyrolitic graphite[120–122], carbon nanospheres, nanoribbons[123], onion-like structures[124], fullerenes[125,126], and covalent triazine frameworks[127,128]. They have been developed to target various applications and/or improve basic scientific knowledge. Recently Sakaushi et al investigated amorphous covalent triazine-based frameworks (ACTFs) synthesized from

p-dicyanobenzene. In their discussion they compared crystalline and amorphous CTFs, showing BET surface areas of 1140 and 792 m^2/g respectively[127]. The pore structure of these materials was of key interest, and was controlled by the crystallinity through the adjustment of the p-dicyanobenzene/$ZnCl_2$ ratio during fabrication. A pore size distribution between 1-2nm was obtained for the crystalline material vs. 0.7-0.9nm for the amorphous material. The combination of high surface area and pore structure control with the high degree of nitrogen coordination (-C_3N_3-) makes this an interesting material for many applications.

Onion-like carbon structures are of interest because the surface is fully accessible to ion adsorption due to an almost perfect graphite network with a high degree of curvature. Additionally, the graphitic nature of these supports provides desirable features for their use as a supporting material. Nitrogen-doped onion-like carbon materials have been synthesized by heat treatment in the presence of Co and Fe species[124]. XPS analysis reveals nitrogen contents were attained at levels near 6 at.% with slightly more sp^3 hybrid character then sp^2, while metal species were detected at around 1 at.%.

There has also been recent interest in covalent grafting of nitrogen-containing species onto carbonaceous structures (commercial powders, nanotubes, graphene, etc.). This type of carbon modification permits organic layers to be attached to solid conducting substrates, which make them attractive (because of chemisoprtion) for biosensing, microelectronics, and photovoltaics. The covalent bonds in these systems are difficult to obtain, but are essential for their use in energy and sustainability applications. Unfortunately, weak physisorption bonds, detrimental toward the utility of these materials, frequently form instead of the covalent type, creating instability[129,130]. Because these materials contain very low nitrogen amounts and frequently have high concentration of physisorbed species, we limit discussion of these materials, referring readers to an interesting review focused on this topic[129].

While all of these materials are focused on application-based integration, basic scientific studies have also been carried out using highly oriented pyrrolitic graphite (HOPG). The well ordered, consistent surface structure of HOPG enables studies of the mechanism of nitrogen incorporation as well as studies of the interactions between carbon-nitrogen composites and supported ad-atoms/nanoparticles. HOPG has been modified with nitrogen by ion implantation to create C-N structures containing ~8at% nitrogen[120,75]. High-resolution XPS scans revealed a wide range of functionalities present after implantation ranging from ~403ev to ~397ev in binding energy.

3. Theoretical Studies

As our understanding of structures and reactions has advanced, areas stretching from synthesis to performance have become more and more theoretically grounded. Through quantum mechanical modeling, density functional theory (DFT) can provide invaluable insight into the energetic shifts of carbon as a function of nitrogen modification and help elucidate the role of specific functional groups on stability and performance for specific applications. These insights can help direct future study and give validity to current hypotheses or raise valuable questions. Herein we provide a discussion on the current revelations provided to the community through theoretical methods.

In order to increase the effectiveness of experimental research it is of great benefit to understand conceptually and mathematically the underlying chemical phenomena. To this

end theory can give insight into properties such as structure, absolute and relative (interaction) energies, reactivity or other spectroscopic quantities, dipoles and higher multipole moments, vibrational frequencies, and electronic charge distributions.

Computational chemistry frequently involves a delicate dance between residual error minimization and computation time. As such, all computational chemistry approaches, including both *ab initio* and semi-empirical approaches involve approximations. These range anywhere from simplified forms of first-principle equations, which are easier/faster to solve, to approximations limiting the system size (i.e. periodic boundary conditions). Because of these limitations, among the carbon allotropes, graphene and its cylindrical analog (CNT's) are typically the best suited for computational study.

3.1 Electronic Effects

In 2012, Schiros et al. used x-ray adsorption spectroscopy combined with DFT to show the overall electronic effect of the different bond structures in N-doped graphene[131]. In this study, the extra electron from the single N defect was shown to be distributed in the local network (electron donation) of carbon π-states and create an n-type effect. However, multi-defects such as pyridinic species have the opposite effect, insomuch as the two electrons fill the σ-bonds of the carbon neighbors, two electrons form a lone pair in the graphene plane, and the remaining electron occupies the N π-state. Thus, the pyridine-like defect has the equivalent occupation of a nominal carbon in graphene, however a π-electron is missing due to the vacancy site so the system is p-doped, leading to the conclusion that pyridinic nitrogen has an electron withdrawing nature.

More recently, Muhich et al. studied singly and triply bound N-substituted graphene using density functional theory (DFT)[132]. Their results indicated that both n-type singly N-doped graphene and p-type triply N-doped graphene gain electron density; these results were contrary to the study by Schiros[131]. This behavior was attributed to unequal charge sharing in the C-N sp^2 sigma bond and the necessity of occupation for the orthogonal p orbital to maintain the aromaticity of graphene. This work also showed a strong enhancement in adsorption of Pt even at distances well away from the nitrogen site while revealing that migration over the nitrogen atom is unlikely due to the increased energy barrier. This phenomena has also been confirmed through experimental studies using STM mapping[133] and motivates the use of N-doped carbon materials as Pt catalyst supports to mitigate catalyst migration and agglomeration. Muhich et al. also shown that metal sites adsorbed on a pyridine ring are trapped by the strong Pt-N bonds having a greater stabilizing effect than the single N defect[132] (Figure 7).

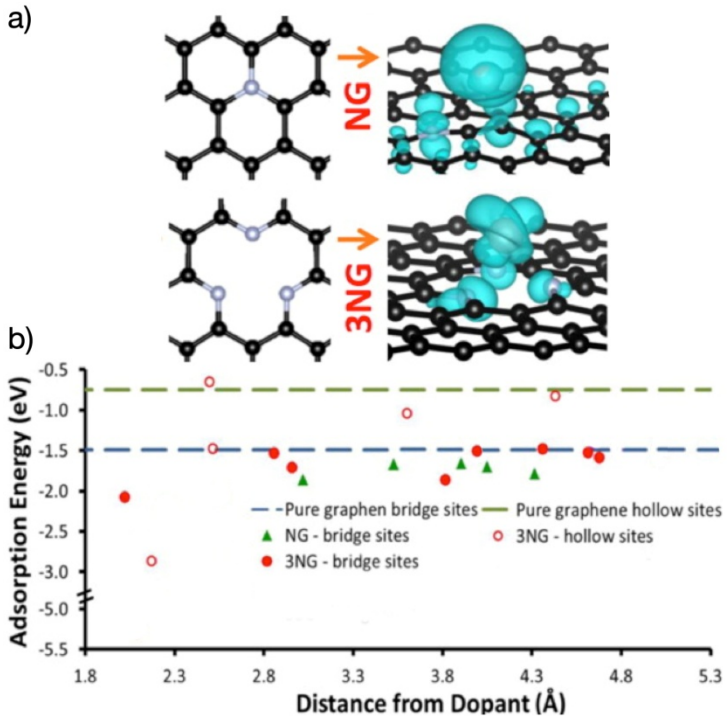

Figure 7: *(a) Electron density of singly and triple doped nitrogen sites. (b)) Pt adsorption energy as a function of distance from the dopant atom. Reprinted (adapted) with permission from Citation*[132]*. Copyright (2013) American Chemical Society.*

A DFT study investigating the effects of N defects in SWCNT's discovered the interesting properties of nitrogen modification on armchair conformations versus those of a zigzag structure[134]. The results showed that zigzag like CNT's exhibit electronic shifts in the Fermi level as a result of the nitrogen adatom in pyridine-like defects. Conversely, in the same defect structure, the Fermi level shifts in armchair CNT's are due to vacancy formation. It was also shown that the resulting Fermi level shifts lead to a metallic nature of N-CNT's at N concentrations as low as 1.6 at.%. At lower concentrations N-CNT's behave as semiconductors [134].

3.1 Applications

Many theoretical studies have focused on examining the effect of N-doped carbon nanostructures for specific applications, including fuel cell supports[135–139], batteries[140–142], [143], [144], hydrogen storage[145,125,146–149,150], supercapacitors[151], and field emission properties[152].

3.2.1. Fuel Cells

A 2009 study combining DFT theoretical applications with experimental results using HOPG highlighted the fact that Pt binding energy modification due to N-doping is likely the principal reason for the improved Pt catalytic activity and metal site 'tethering' in N-doped carbon fuel cell support systems[153,138]. Similar studies investigating the effects of PtRu on nitrogen-modified systems reveal the complicated nature of the bi-functional system and indicate that the behavior is greatly affected by the specific nitrogen functionality employed. Simulations revealed that graphitic N defects consistently improve resistance to dissolution in all considered cases, (dissolution of Pt from Pt, dissolution of Pt from Ru_2Pt_2 and dissolution of Ru from Pt_2Ru_2). However, DFT analysis shows that the effect of pyridinic nitrogen is conflicting. It helps improve resistance to dissolution for Pt from Ru_2Pt_2 but

makes dissolution of Ru from Pt_2Ru_2 more likely. Therefore the stability of PtRu catalysts can be improved through a well-balanced mix of pyrrolic, pyridinic and graphitic N[75].

DFT has also been used to investigate the full reaction path of the oxygen reduction reaction (ORR) on N-doped graphene like surfaces[137,136,125,139]. These studies have summarized the effect of N-doping on different configurations. N located at sites next to the zigzag edge activates the neighboring two carbons along the zigzag edge. On the other hand, the pyridinic N located along the zigzag edge may negatively affect ORR activity, although it is abundant in most samples. Unfortunately, the pyridinic sites appear more stable and so researchers must fight the negative relation between energetic stability and the chemical reactivity [136]. Conversely, it has also been shown that higher concentrations of graphite-like nitrogen groups reduce the energy barrier for oxygen molecule dissociation much more efficiently[139]. Recently other groups have proposed that theoretically, graphitic nitrogen on graphene will precipitate the ORR reaction via a $4e^-$ pathway[137,154]. However, this is much debated and other studies contradict this finding[155]. It is likely specific groups such as graphitic nitrogen may reduce the energy barrier for the $4e^-$ pathway, however the $2e^-$ pathway is overall more energetically favorable (on N-graphene without metal) and a combination of two pathways is inevitable (Figure 8)[139]. It is well documented that the rate-determining step is likely the removal of the adsorped oxygen species, meaning that future catalysts should be designed to improve the kinetics of O_{ads} removal[137,155].

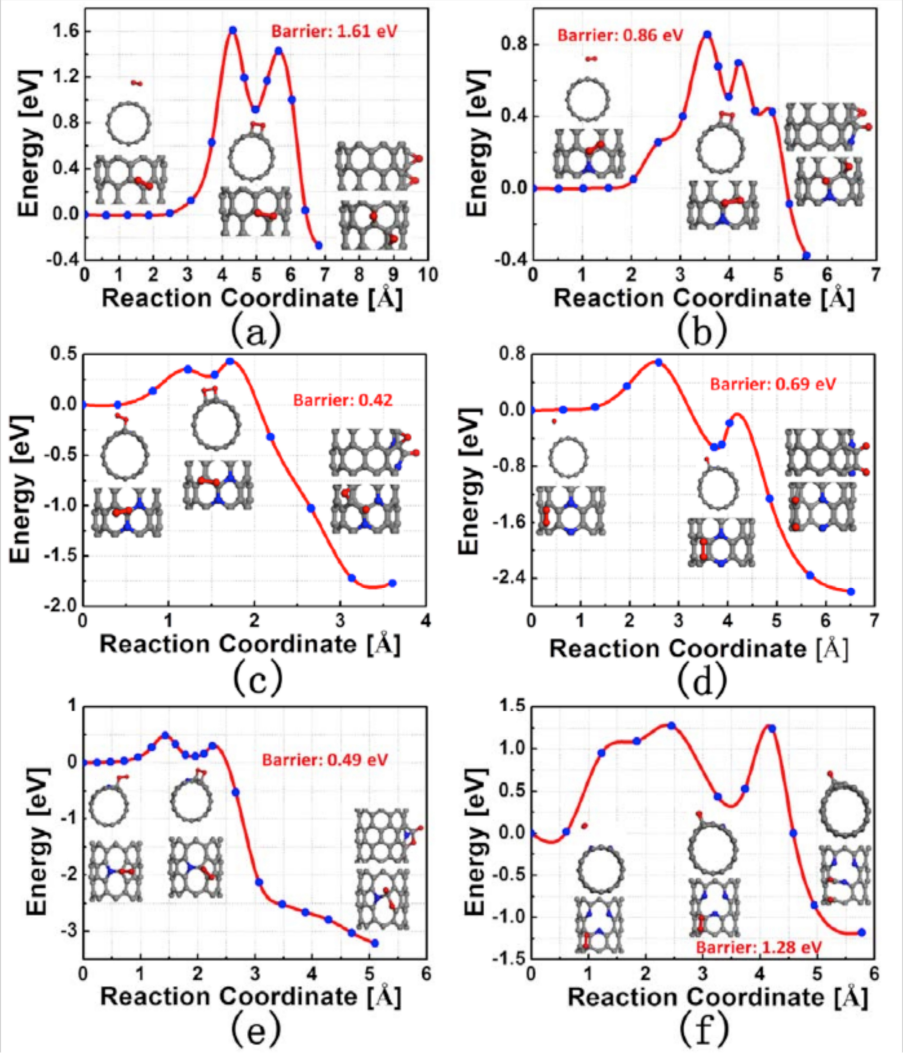

Figure 8: *Minimal energy paths of oxygen molecule dissociation on (a) a pure (8,0) SWNCT, (b) a one nitrogen atom substituted (8,0) SWCNT, (c) a two meta nitrogen atom substituted (8,0) SWCNT, (d) a two para nitrogen atom substituted (8,0) SWCNT, (e) a one nitrogen atom substituted (8,0) SWCNT with a stone-wales defect, and (f) a (8,0) SWCNT with pyridine-like nitrogen atoms. Gray dots, blue dots and red dots represent carbon, nitrogen and oxygen atoms respectively. Reprinted (adapted) with permission from Citation*[139]*. Copyright (2013)Royal Society of Chemistry.*

Non precious metal group (NPMG) catalysis has been the focus of many theoretical studies. In this area it is well believed that the geometrical and electronic structures of Me–N_x clusters are the most important factors in influencing the catalytic activity of Me–N/C electrocatalysts for ORR[154,156–159]. To date, DFT computation studies have explored the progression of ORR on Me–N_x clusters in isolated transition metal-macrocyclic molecules[160,161] and perfect graphene[156,157]. These studies focus on understanding the geometry, stability, ORR pathway, and electronic structure of the Me–N_4 (Me=Fe, Co, or Ni) on carbon. Recent work by Kattel and Wang focused on elucidating the ORR pathway of Me–N/C electrocatalysts. Consistent with experimental findings, the DFT results suggest that Fe–N_4 and Co–N_4 clusters could promote 4e$^-$ ORR on a single active site and that the ORR activity of the Me–N_4 clusters is correlated to the d-orbital electronic structure[162].

Additionally, DFT has also recently been used to predict binding energy shifts in N1s XPS spectra resulting from the Me-N_x structures present in these types of ORR catalysts. Therefore the synergy of experiment and theory could allow researchers to extract critical information from *in situ* high-resolution N1s spectra. This information is needed for the determination of geometry and abundance of ORR active sites in an oxidizing atmosphere, which is critical information that must be evaluated against electrochemical activity for ORR reactions[163].

3.2.2. Batteries

Nitrogen-modified carbon-based ORR catalysts have also been studied for lithium air/oxygen batteries[140–142,143,144]. The results of these studies indicate beneficial effects similar to those observed in fuel cell studies. Results by Yan et al. show that N-doping can decrease the energy barrier of graphene from 2.39eV (undoped case) to 1.20 eV, increasing the energetic feasibility of O_2 disassociation [142]. The effect of N on lithium intercalation into carbon has also been studied. Ma et al. used first principle calculations to investigate three different nitrogen defect structures, pyridinic, pyrrolic, and graphitic, in order to study the electronic properties and adsorption mechanism of single and multiple Li atoms[164]. This work showed that pyridinic nitrogen is the most beneficial for Li intercalation and gives rise to the highest storage capacity. This was attributed to the fact that the single atom Li absorption energy on pyridinic sites was increased by ~40% (compared against pristine graphene) and was energetically more favorable then the formation of Li clusters, which tend to form on pristine graphene. Computational results indicated that N-graphene has the potential to possess reversible capacities of 1262 mAh/g[164]. A more recent theoretical study by Kong et al. studied various pyridinic clusters and found that a 4 pyridinic cluster is the best candidate for Li adsorption[143]. In this work it was also shown that this structure enhanced Li mobility and increased the strength of Li adsorption. Comparing these results with recent experimental findings shows that the steep reduction in Li capacity observed for N-modified anodes after cycling can be attributed to their enhanced Li adsorption. It can be hypothesized that the strong Li-pyridinic attractions can allow the Li atoms to stay on the surface even after multiple charge-discharge cycles. While nitrogen modification in these systems is still very beneficial, these positive effects decrease over the lifetime of the anode. As such, focus needs to be placed on maintaining Li capacity through creative means.

3.2.3. Hydrogen Storage

In the arena of hydrogen storage, theoretical studies have explored the effects of dispersed Li on N graphene at standard temperature and pressure. The results showed the maximum number of adsorbed H_2 molecules to be three for pyridinic and pyrrolic species, which can be adsorbed and desorbed under the same conditions[147]. Lu et al. explored a similar system by studying the effect of nitrogen on a 2-D porous polymeric network. Authors showed that the increasing number of N in an aromatic ring enhances the binding energies between hydrogen molecules and pre-adsorbed Li atoms from $1H_2$ to $3H_2$. While these studies have focused on the molecular adsorption of H_2, a novel strategy of applying an electric field to N-graphene allows for atomic H adsorption. Theoretically, materials used in this way could reach hydrogen uptake values of 7.23 wt% at complete hydrogenation, well above the U.S. Department of Energy (DOE) target. Hydrogen can then be released through another voltage change, adding utility and interest to this type of system because the band gap of N-doped graphene is increased to 3 eV after 2 H atoms are adsorbed. These results suggest that hydrogenated N-doped graphene could display photocatalytic activity and solve the band gap problem of graphene for nanoelectronic applications[145]. Overall, the combination

of theoretical calculations with experimental observations greatly enhances the community's understanding of doping mechanisms, the effects of doping on adatom adsorption, as well as the effects of doping on the electronic properties of these materials. This enhanced understanding can be applied to a variety of systems to enable the tailoring of carbon structures to fit various specific applications.

4. Applications

Carbon-nitrogen nanostructures are ultimately intended for integration into important, industry-relevant applications. The goal is to determine which functionalities and properties are most beneficial for a desired application and amalgamate that knowledge into systems that improve performance and efficiency. Within the last five years, research has greatly improved our understanding of how C-N structures can benefit applications ranging from fuel cells to batteries, hydrogen storage to CO_2 capture, and supercapacitors to photocatalysis. This section discusses recent findings related to the effects of nitrogen on these various applications and draws conclusions for future study and improved integration.

4.1. Fuel Cells

The following paragraphs discuss progress in N-modified carbon-supported catalyst systems for methanol electrooxidation and oxygen electroreduction, starting with carbon-supported precious metal catalysts, followed by non-precious metal catalysts (transition metal based catalysts) and finally, nitrogen-functionalized metal-free catalysts.

4.1.1. Precious metal N-containing catalyst systems for methanol electrooxidation:

State-of-the-art methanol electrooxidation catalysts typically consist of carbon-supported Pt-Ru alloy nanoparticles. A bimetallic Pt-Ru alloy, instead of pure Pt, is generally used as it shifts the onset potential to lower values and eliminates poisoning from CO intermediates. Nitrogen functionalized carbon supports are interesting for these applications because the nitrogen modification can improve the interactions between the carbon support and the metallic nanoparticles, leading to improved catalyst activity and durability.

While a few authors have examined the role of nitrogen-doping in the enhancement of performance for carbon-supported Pt-Ru catalysts, most papers discuss the effects of nitrogen doping on carbon-supported Pt catalysts[165,63,56,97,33,21,166,167,153,138,168,169] even though these pure Pt-based catalysts are not optimal for methanol oxidation applications. Several classes of nitrogen-doped carbon materials have been investigated in the past 5 years, including carbon blacks [170,76,171–173,75,174], carbon nanotubes[175,56,63,98] , mesoporous carbons , carbon shells[167],porous carbon nanospheres[168,169], carbon nitride[116], graphene[33,21,35] and highly oriented pyrolitic graphite (HOPG) [121,176,75,153,138].

N-doping of CNT's for fuel cell applications has been achieved by direct synthesis using chemical vapor deposition (CVD)[56], post-treatment with nitrogen plasma[175] or polymerization of aniline[63]. Carbonization of polyaniline/aniline has also been used to incorporate nitrogen into ordered mesoporous carbons [166,165] and to synthesize nitrogen-doped carbon shells[167]. N-doped porous carbon nanospheres have been fabricated by carbonization of polypyrrole nanospheres, followed by chemical activation to introduce porosity[168,169]. Melamine precursors have also been employed to incorporate nitrogen into the graphene nanocomposites[35].

Shao et al. explored doping of graphene using ammonia treatment and a one-pot synthesis route using N-methyl-2-pyrrolidone as nitrogen precursor[33], while Pan et al. utilized a polymerizable ionic liquid to control carbon yield, nanostructure and nitrogen concentration in nitrogen-doped carbon/Pt nanoparticle hybrids[97]. These materials showed nitrogen in the range of 8.27-15.29 %. O'Hayre et al. have studied effect of nitrogen ion beam implantation onto the structural and chemical modification of highly-oriented pyrolytic graphite [120,121,176,75,153,138] and later applied same method to incorporate nitrogen into carbon blacks[170,173,171,172] and commercial catalysts [177].

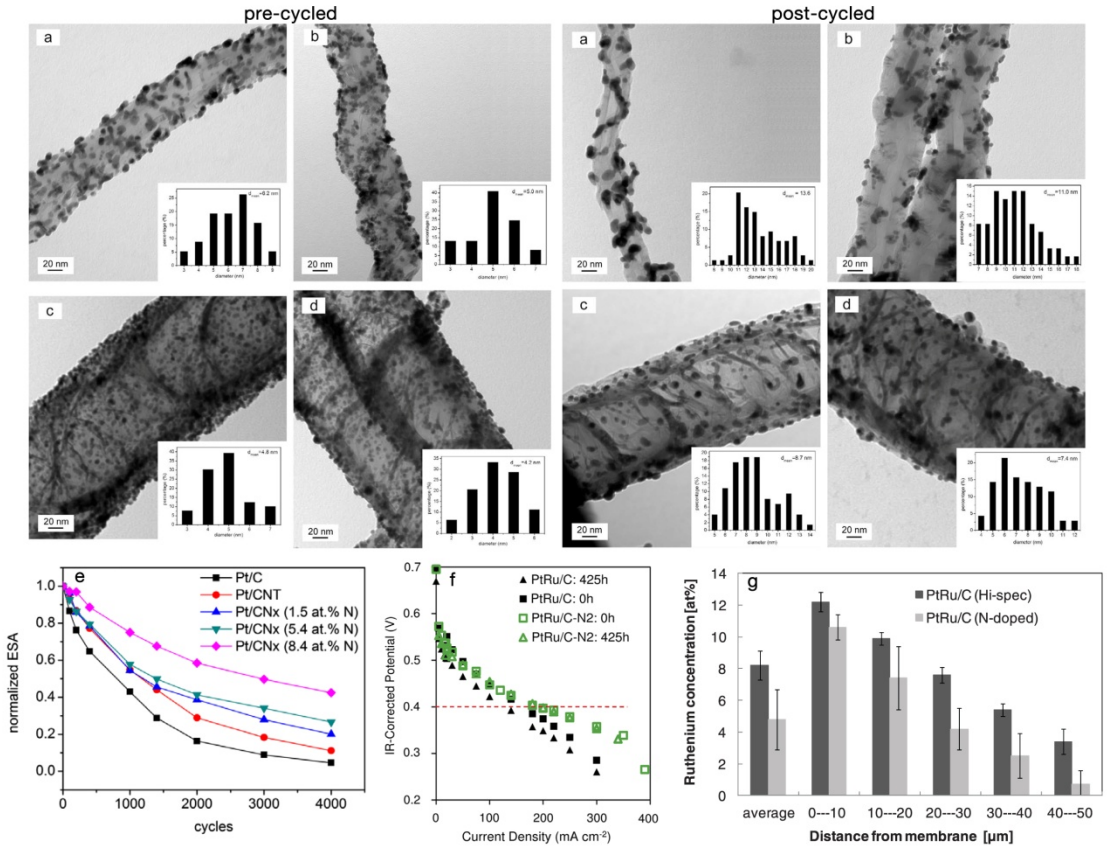

Figure 9: *TEM images and size distribution histograms (insets) of Pt electrocatalysts before and after ADT. (a) Pt/CNT's; (b) Pt/N-CNT's (1.5 at.% N); (c) Pt/N-CNT's (5.4 at.% N); (d) Pt/N-CNT's (8.4 at.% N) and (e) the comparison of the degradations of the five catalysts. on the structure of CNT's. Reprinted (adapted) with permission from Citation[68]. Copyright (2009)* Elsevier *(f) the effect of N-doping on performance of PtRu anode. Reprinted (adapted) with permission from Citation[76]. Copyright (2014)* Elsevier *(g) the effect of N-doping on Ru crossover in DMFC made with PtRu anode. Reprinted (adapted) with permission from Citation[178]. Copyright (2012) The Electrochemical Society.*

A review paper published in 2010 highlighted the effects of nitrogen doping on the performance of methanol electro-oxidation catalysts, concluding that irrespective of the type of the carbon support and doping method, when compared to undoped counterparts, the N-doped systems generally show improved MOR performance [179]. Specifically, N-doped catalyst systems show improved catalyst dispersion[153,167,75,165,166,56,168,169], lower onset potential[175,153,166,167,169,180], increased current produced per catalyst surface area (specific

activity)[175,167] or per metal catalyst mass (mass activity)[166,168,169] and exhibit improved stability. The evidence that nitrogen modification improves dispersion of carbon-supported precious metal nanoparticles and enhances their durability is strong. Figure 9 a-d shows the effect of nitrogen concentration on the pre- and post-cycled Pt particle size distribution and the respective benefit to the electrochemical surface area. The evidence that nitrogen modification enhances intrinsic catalytic activity is less clear-cut.

It is well documented that the nucleation and dispersion of metal nanoparticles on carbon materials with high graphitic content is quite poor and typically requires surface pretreatment. Incorporation of nitrogen into CNT's provides sites for preferential nucleation, without need for pretreatment [56]. Similarly, incorporation of nitrogen into the structure of graphitic Vulcan through ion beam implantation greatly enhances the nucleation of uniformly dispersed Pt nanoparticles[75]. Generally, catalyst nanoparticles supported on undoped and N-doped carbon differ in their initial density, dispersion, size and composition. It is observed that N-doping alters the nucleation and growth of nanoparticles in a beneficial way, leading to improved dispersion and smaller particle sizes[153,167,75,166,165,56,169]. Guo showed that incorporation of nitrogen into ordered mesoporous carbon enables dense dispersions of Pt nanoparticles at dramatically increased Pt loading[165]. Lei et al compared a series of nitrogen-containing ordered mesoporous carbons synthesized in the temperature range of 600-950 °C, and showed that the nitrogen concentration was critical to the dispersion of the Pt nanoparticles[166]. Within the set of materials produced, the authors reported BET surface areas from 988 to 1166 m^2/g, pore sizes from 2.7 to 3.3 nm and nitrogen concentrations from 9. 6 to 4.8 at.%. Despite relatively comparable BET surface areas, the increase in nitrogen concentration from 4.8 % to 9.6 % led to a systematic decrease in the Pt nanoparticle size from 4.0 to 2.4 nm. The authors also discussed the interplay between the N concentration and particle size in terms of their effect on the CO stripping peak. The materials synthesized at the lowest temperatures possessed the highest N contents and exhibited the highest CO tolerance, while the materials synthesized at the highest temperatures showed lower nitrogen content, but larger pore size. The materials synthesized at the highest temperatures also showed lower charge transfer resistance and demonstrated the best mass activities for methanol oxidation. Lei et al also explored the effect of nitrogen by using a series of nitrogen-doped carbon shells pyrolyzed in the temperature range of 400-950 °C; material synthesized at 900°C showed the best catalytic performance towards oxidation of methanol.

Pt and PtRu supported on N-doped porous carbon nanospheres show enhanced dispersion and particle size as well as improved onset and mass activities[169]. Authors also reported that N-supported PtRu retained better performance even after durability cycling. For bimetallic precious metal nanoparticles such as PtRu, nitrogen functionalization of the carbon support can change the Pt-to-Ru composition due to altered nucleation and growth kinetics. For example, PtRu nanoparticles grown on ammonia-treated N-containing CNT's also contained an unalloyed hexagonal Ru phase that appeared to be least partially responsible for enhanced activity[175].

In addition to the typical catalyst degradation mechanisms (i.e. dissolution/reprecipitation, migration/coalescence, support detachment) experienced by carbon-supported Pt-based catalysts, PtRu/C anode catalysts experience an additional degradation mechanism associated with the dissolution of ruthenium, which crosses over the electrolyte and contaminates the cathode. Modification of the catalyst-support interactions though nitrogen

modification has been shown to improve PtRu catalyst nanoparticle stability while also mitigating Ru crossover and particle-growth mechanisms[173,171,170,178,121].

Since N-doping alters the metal nanoparticle nucleation dynamics and can therefore affect the initial particle size and dispersion of the supported metal nanoparticles, this can make it difficult to assess the effect of N-doping on subsequent catalyst durability, since the morphological starting point for doped and undoped catalyst systems will be different. In order to address this issue and isolate the effect of nitrogen functionalization on the stability of PtRu nanoparticles independent of their effect on metal nanoparticle nucleation, O'Hayre et al. conducted a series of experiments utilizing PtRu nanoparticles deposited via sputtering from a single-alloyed PtRu target [120,121,176,75,153,138], which led to initial PtRu nanoparticle coverage, dispersion, and particle size distributions that were identical for nitrogen-modified and unmodified carbon supports. PtRu nanoparticle stability was probed by accelerated degradation testing using a series of model HOPG substrates with varying nitrogen concentrations (controlled via ion implantation dosage) but identical starting PtRu nanoparticle composition, size and coverage [121]. It was found that low implantation dosages had an overall negative effect on catalyst stability, presumably due to the presence of implantation-induced physical defects and oxygen groups associated with the nitrogen functionalities present at low dosages. These samples were similar in their stability to those exposed to Ar^+ irradiation, which introduced physical defects that had a beneficial effect on nucleation but a detrimental effect on durability[153]. Samples implanted at higher nitrogen dosage, however, possessed a mixture of physical defects, oxygen functionalities and significantly higher amounts of nitrogen (up to 8 at% N prior to metal deposition). The high nitrogen concentrations led to the formation of clustered multi-nitrogen defects and also led to great improvement in PtRu nanoparticle stability (specifically preventing nanoparticle agglomeration by migration/coalescence). Through analysis of datasets containing electron energy spectral images, it was demonstrated that only regions with the highest nitrogen concentration offered improved stability after accelerated degradation testing[75]. Within the areas of best stability, PtRu nanoparticles appeared to be surrounded by nitrogen defects, suggesting that the incorporation of nitrogen next to the catalyst nanoparticles is of utmost importance in preventing migration[75]. This effect was also later demonstrated by testing post-doped commercial PtRu/carbon catalysts [177]. Further, it was shown that stability of PtRu nanoparticles on N-doped HOPG substrates could be additionally improved by the incorporation of fluorine. In this "co-functionalized" system, nitrogen is believed to mitigate migration/coalescence and fluorine is hypothesized to improve resistance to metal dissolution [176].

The beneficial effect of N-doping on the stability of PtRu nanoparticles has also been demonstrated with the N-doped carbon black supports such as Vulcan black[170,173,171,172]. Investigation of catalyst stability with in situ small-angle x-ray scattering (SAXS) has revealed remarkably improved durability of PtRu nanoparticles on N-doped carbon blacks compared to an unmodified carbon blacks[173,170,62]. N-doped supports have shown better retention of electrochemically active catalytic sites when compared against undoped in-house materials and commercial references [170]. Long-term stability of PtRu supported on N-doped Vulcan has also been investigated in complete direct methanol fuel cells, revealing improved fuel cell performance as well as mitigation of metal dissolution and ruthenium cross-over after durability testing (figure 9 (f) and (g))[171,178]. Overall the role of specific nitrogen functionalities is hard to elucidate and as seen above most studies in this application show that increasing nitrogen content, regardless of functionality, is the most

important. Every work reports presence of multiple functionalities, among them nearly every study mentions pyridinic nitrogen.

4.1.2. Precious metal N-modified catalyst systems for oxygen electrooxidation:

As previously noted, when compared to methanol electrooxidation, fewer studies have been completed on Pt and Pt-alloy supported N-doped carbons investigating oxygen electroreduction. Most studies have focused on the improved Pt nanoparticle dispersion and stability provided by N-doping, rather than on the electrocatalytic properties for ORR. Among the N-doped carbon materials studied for ORR are N-CNT's [181–184,62,185,68], mesoporous carbons [186], porous carbon nanospheres [168], carbon blacks [187], graphene[38,188] and graphene nanoplates[181–183,62].

Chen et al. demonstrated control of nitrogen content in CVD-grown carbon nanotubes through the use of a melamine precursor[181]. Their work clearly demonstrated that with increasing nitrogen concentration, the average Pt particle size decreases and the size distribution narrows. In addition, the authors used accelerated degradation testing to demonstrate that nitrogen helps to stabilize the supported nanoparticles, evident from the analysis of nanoparticle size distributions and improved retention of active surface area (11.2 % on undoped CNT's, vs. 20.2 %, 26.6 % and 42.5 % on CNT's doped with 1.5, 5.4 and 8.4 at% nitrogen, respectively). Another work focusing on N-doped CNT's compared various nitrogen precursors and found that nitrogen-rich ethylendiamine helps incorporate more nitrogen (4.74 at%) than the less nitrogen-rich pyridine precursor (2.35 at%)[182]. Both types of N-containing CNT's demonstrated more uniform Pt particle size and increased ORR activity compared against the unmodified catalyst material. During MEA testing, catalysts with higher nitrogen contents showed better overall performance metrics, including enhanced nanoparticle dispersion and substantial increases in the power density. Saha et al. also reported smaller nanoparticle sizes (2.6 nm) and more narrow particle size distributions on the N-doped CNT's as compared to undoped CNT's (5.89 nm); the improved particle size distribution led to a 36% improvement in active surface area and higher current density[184].

A series of nitrogen-doped ordered mesoporous carbons for use as ORR catalyst supports were prepared by pyrolysis of carbon and Pt precursors using a silica SBA-15 template functionalized with 3-[2-(2-aminoethylamino)ethylamino]propyl as the nitrogen source[186]. Nitrogen levels in the range of 0 to 3 wt% were achieved, and with exception of one test, all samples followed the trend of improved Pt nanoparticle dispersion with increasing nitrogen concentration. The dominant functionalities were graphitic and pyridinic nitrogen and the pyridinic fraction increased with increasing total nitrogen concentration. Electron energy loss spectroscopy mapping of carbon and nitrogen revealed that nitrogen was not homogeneously dispersed in these materials, displaying enrichment along the outer rims. The best electrocatalytic activity, durability and tolerance to methanol were reported for the materials with 2.2 wt% nitrogen. Methanol tolerance is important for ORR cathode catalysts in direct methanol fuel cells in order to mitigate the deleterious effects of methanol crossover at the cathode.

Ramaprabhu et al have investigated Pt and Pt_3Co alloy nanoparticles supported on N-doped graphene, where 5.9 at% N-doping was achieved by coating graphene with polypyrrole and treating it at 800°C in inert atmosphere[188]. Samples showed contributions from pyridinic, pyrrolic, graphitic and oxidized nitrogen groups, with pyridinic nitrogen being the main component. Pt and Pt_3Co were deposited onto N-doped graphene by a modified-polyol reduction method and showed higher electrochemical surface area (ECSA) than that of

commercial Pt/C. The high ECSA was attributed to the uniform dispersions of nanoparticles, achieved due to the presence of nitrogen groups. Both samples also showed maximum power densities higher than those of commercially supported Pt or PtCo catalysts and demonstrated good stability. Liu et al. demonstrated Pt supported N-doped porous carbon nanospheres with excellent dispersion and small particle size as well as improved half-wave potentials and mass activities [168]. Popov et al. developed a nitrogen-modified carbon composite (NMCC), prepared from ethylene diamine, $Co(NO_3)_2$ and carbon black[187]. The authors first compared the performance of Pt/C, Pt/NMCC and PtPd /NMCC catalysts with various Pt/Pd ratio and reported that the Pt/NMCC material showed best mass activity. Mass activities of PtPd/NMCC catalysts varied due to differences in the particle size and alloying effects. Fuel cell testing revealed that the NMCC-supported catalyst had higher initial catalytic performance and was also more stable than the unmodified carbon black support due to higher graphitization.

As discussed in the materials section, pyrolysis of ionic liquids using CNT's as a template was used to investigate the electrocatalytic performance of Pt. These materials contained low overall N concentration, but possessed a reasonable (~8%) concentration of surface C-N bonds. While Pt-mass based activities of the undoped and N-doped materials were very comparable, author's observed major differences in the stability of these materials, demonstrating the beneficial effect of surface nitrogen groups towards stabilization of the Pt nanoparticles. In this study, ECSA losses were reduced from 33% to 27% and more significantly, the average particle size growth was reduced from 45% to 22%, suggesting reduced dissolution/ripening and/or migration/coalescence due to nitrogen functionalization[62].

4.1.3. Non-precious metal N-modified catalyst systems for oxygen electroreduction:

N-containing non-precious metal catalysts (NPMCs) derived from precursors of carbon, transition metals, and nitrogen by means of heat treatment have been studied for years, but the recent years have been transformational, with major advances in the oxygen reduction performance. Within the past 5 years, several detailed reviews of nonprecious metal catalysts for ORR have appeared in the literature [189–192].

In general, various precursors and synthesis routes have been explored in the search for the most active and stable catalysts. Despite this vigorous activity, however, the precise nature of the active sites in this class of materials is yet to be determined. The mechanism of oxygen reduction can follow several pathways, i.e. proceeding via two, four or two-by-two electron transfer. In these systems, identification of the active site is challenging because these materials are typically complex and possess many different species that could potentially support the different pathways. The most widely used techniques employed for investigation of the catalyst composition and structure is X-ray photoelectron spectroscopy (XPS) and transmission electron microscopy (TEM). In search of the nature of the active sites, scientists have also employed a variety of other techniques, including X-ray absorption techniques (XAS), time-of-flight secondary ion mass spectroscopy (ToF-SIMS) and Mössbauer spectroscopy[193–201]. Several studies have additionally employed sophisticated statistical analyses such as principal component analysis to determine correlation between ORR activity and parameters obtained from spectroscopic techniques[202,203,193,204].

Published in 2009, a cross-laboratory study of non-noble-metal electrocatalysts compared electrocatalysts synthesized by different groups using several routes: 1) pyrolysis of a single precursor based on a metal-N_4 chelate, 2) pyrolysis of two separate precursors for metal and nitrogen, 3) second pyrolysis of materials derived by 1 or 2 under reactive atmosphere of O_2, CO_2, NH_3 or N_2/H_2) and 4) pyrolysis of metal precursors under NH_3[205]. The conclusion of this work was that total nitrogen content appeared not to have a direct correlation with the activity, but micropores produced during heat-treatment were found to be important as they were hypothesized to host N-containing active sites. Later, the Dodelet group demonstrated significant improvement in the current and power densities by focusing on optimization of the synthesis to maximize the amount of active sites hosted between graphitic sheets within micropores, with the active site proposed to be pyridinic nitrogen coordinated to iron[72] (See Figure 1). Pyrolysis of chloro-iron tetramethoxyphenylporphyrin (Cl-FeTMPP) supported on a non-microporous carbon in NH_3 led to a more active and less stable catalyst than heat-treatment in argon environment[206,207].

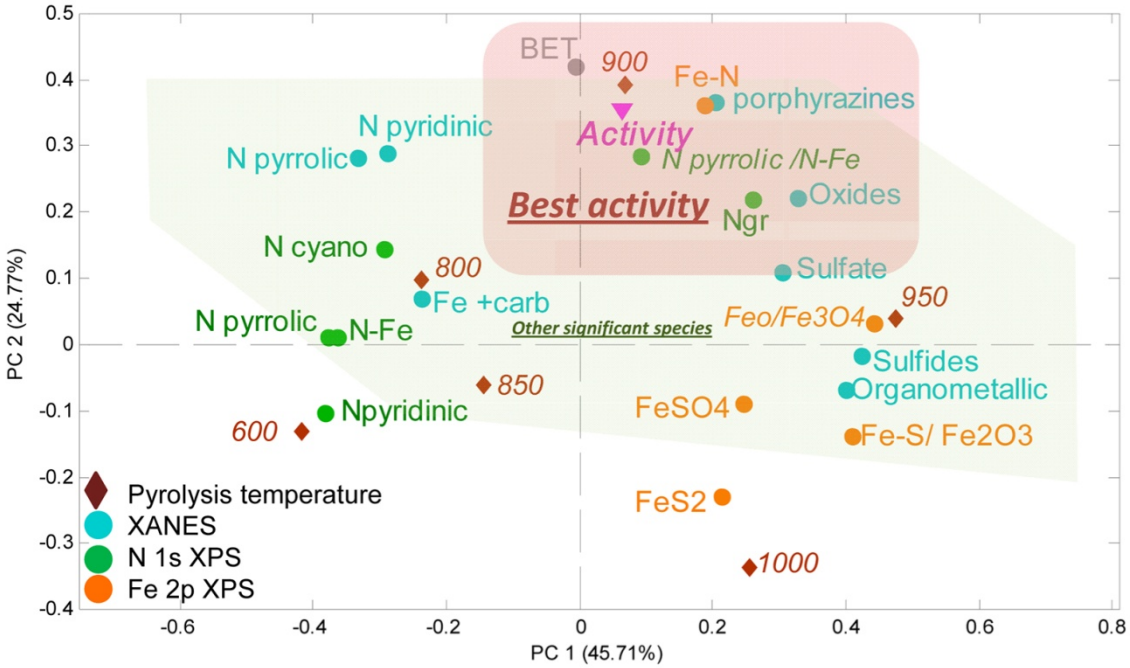

Figure 10: *Correlation between XANES, XPS, and BET data and ORR activity for PANI–Fe–C using principal component analysis. All catalysts after heat treatment, acid leach, and a second heat treatment. Reprinted (adapted) with permission from Citation*[193]*. Copyright (2012) American Chemical Society.*

In attempts to increase the density of active sites, a group from Los Alamos National Laboratory (LANL) explored materials derived from cyanamide and polyaniline. A cyanamide precursor was employed in efforts to increase the nitrogen content; however, authors reported lower than expected nitrogen concentration and additional incorporation of sulfur[208]. NPMC based on pyrolysis of polyaniline showed high selectivity for four-electron oxygen reduction when materials contained both nitrogen and metal[71]. Authors explored the effect of pyrolysis temperature in the range of 400-1000°C, finding 900°C to be the optimum temperature for maximum activity and stability. The unique characteristic of this material was the high degree of graphitization that occurred in the form of graphitized

onion-like carbon shells over the metal-rich particles and graphene-like sheets. These graphitic structures were hypothesized to improve stability and host active sites[71,124]. For the iron-based catalyst, increasing the heat-treatment temperature led to an increase in the ratio of quaternary (Figure 1) to pyridinic N species, but because the total nitrogen content decreased, the correlation between quaternary nitrogen species and activity could not be directly depicted[194]. In addition, the authors also investigated the effect of metal type (Fe or Co) and metal loading on the catalyst composition, morphology and resulting performance. It was noted that compared to Co-based catalysts, more active Fe-based catalysts showed higher amounts of graphitic nitrogen, but authors discussed the unlikeliness for this type of nitrogen to be the most active catalytic site; instead the apparent correlation might have been associated with beneficial morphological changes. In general, the authors didn't find strong direct correlations between activity and specific nitrogen functionality[194]. Correlations between XANES, XPS, BET and ORR activity for a polyaniline-iron-carbon catalyst revealed close correlation between ORR activity, Fe-N content, BET, and microporous surface area. The authors of this study also observed correlation of ORR activity to the total amount of graphitic and quaternary nitrogen and the ratio of pyrrolic N to Fe-N species (Figure 10). These findings showed the importance of the relative distribution of nitrogen functionalities in determining catalytic performance[193]. Aiming at improving the stability of polyaniline-derived catalysts, Wu et al. increased catalyst graphicity by using CNT's as the support[209]. Fe-N_x centers and quaternary nitrogen incorporated into carbon structures have been proposed as possible active sites in iron-imidazole-derived catalysts[210]. Ramaswamy also investigated the role of the carbon basal plane in more detail, demonstrating that changes in the transition metal redox potential are closely related to pyrolysis-induced integration of the Fe-N_x centers into the π-electron-deficient environment of the carbon[195].

Another approach to increase the density of nitrogen-containing active sites was proposed by Kothandaraman et al. through the pyrolysis of nitrogen and iron precursors, mixed with high surface area carbon, performed at high pressure in a closed container[211]. For materials prepared using high-pressure pyrolysis, the concentration of incorporated nitrogen and the corresponding ORR activities were greatly affected by the structure and composition of the carbon support[212]. Byon investigated surface functionalization of multi-walled CNT's for incorporation of sites participating in ORR and observed higher ORR mass activity when materials possessed higher amounts of Me-N_x (where x~4) as well as greater Fe/C ratios [196]. Arechederra et al. demonstrated incorporation of nitrogen and iron or cobalt into carbon nanotubes from phthalocyanines using low temperature solvothermal synthesis[213].

Several reports have discussed self-supporting catalyst materials prepared without carbon support using sacrificial silica templates[202,214–216,198]. Serov et al. showed that performance of iron-aminoantipyrine-derived catalysts prepared with a sacrificial support had a greater density of active sites as compared to a carbon-supported catalyst. The best performance was obtained for the catalyst pyrolyzed at 800 °C. At higher pyrolysis temperatures the performance dropped, most likely due to decomposition of active sites. Doubling the amount of the nitrogen precursor relative to the amount of transition metal resulted in significant improvement in the catalytic activity. Further increases in the amount of the nitrogen precursor, however, led to a drop in the performance[217]. Olson et al. prepared catalysts based on pyrolyzed porphyrins with nitrogen and cobalt content of 5 at% and 1.24 at%, respectively. The catalyst was subjected to various treatments with the objective of selective removal/enrichment of catalyst with different moieties. Authors reported a decrease in the halfway potential upon removal of either Co-N_x or Co_xO_y/Co. It was

hypothesized that oxygen reduction follows two-by-two electron pathway, where the first step occurs on the Co-N_x and second on Co_xO_y/Co. Materials depleted in active Co-N_x and Co_xO_y/Co showed correlation between high concentration of graphitic carbon and graphitic nitrogen and lower amounts of produced peroxide, suggesting that these species might contribute to decomposition of peroxide[202]. In the absence of transition metal, N-containing catalysts derived from poly(ethyleneimine) showed a high peroxide yield, which was significantly reduced with the addition of iron[214]. Catalysts derived from iron and 4-aminoantipyridine, which had nitrogen and iron contents of 3.5 at% and 0.1 at% respectively, also followed the 2x2 electron transfer pathway. This material was shown to be effective in acid and alkaline media and was found to be especially good at reducing peroxide[217,215]. Other reports also evaluated activity of the NPMC's at different pH, demonstrating the potential of these materials in alkaline media[218,219,203]. In these studies, iron and nitrogen-containing electrocatalysts were shown to have 7-10 times higher ORR activity in alkaline media when compared to acid media[218]. Investigation of cobalt-polypyrrole electrocatalysts in alkaline media suggested dual-site mechanism where Co-N_x acted as an active site for the $2e^-$ process[203].

NPMC catalysts based on graphene have been studied in acid[220] and alkaline media[221,222,197]. Byon reported synthesis of NPMC based on heat-treatment of chemically reduced graphene in the presence of iron salt and graphitic carbon nitride. Increased integration of Fe-N_x centers were observed for temperatures between 600 and 700°C. This material contained ~5 at% of nitrogen and 0.4 at% of iron, where on average, the Fe was coordinated to 3 nitrogen atoms (based on EXAFS analysis)[220]. Similar to observations in acid media, the ORR performance and stability of the N-doped materials was improved by incorporation of iron[222] or cobalt[221,197] demonstrating the necessity for both nitrogen and transition metal.

In addition to non-precious metal N-containing catalysts derived from pyrolysis of transition metal and nitrogen precursors, N-functionalization was also demonstrated for catalysts based on carbon-supported high-loading transition metal oxides[223–228]. Liang et al. reported on the effects of nitrogen doping on the nucleation and growth of Co_3O_4; demonstrating the reduction of particle size from ~12-25 nm to ~4-8 nm. Additionally, incorporation of nitrogen resulted in positive ORR peak potentials, higher peak currents and more positive halfway potentials as well as lower peroxide yields. Authors reported the results of XANES analysis indicating a bond formation between Co_3O_4 and N-doped graphene[223–226]. Later, authors also described electrocatalysts based on manganese-cobalt oxide and graphene[229] and reported high-performance hybrid catalysts based on cobalt oxide and N-doped carbon nanotubes[224]. He et al. also reported narrow nanoparticle size and synergistic effects between N-doped graphene and cobalt oxide. Authors reported that addition of nitrogen and cobalt oxide improved ORR activity and four-electron selectivity, while the addition of nitrogen only improved the onset and half-wave potentials. Spectroscopic analysis, paired with DFT, were used to hypothesize that pyridinic nitrogen species in N-doped graphene might be coordinated to cobalt ions[225]. Impressive ORR performance in alkaline media was demonstrated for carbon-nanotube/carbon nanoparticle composites synthesized from iron acetate and cyanamide[226]. Nitrogen surface groups were also shown to improved stability of iron nanoparticles, decreasing their sintering[230].

4.1.4. Metal-free N-containing catalyst systems for oxygen electroreduction:

Many groups report that ORR performance of carbon material could be significantly improved upon doping with nitrogen even in the absence of nitrogen-coordinated

transitional metal complexes. Increases in the current densities and decrease in the overpotential are observed for metal-free N-doped systems when compared to undoped references. Most of the studies focus on N-doped CNT's and graphene, but a few also report on carbon blacks[231,232], porous carbons[233,88] carbon nanoshells[234] and carbon nitrides[235]. Some groups also investigated composite structures made with both CNT's and graphene[236,237]. Based on the fact that many studies use iron during the synthesis, and treatments utilized to remove the iron might not be 100% efficient, most "metal-free" materials might actually still have some trace transition metal sites that might be responsible for the observed effects. Therefore there is a debate among researchers whether truly "metal-free" N-doped carbons are as active as reported.

Vertically aligned CNT's showed significant improvement in kinetics of ORR in both acid and alkaline media[238]. Gong et al. evaluated vertically aligned N-doped CNT's in alkaline media and reported high electrocatalytic activity, a four-electron pathway and good stability after potential cycling. Authors synthesized vertically aligned N-doped CNT's using pyrolysis of iron and nitrogen containing precursor, iron (II) phtalocyanine, with and without NH_3, followed by removal of residual iron[239]. Vertically aligned N-doped CNT's produced from ferrocene under ammonia [240] also showed improved onset and peak potential, but due to lower amount of doped nitrogen underperformed as compared to the phtalocyanine-based materials. The same work also discussed vertically aligned CNT's doped with boron and demonstrated that CNT's co-doped with nitrogen and boron show synergistic effect on ORR performance, meanwhile CNT's doped with boron only are less effective than N-doped material [240]. Good ORR activity was demonstrated for N-doped CNT's and N-doped graphene obtained from melamine with and without assistance from metal atoms [241,54,242,34]. McClure et al. synthesized N-doped carbon nanowall electrodes without a metal catalyst and observed an increase in kinetic current density and the number of electrons transferred per O_2 as total nitrogen concentration increased, specifically graphitic nitrogen and pyridine-N-oxides[243]. Investigation of CNT's doped with nitrogen by ammonia treatment revealed a gradual positive shift in onset potential and an increase in the limiting current when the temperature increased from 200°C to 800°C. The increase in the temperature associated with reduction of the total amount of nitrogen and oxygen functionalities, was, however, accompanied by a relative increase in quaternary nitrogen with respect to pyridinic and pyrrolic groups, suggesting the importance of the formation of quaternary nitrogen for the improvement in the ORR performance[59]. Higher temperature treatment (which decreases the amount of nitrogen) and higher loading of polypyridine precursor on the surface of the carbon black (which increases the amount of nitrogen) were beneficial for ORR activity[244]. Higher temperature was also shown to be beneficial to ORR activity of nitrogen-rich mesoporous carbon materials[245]. Surface coatings rich in pyridinic and quaternary nitrogen groups obtained by pyrolysis of cyanamide result in improved onset potential and ORR kinetics [246]. Likewise, Liu also reported pyridinic and quaternary nitrogen as proposed ORR sites [247].

Improvements in ORR activity as a function of nitrogen concentration were reported for CNT's synthesized from pyridine[248], diamine[249] and melamine[242] precursors. Interesting findings in regard importance of clustering of nitrogen atoms were reported by Zhang et al. Authors discussed that the number of active sites per dopant atom is maximum when clusters consist of two nitrogen atoms. Further increase in the cluster size reduces the number of active sites[150]. For the pyridine-based materials, a small increase in the nitrogen concentration had a large effect on the limiting current density and H_2O selectivity and a smaller effect on the onset and half-wave potential[248]. Similarly, an increase in nitrogen

concentration had no effect on onset potential, but led to an increase in the current density for the melamine-derived graphene[34]. Materials derived from diamine with different nitrogen to carbon ratios showed a larger range of nitrogen concentrations (1.2-4.74 at.%), which was associated with a higher degree of edge plane defects arising from pyridinic species[249]. N-doped CNT's synthesized with ethylenediamine showed improvements in onset and half-wave potential, limiting current density, number of electrons transferred, and H_2O selectivity when compared to CNT's made with pyridine. This effect was attributed to the higher nitrogen concentration and surface defects[250]. Chen et al. also compared CNT's synthesized from ferrocene and iron (II) phtalocyanine, and concluded that when the nitrogen concentration is similar, CNT's with more surface defects perform better. In this work, the authors employed an acid treatment process to remove iron seed atoms, but reported that about 0.2-0.27 at% of the iron remained, which is near the same level as previously discussed in the NPMC catalysts section[251]. Zhao correlated ORR activity to the concentration of species at binding energies of 398.3 and 401.5 eV rather than the total nitrogen content[252]. Singh et al. reported correlation between pyridinic N and ORR activity of CN_x grown on two different substrates[253]. Biddinger suggested that the total amount of nitrogen or nanostructure on its own are not so important; rather it is the amount of nitrogen incorporated into graphitic structure that matters [254]. Taking into account these observations, it is clear that there is a need for systematic studies aimed at understanding the importance of specific functionalities, in addition to total nitrogen content.

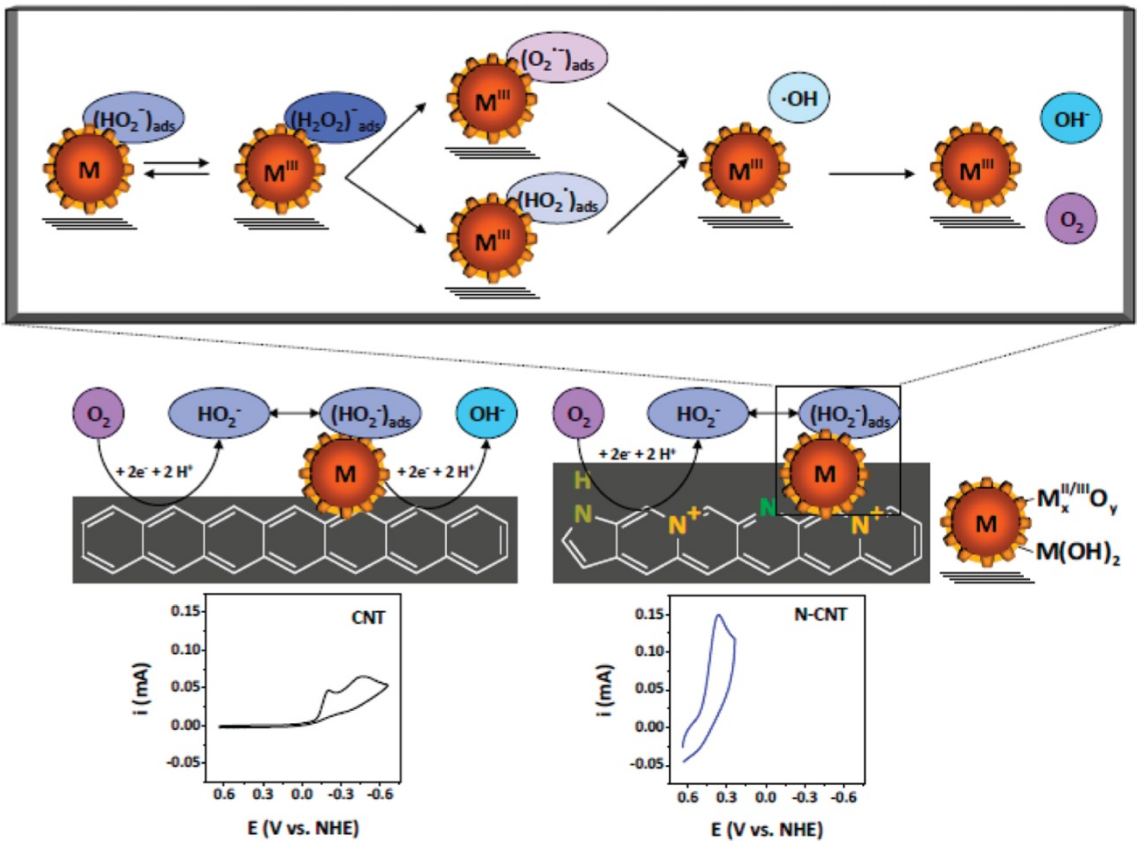

Figure 11: *Graphical Representation of Proposed ORR Mechanism at CNT versus N-CNT Electrodes with Representative Cyclic Voltammograms for CNT's and 6.3 at. % N-CNT's in 1 M*

Na_2HPO_4 (V vs. NHE). Reprinted (adapted) with permission from Citation[52]. Copyright (2011) American Chemical Society.

Since a lot of N-doped materials do contain small amounts of metal, investigations aimed at evaluating the effect of nitrogen vs. the effect of residual metal/metal oxide phase are important. Masa et al. compared the performance of catalysts made without metal precursor, with metal precursor and with addition of trace amounts of metal and showed that the performance of the metal-free materials was the lowest and was significantly effected by the addition of iron even at very low concentrations (0.05%) [255]. A mechanistic study by Wiggins-Camacho et al. concluded that both nitrogen groups and residual surface metal oxide/metal phase participate in the ORR on N-doped CNT's. The authors correlated the gradual shift in ORR on-set potential with the increase in the nitrogen content. In addition, reduction potential was correlated with an increase in the amount of pyridinic species and a decrease in the pyrrolic species. This work suggested that on N-doped CNT's, the reaction undergoes a "pseudo"-four electron pathway, where the first step of two-electron electrochemical reduction of O_2 is followed by chemical disproportionation. The last step occurs faster on the CNT's with larger concentrations of nitrogen and involves the iron oxide/iron sites stabilized by the pyridinic nitrogen groups (See Figure 11)[52]. The mechanistic investigation of ORR on N-doped CNT's in alkaline media conducted by Vazquez-Arenas proposed parallel two and four electrochemical electron pathways of ORR on N-doped CNT's in alkaline media[256]. N-doped CNT's were also investigated in neutral pH phosphate buffer solution suggesting a four-electron pathway[257]. Deak et al. used carbon monoxide and cyanide to probe the active sites in CN_x, suggesting that metal centers are not involved. In contrast, Li observed more than 100 mV decrease in the onset potential and changes to the diffusion-limiting current in the presence of cyanide ions, indicating the involvement of iron in the ORR. Moreover, aberration-corrected STEM-ADF and EELS mapping of graphene sheets that were active for the ORR showed the presence of iron and nitrogen atoms in close proximity to each other [258].

Beyond CNT's, metal-free N-modified mesoporous carbons have also been investigated as ORR electrocatalysts. Silva et al. investigated mesoporous carbons derived from polyaniline and concluded that high catalytic activity of metal-free materials was most likely due to synergistic effect of nitrogen and oxygen functionalities[88]. Another class of N-doped porous carbons that showed promising ORR activities was derived using porous organic framework as sacrificial template[233].

In recent years, many groups have studied N-doped graphene as an efficient catalyst for ORR in alkaline media with performance comparable to that of commercial Pt/C catalysts[16,29,259]. Qu et al. reported large area synthesis of N-doped graphene using ammonia. This material showed great catalytic activity via a four-electron pathway and long-term stability[16]. Geng et al. employed an ammonia treatment at temperatures of 800-1000 °C to incorporate 2-2.8 at% of nitrogen. The authors suggested that nitrogen species located at binding energy of 401.3 eV might be responsible for the improvement in onset potential. The largest shift in the onset potential and close to four-electron reduction process was reported for the material pyrolyzed at 900°C [29]. Niwa analyzed three sets of materials using XAS to propose the importance of graphitic nitrogen over the pyridinic nitrogen[260]. To facilitate the formation of graphitic nitrogen species (at 401-401.2 eV), Lin et al. reported pyrolysis of graphene oxide with polypyrrole[261] or polyaniline[262] being the N source[261].

Another approach using a thermal annealing process with urea resulted in nitrogen concentrations close to 2-3 at %[263]. High levels of nitrogen (~10.6%) were achieved using a solvothermal method employing ammonia as both the nitrogen source and the reducing agent[264]. Investigation by Luo et al. showed a two-electron reduction mechanism on graphene doped with pyridinic nitrogen, suggesting that these species may not be as beneficial for ORR as other functionalities[15]. In contrast, the activity of hollow mesoporous carbon with graphene-like structure was attributed to the availability of pyridinic nitrogen[265]. This could be explained using a study by Brun et al. which discussed the fact that selectivity for the 2e- vs. 4e-electron pathways can be controlled by tuning the pyrrolic/pyridinic nitrogen ratio[266]. More recently, Guo et al. reported that the pyrrolic nitrogen species present in materials pyrolyzed from blood protein in the presence of carbon black are possible catalytic sites for four-electron transfer [267]. Lai et al. compared ammonia treatment vs. pyrolysis of polyaniline and polypyrrole and reported preferential formation of graphitic and pyridinic N via the first route and pyridinic and pyrrolic N via the second [268]. Authors also reported positive effects from graphitic N on the limiting current density and from pyridinic N on the onset potential.

4.3. Batteries:

Carbonaceous materials doped with nitrogen have been vigorously explored for application in non-aqueous Lithium-air batteries. In these applications, the oxygen reduction reaction at the cathode is similar to the ORR reaction at the fuel cell cathode and therefore many of the advantages discussed in the previous sections also apply to this field of research.

Li et al. evaluated the performance of N-doped graphene nanosheets with 2.8 at% nitrogen and demonstrated several improvements over undoped material: First, the N-doped material showed higher discharge plateaus at various discharge current densities and specifically demonstrated 40% higher discharge capacity at a current density of 75 mAg^{-1}. Secondly, the onset potential, current densities and the number of transferred electrons were also improved. Analysis of discharge products revealed more uniform distribution of the particles, indicating a larger number of active sites[30]. N-doped CNT's with nitrogen concentration of 10.2 at% showed 1.5 times higher specific discharge capacity as compared to undoped CNT's. N-doped CNT' were also employed in binder-free Li-air batteries[269]. The performance of exfoliated N-doped graphene showed a shift in the onset potential and a predominant four-electron transfer clearly attributed to nitrogen-doping. These promising results were demonstrated in Lithium-oxygen and Zinc-air battery single cells [270]. N-doped CNT's and N-doped carbon fibers have been investigated as efficient catalysts for Zn-air batteries[271,272]. For example, electrocatalytic activity of carbon fibers produced from polystyrene and polyacrylonitrile was attributed to developed porosity and enrichment with nitrogen[272].

Wu et al. discussed graphene-rich nanocomposites prepared from polyaniline and a cobalt precursor, which were supported on commercial MWCNT's. The temperature of the heat-treatment was shown to be an important factor that affected the nitrogen speciation and in turn improved ORR performance. The authors discussed the formation of desirable functionalities located at 398.6 eV and 401.3 eV (assigned to pyridinic and quaternary nitrogen groups respectively), which they suggest may have been preferentially formed due to the addition of cobalt [273].

Recently, Park et al. reported on a bi-functional nanocomposite made of N-doped CNT's and graphene. The role of the N-doped CNT's is two-fold; in addition to providing catalytic sites, they also connect the graphene sheets and compensate for the loss of conductivity in the graphene resulting from the synthesis via the thermal annealing route. The material was also highlighted for its excellent oxygen evolution reaction (OER) performance [274].

Kichambare et al. investigated mesoporous carbons made with a mix of N-doped Ketjen black and Calgon black[275,276]. A two times higher cell discharge capacity of the N-doped material was attributed to higher electrocatalytic activity and increased porosity of the N-doped material, thereby leading to higher oxygen diffusivity[275]. The importance of pore structure, in conjunction with high nitrogen content (~6.59 at%), was also discussed by Nie[277]. Excellent electrocatalytic activity observed in molybdenum nitride/N-doped carbon nanospheres was attributed to the nanostructure and the synergy between the molybdenum nitride and the N-doped carbon nanospheres[278]. Hybrid catalysts based on MnO_2 nanotubes and N-doped exfoliated graphene have been shown to have increased ORR activity because of defect sites introduced by doping[279].

Various N-doped carbonaceous materials were also explored for application as efficient anode materials in lithium-ion batteries (LIBs) and emerging sodium ion batteries (NIBs). In these systems the purpose of nitrogen doping is to improve the intercalation properties and increase specific capacity. Here it is beneficial to grow N-doped materials directly on the current collector substrate to improve the adherence and electron transport. Due to their modified electron transport, however, the N-doped carbons often display non-ideal voltage versus capacity plateaus. The capacitor-like sloping V vs. capacity profile of N-rich carbon anodes for both lithium ion and sodium ion applications reduce the total energy density of the cell by limiting the working voltage window and making it difficult to design devices that behave analogously to commercial LIB technology. In fact, where N-rich carbons may have the highest use is in Li ion and Na ion capacitors[280].

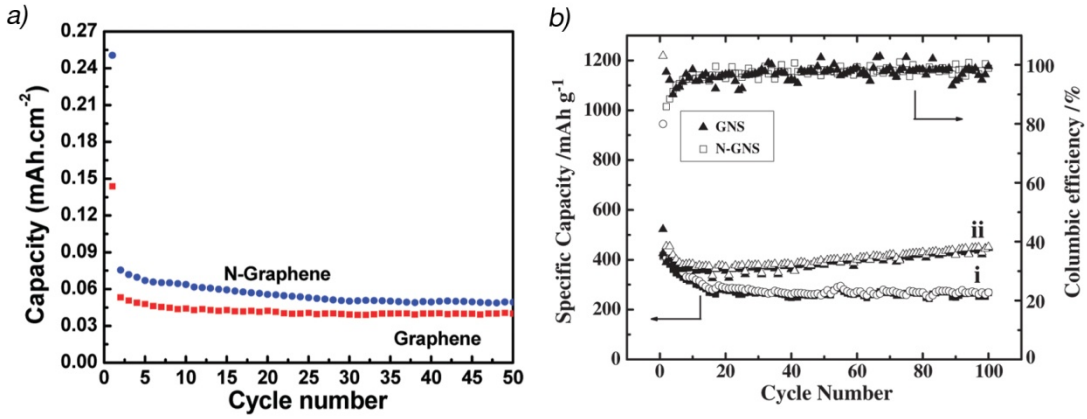

Figure 12: *a) Electrochemical performance of graphene films grown on Cu foil, galvanostatically cycled in Li half cells. Variation in discharge capacity vs. cycle number for the pristine graphene and N-doped graphene cycled at a rate of 5 mA/cm2 between 3.2 and 0.02 V vs. Li/Li+ in 1 M solution of LiPF6 in 1:1 (v/v) mixture of ethylene carbonate (EC) and dimethyl carbonate (DMC) as the electrolyte. Reprinted (adapted) with permission from Citation [281]. Copyright (2010) American Chemical Society. b) Reversible charge/discharge capacity verse cycle number of (i) graphene-nanosheets and (ii) N-graphene-nanosheets Reprinted (adapted) with permission from Citation[282]. Copyright (2011) Elsevier.*

A 2010 report published by Reddy et al. examined the benefits of N-doping for graphene films. The addition of nitrogen dopants led to a nearly two times increase in the reversible discharge capacity (Figure 12a). N-doped films contained about 9 at% nitrogen, with pyridinic nitrogen as the predominant functionality. The effect of nitrogen on performance was explained by the presence of a large number of surface defects associated with nitrogen doping[281]. Several groups discussed that N-doping improves the reversible capacity, rate capability and long-term cycling stability related to enhanced kinetics, as well as the number of active sites, and contributes to more stable interfaces[30,283,284]. Materials with higher levels of nitrogen demonstrate higher reversible specific capacity and rate capacity[285]. Li et al. didn't detect a noticeable change in the initial Li^+ intercalation/de-intercalation associated with doping of ~2.8 at% nitrogen into graphene nanosheets, but reported a remarkable difference in the cycle performance of undoped and N-doped materials[282]. In the N-doped material an increase in the specific capacity was observed starting at 17th cycle and continuing until it reached a maximum at around 501st cycle. Conversely, the undoped graphene demonstrated a typical decrease in the specific capacity (Figure 12b). The authors attributed this effect to the gradual increase in the defects of the already disordered structure of N-doped material. The benefits of the surface defects introduced by N-doping can be effectively combined with benefits of sandwich structures, in which nanoparticles or arrays are sandwiched between graphene sheets[20].

Dispersion and stability of active nanoparticles in graphene-based hybrid anodes can be greatly enhanced via modification of graphene with nitrogen. These properties of N-doped graphene were explored in the hybrid materials with nanoparticles of SnO_2[26,286,20], Fe_2O_3[287], Fe_3O_4[288], TiO_2[289,290], MnO[291] and NiS[292] demonstrating synergy between the N-doped support and the nanoparticles.

Increase in the specific charge capacities and improvement in rate capability of carbon nanotubes[293–295] carbon nanofibers[296,102] and mesoporous carbon materials[297,298] upon nitrogen doping has been reported by several groups. CNT's with 16.4 at % of nitrogen showed better rate capability and about a two times higher reversible capacity when compared against undoped CNT's[293]. Characterization of a series of N-doped CNT's with nitrogen content ranging from 1.23 to 2.89 at % produced with an acetonitrile precursor revealed that higher nitrogen levels lead to an increase in the first-cycle discharge capacity. The authors suggested that the irreversible capacity is related to the amount of pyridinic nitrogen. The best electrochemical performance was observed for material with the lowest N-content that had the highest relative amount of graphitic nitrogen[294]. Ren et al. investigated CNT's doped with similar amount of nitrogen (1.21-2.83 at %) using melamine as a nitrogen precursor and found that higher nitrogen concentrations not only increase the first discharge/charge capacity, but also increase reversible capacity[295]. A storage capacity of 1780 uAhg-1 was reported for N-doped mesoporous carbons obtained from biomass-derived proteins, the result of an efficient combination of high surface area, graphitization and high nitrogen content (up to 10.1 at%)[297]. Porous nanostructure and high nitrogen content (~13 %) of N-doped carbon capsules resulted in high rate capacity and good cycling performance[299].

The performance of electrode materials (e.g. oxides) with low conductivity can be improved by carbon-coating, where N-doped carbon coatings provide additional benefits as compared to undoped coatings. For example, N-doped carbon coatings were used to improve rate capability and cycling performance of Li_4TiO (LTO)[300,301] and $LiFePO_4$[302]. Using experimental and theoretical studies, Ding et al. suggested that doping nitrogen into carbon coatings improves interfacial stability and electric conductivity[300]. Improvements in storage capacity, rate capability and/or cyclic performance were also reported for other nitrogen-doped carbon-coated anode materials, including SiO, TiO_2 and $CoSnO_3$[303–305]. In addition to the battery applications discussed above, N-doped materials have also been evaluated for vanadium redox flow batteries[306–308], and lithium-sulfur batteries [64,309,310] with promising results. The benefit of N-doping towards improving capacitance of various types of batteries had been clearly demonstrated and further improvements in the performance are expected as the field advances fundamental understanding of N-doping.

4.4. Supercapacitors

Carbon materials have been used for decades in capacitor applications. The capacitance of high-surface area carbon-based materials with good conductivity and fast electron transfer rate can be further improved though functionalization with heteroatoms such as nitrogen or oxygen groups. Functionalization is believed to increase the capacitance through pseudo-capacitance effects, i.e. via additional Faradaic reactions.

Comprehensive analysis of the pore structure in conjunction with deconvolution of the type of functional groups present is critical to understand the contributions to capacitive performance. This is particularly essential for highly porous materials, where pseudocapacitance is superimposed onto a more significant contribution from double-layer capacitance. In organic electrolytes, the pore size plays a particularly important role. In aqueous electrolytes, the porous structure still greatly controls capacitance, but the psueodcapacitive effects of heteroatom functionalization are more clearly resolved. Capacitive enhancement due to nitrogen functionalization has been shown by comparing highly-porous nitrogen-containing carbons and porous carbons with no nitrogen, but similar textural characteristics[311]. Furthermore, significant (e.g. 2X) capacitive enhancement has been observed upon the addition of surface nitrogen to porous carbon already containing nitrogen in the bulk[312]. In addition to increased capacitance due to pseudocapacitive effects, the enhancement in the electrochemical properties of N-containing carbon supercapacitor materials has also been attributed at least in part to improved wettability [312–315].

Hulicova-Jurcakova et al. synthesized ammonia-treated low surface-area non-porous carbon materials prepared from melamine-mica composites which demonstrate excellent cycleability and three times higher gravimetric capacitance than untreated composites. Materials pre-oxidized prior to ammonia treatment exhibited higher nitrogen content, larger concentration of pyrrole-like nitrogen groups and showed improved pseudocapacitance[80]. Others also reported pseudocapacitive effects in the presence of positively-charged pyrrole species detected at XPS binding energies of 400.0-400.3 eV[316,317], [318]. In another study, Hulicova-Jurcakova et al. modified coconut-shell-based microporous carbons with nitrogen functional groups from urea and melamine precursors to investigate the combined effect of nitrogen and oxygen functional groups[319]. Pyridinic and pyrrolic nitrogen groups (along with quinone oxygen groups) had the largest effect on capacitance, meanwhile the positive charge of quaternary and pyridinic-N-oxides also improved capacitance, particularly at high current loads. Amino-functionalization of carbon

nanotubes was also shown to enhance capacitance[320]. Lai et al. compared the effect of various surface functionalities on the capacitance of graphene/polyaniline composites and found that among chemically-reduced (RG-O), nitrogen-doped RG-O and amine-modified RG-O, the latter had the highest capacitance, reaching up to 500 F/g (in acid electrolyte)[321] (see Figure 13). Researchers also examined supercapacitor performance for surface-functionalized graphene/polypyrrole composites. In this study, an amine-modified graphene/polypyrrole composite showed higher capacitance than unmodified graphite oxide, but both were clearly outperformed by composites made with N-doped graphene, which demonstrated a high specific capacitance of 393.67 F/g.[314] This performance was attributed to improved electron transfer efficiency and surface wettability. In a similar vein, composites of polyaniline and graphene functionalized with oxygen groups outperformed nanocomposites made with oxygen functionalized graphene and metal oxides such as RuO_2, TiO_2 and Fe_3O_4 [322]. About 4 times higher capacitance was observed for the nitrogen-plasma modified graphene as compared to pristine graphene; the enhancement was linked to nitrogen sites at the basal planes of the graphene[41]. In 2012, a report used direct synthesis to fabricate C_3N_4 coated graphene, which had a surface area of 465 m^2/g, large pore volume, and 10.8 at.% N. This material performed well in electrochemical testing because of easy ion transport as well as good conductivity. The resulting material showed a capacity of 302 F/g in a 6M KOH electrolyte[323].

The effect of carbonization temperature on the nitrogen content, speciation, pore structure, and their respective contributions toward capacitance have been studied by many[313,316,312,324]. N-containing porous carbon nanofiber papers with moderate to low surface areas, carbonized at temperatures 700-1000°C, demonstrated the effect of pyridinic and pyrrolic functionalities on activity in aqueous media[324]. Evaluation of nitrogen-doped porous carbon derived by pyrolysis of nitrogen-containing salts in the 600-900°C temperature range revealed maximal pseudocapacitance for the 600°C pyrolysis temperature, which was correlated to a large amount of pyridinic and pyrrolic groups. Samples pyrolyzed at 800 and 900°C showed decreased capacitance despite higher surface areas; authors attributed this to poor functionalization. The sample pyrolyzed at 700 °C showed the highest overall capacitance (245 F/g, alkaline electrolyte), the result of a good balance between surface area and nitrogen content. In a similar vein, the effect of synthesis temperature on the performance of terephthalonitrile-derived nitrogen-rich networks was studied, identifying important differences between materials produced below 550°C vs. those synthesized at temperatures above 550°C. While it is typically reported that nitrogen content decreases with increasing carbonization temperature, in general, nitrogen-doped porous carbons synthesized from ionic liquid precursors have allowed researchers to obtain higher nitrogen content even at high carbonization temperatures [93,81,325].

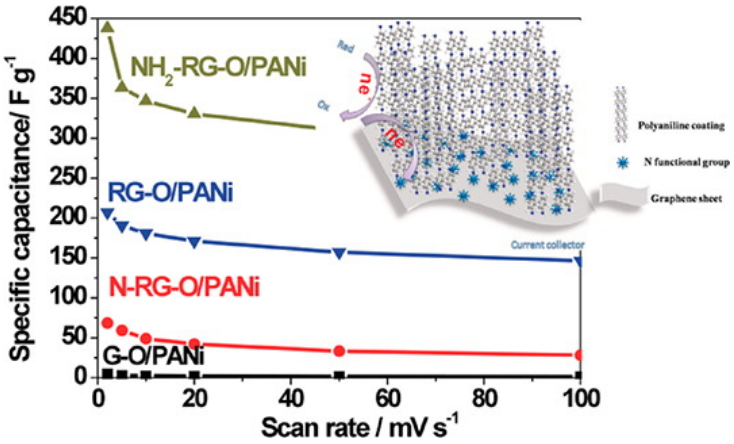

***Figure 13**: Performance of 10 wt% PANi as a function of scan rate (from 2 to 100 mV/s) in 1M H_2SO_4 electrolyte. Reprinted (adapted) with permission from Citation [321]. Copyright (2012) American Chemical Society.*

Motivated by a focus on sustainability, nitrogen-doped porous carbons have been prepared from gelatin using an activation process involving NaOH[109] as well as via a dual carbonization method without physical/chemical activation[326]. Xu et al. reported capacitance in the range of 172-385 F/g (alkaline electrolyte) for materials with nitrogen concentrations ranging from 9.26% to 0.88 at% and BET surface areas from 323-3012 m^2/g. The highest capacitance was observed for the samples with highest BET surface area and lowest N content. Nevertheless, pseudocapacitive effects were obtained in the samples with the highest nitrogen content, and despite much lower BET surface area, these samples still demonstrated capacitance reaching 172 F/g. Carbon spheres derived from polypyrrole nanospheres by carbonization showed poor capacitance despite their high nitrogen content (up to 14. 3 %), although the materials had surface areas below 100 m^2/g. The authors reported much improved capacitance once the carbon nanospheres were chemically activated using potassium hydroxide to obtain microporous carbon spheres with higher BET surface area (1080 m^2/g) and significantly lower nitrogen content (around 2.2 %)[84]. A similar trend was observed for templated porous carbon treated either with potassium hydroxide or carbon dioxide: after treatment, the nitrogen content decreased while porosity increased[327]. In general, the synthesis and treatment approaches that lead to high nitrogen content tend to favor low surface area, while procedures to enhance surface area tend to also decrease nitrogen content. It is clear that there is still significant need for further innovations in synthesis so that materials can be obtained with high nitrogen concentration while also achieving high porosity.

Wu et al. reported that graphene aerogels show enhanced pseudocapacitive contribution upon doping with either nitrogen or boron. Moreover, the authors reported that materials

***Table 1 (goes here):** Reports within the last 5 years on N-modified carbon supercapacitors.*

co-doped with nitrogen and boron demonstrate a synergistic effect[328]. Generally, carbon materials doped with nitrogen and boron show higher specific capacitance than their undoped counterparts. For example, Konno el al. reported specific capacitance for a B/C/N composite measured in sulfuric acid that exceeded 300 F/g[329]. Guo el al. reported specific capacitance values for boron and nitrogen co-doped porous carbons of up to 268 F/g in

potassium hydroxide electrolyte[315]. Comparable specific capacitance values were achieved for boron and nitrogen substituted carbons synthesized using a combination of polyborazine as the nitrogen/boron precursor and coal tar pitch as the graphitizing precursor. This method allowed for the simultaneous incorporation of N and B at high concentrations (10 and 14 at %, respectively) and it was suggested that boron aided the stabilization of nitrogen during the pyrolysis[330]. Increasing the pyrolysis temperature during the growth of boron and nitrogen-doped aligned nanotubes synthesized from melamine diborate enhanced the incorporation of both dopants. Promising electrochemical performance and pseudocapacitance has also been shown for glucose-derived microporous carbon co-doped with nitrogen and phosphorus using ammonium phosphate as a phosphorus and nitrogen precursor[331]. Table 1 compares some advances made in the supercapacitor field, using nitrogen doping, over the last 5 years.

4.5. Hydrogen Storage

High surface area carbon materials such as CNT's and graphene continue to see interest as physisorption materials for hydrogen storage applications. Surface properties of the support, such as surface area, nanostructure and composition are well known to have dramatic effects on the hydrogen storage properties of these materials. Altering the composition and nanostructure through targeted functionalization of the support [16] and design of the pores that promote two-wall interactions[332] have proven to be beneficial approaches to increase the hydrogen binding energy. Direct effects from functionalization, however, are debated, as it is hard to separate their influence from the effects of porosity/texture. The microporosity of the support is believed to be the major player, while functionalization is believed to play a more minor role.

Giraudet et al. created and compared the physical adsorption properties of two classes of nitrogen containing carbon materials. Mesoporous carbon was enriched with nitrogen though ammonia treatment, maintaining a surface area above 1300 m^2/g while enabling 1.2-3.9 wt% nitrogen doping levels. A variety of nitrogen functionalities were observed depending on the treatment temperature, yielding hydrogen uptake values from 0.18-0.24 wt% H_2, at 298 K and 4.5 MPa. For the second set of materials, the authors used a hard silica template to synthesize carbon nitrides with up to 20 wt% nitrogen content, consisting of pyridinic and pyrrolic functionalities with high pyridine to pyrrole ratios. This set of materials showed hydrogen uptake values of 0.03-0.05 wt%, at 298 K and 4.5 MPa. The authors concluded that physical characteristics, such as the specific surface area, determined the amount of adsorbed hydrogen, and that the nitrogen groups had no impact. However, the authors did report that nitrogen groups participate in the oxidation reaction during electrochemical adsorption of hydrogen. Later, Giraudet et al. reported on the improved hydrogen-storage properties of nitrogen-enriched mesoporous carbons doped with nickel nanoparticles. Electrosorption of hydrogen benefited from incorporation of nickel, but the combined effect of nitrogen and nickel was negative[114].

Jiang et al. have combined a doping and activation approach that changes the textural characteristics of the carbon[333] . First, the authors showed that pristine ordered mesoporous carbon nitride, despite having half the surface area of ordered mesoporous carbon CMK3, gave similar hydrogen storage performance. This result suggested that the nitrogen dopants may have somehow compensated for the difference in the specific surface area. Second, they demonstrated activated nitrogen-containing carbon spheres with a unique hollow structure that yielded a hydrogen uptake of 2.21 wt.% at 298K and 8 MPa.

The authors concluded that hydrogen physical adsorption is facilitated through the unique structure and texture of the material, while nitrogen activates the absorbent and increases defect site density and the binding strength of hydrogen to the carbon.

Activation of hydrogen near the nitrogen sites was also suggested by the work of Parambhath et al., who employed nitrogen plasma treatment to dope exfoliated graphene, leading to a 66% increase in the hydrogen uptake[44]. A further 272% increase in the hydrogen uptake was achieved by depositing Pd nanoparticles over the nitrogen-doped graphene, where uniform metal dispersion was facilitated by the modification of graphene with nitrogen heteroatoms (Figure 14). Moreover, the addition of nitrogen strengthened the binding between the Pd nanoparticles and the graphene support, preventing the detachment of Pd nanoparticles and thus facilitating continuous migration and diffusion of hydrogen to the adsorbate surface. Authors reported hydrogen uptake capacities of 1.97 and 4.4 wt% at 25°C using 2 and 4 MPa respectively. Later, the same group reported similar hydrogen uptake capacity (4.3 wt% at 25°C and 4 MPa hydrogen pressure) for Pd nanoparticle decorated nitrogen-doped graphene synthesized using a one-step green approach. The in-situ process uses solar radiation and combines the formation of graphene nanosheets, nitrogen doping, and the reduction of the Pd nanoparticles in one step[334]. The graphene materials reported in these two papers had similar concentrations of nitrogen, ~7 at% (Figure 14).

Nitrogen-doped carbon nanotubes (~1.5 at% nitrogen) with a bamboo-like structure and a specific surface area of 135 m^2/g, synthesized by the pyrolysis of melamine, showed hydrogen uptake of 0.17 wt% at 298 K and 19 bar [335]. Nitrogen-enriched graphitic carbon with a carbon-to-nitrogen ratio of 1:1.12 and a low BET surface area of ~10 m^2/g gave a hydrogen storage capacity of 0.34 wt% at 298 K under 100 bar. Jin et al compared pristine and heteroatom (boron, phosphorus or nitrogen) –substituted carbon scaffolds, reporting enhancement in reversible hydrogen physisorption capacity and hydrogen binding energy for all heteroatom-substituted materials [336].

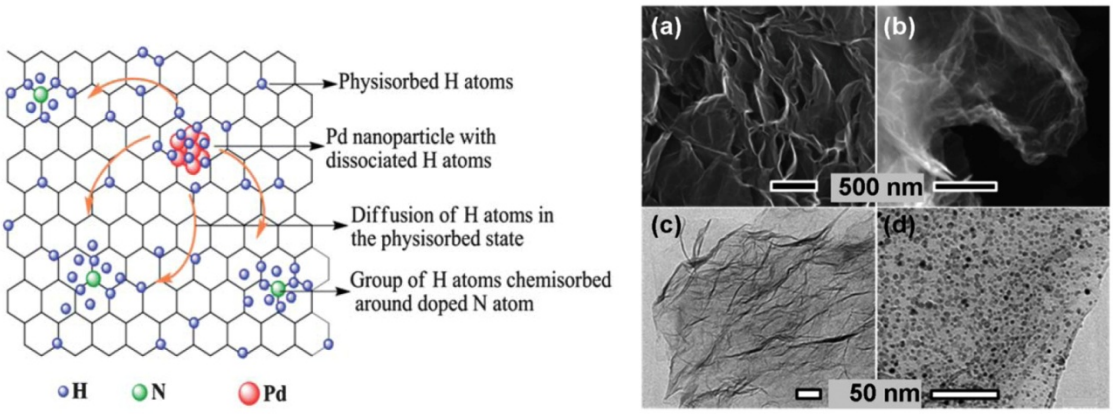

Figure 14: *(1) Hydrogen adsorption mechanism schematic on Pd/N-graphene Reprinted (adapted) with permission from Citation[145]. Copyright (2013) Royal Society of Chemistry. (2) Scanning electron micrographs of (a) N-HEG and (b) Pd-N-HEG depicting the folds in graphene layers. Transmission electron micrographs of (c) N-HEG and (d) Pd-N-HEG. A uniform dispersion of Pd NPs on N-HEG support is clearly visible. Reprinted (adapted) with permission from Citation [44]. Copyright (2012) American Chemical Society.*

Table 2 (goes here): *Research in the last 5 years on hydrogen storage*

Nitrogen dopants, along with vacancies and other dopants including P and B, can adjust the binding energy between the hydrogen and Pt atoms without inducing a negative effect on hydrogen storage capacity[148]. The binding energy between N and Pt is rather strong, and thus the binding energy of the second hydrogen increases such that release occurs only when the pressure is reduced to ambient conditions [148].This is contrary to sidewall vacancies where two hydrogen molecules can adsorb and desorb easily, and thus have the potential to improve hydrogen storage capacities at higher pressures. It is important to note that this study was limited to single defects and authors suggested that clustered defects should be further investigated. Liu et al. have explored the effect of substitutional nitrogen, ranging from 1 to three N atoms in the aromatic ring, on hydrogen adsorption in Li-decorated porous graphene. They observed a clear trend for multiple hydrogen adsorptions, where increasing the number of substitutional nitrogen atoms leads to stronger adsorption energies[337]. Comparing graphitic, pyridinic and pyrrolic nitrogen defects in the Li-decorated graphene system, Lee concluded that as compared to pristine and graphitic structures, pyridinic and pyrrolic structures are more stable, leading to better dispersions of Li atoms without clustering. The pyridinic and pyrrolic graphitic structures were also shown to adsorb and desorb up to a maximum of three H_2 molecules under ambient conditions [147]. A recent theoretical study of four-nitrogen divacancy defects in CNT's suggests that these defects may be more favorable than pyridine-like defects, as they have strong, agglomeration-preventing interactions with Ca atoms and meet the requirements for hydrogen adsorption energy[149]. A first-principles study conducted on graphitic carbon-nitride nanotubes (g-C_3N_4), assuming a heptazine-like structure, reported a configuration where hydrogen atoms chemisorbed to each alternate nitrogen atom. The authors predicted fast uptake rates due to easy access to the interior of the tube and a storage capacity close to 5.45 wt% H_2[146].

Ao et al. have proposed a novel approach to lower the energy barrier for the dissociative adsorption of hydrogen on graphene based on N-doping and the application of an electric field normal to the graphene surface[338]. Further study suggests that the electric field facilitates the dissociative adsorption and diffusion of hydrogen while removal of electric field can be used to release hydrogen[145]. N-doped graphene was also reported to be an effective additive to $NaAlH_4$ to assist with hydrogenation and dehydrogenation reactions. The research team demonstrated that the addition of N-doped CNT or N-doped graphene to $NaAlH_4$ promotes rehydrogenation as hydrogen molecules are more easily activated on the nitrogen sites [339]. In contrast, the addition of undoped carbon materials doesn't improve rehydrogenation, whose benefit is limited only to dehydrogenation[340–343]. Table 2 helps show the recent advances in hydrogen storage.

4.6. CO_2 Capture

Carbon-based materials considered for CO_2 capture must meet several requirements including large adsorption capacity, fast adsorption and desorption kinetics, high selectivity and facile regeneration. It has been previously established that adsorption of CO_2, which is acidic in nature, can be improved using nitrogen sites that are basic in nature[344]. Carbonaceous materials with amine groups were produced from biomass in a two-step process consisting of hydrothermal carbonization of glucose and modification with branched tetramine. These sorbent materials possessed high nitrogen content (5.27 and

10.75 wt%) but very low specific surface areas (less than 20 m^2/g) and authors suggested that these materials would benefit from further optimization of the channels and surface area[345]. Low cost soybean was used to synthesize carbon with a surface area 811 m^2/g, enriched with pyridinic and amide nitrogen groups[346].

Development of sorbent materials used for CO_2 capture, similar to those used for hydrogen storage, requires consideration of the interplay between textural characteristics and functional groups. Jones et al., in their recent review of sorbents for CO_2 capture, highlighted conflicting trends for the adsorption capacities of activated carbons treated with ammonia at higher temperatures, with one group reporting an increase in the CO_2 uptake and another group demonstrating a decrease[344]. The decrease in the hydrogen uptake was related to the blockage of pores. Results across the field suggest that if the surface area and pore structure are equivalent, N-doped materials provide better characteristics than undoped counterparts. However, it appears difficult to incorporate significant quantities of nitrogen and maintain high surface area and pore structure at the same time.

Hao et al. studied the effect of temperature for a series of nitrogen-doped porous carbon monoliths pyrolyzed at 400-800°C. Despite a low BET surface area of 42 m^2/g, the sample treated at 400°C showed a moderate CO_2 absorption capacity of 1.87 mmol/g. Samples synthesized at 500-800°C had an order magnitude higher BET, with the sample pyrolyzed at 500C demonstrating the highest CO_2 capacity of 3.13 mmol/g. In this group of samples, nitrogen content slightly decreased but surface area slightly increased, thereby leading to relatively similar CO_2 adsorption capacities [83].

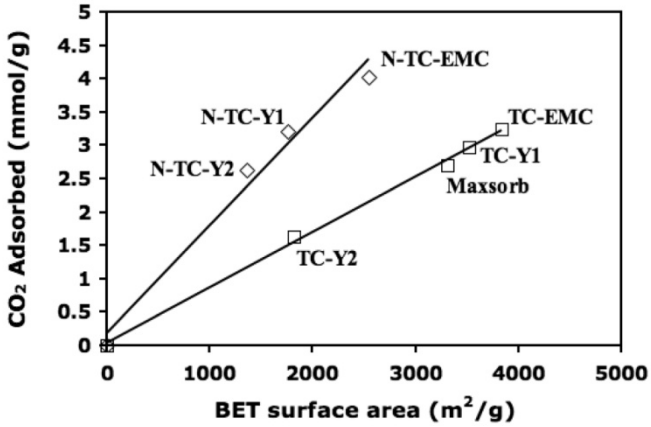

Figure 15. *Relationships between the CO_2 adsorption capacities (at 298 K and 1 atm) and BET surface area of nitrogen-doped carbons and undoped carbons. The N-doped carbons contain 6-7 wt % nitrogen. Reprinted (adapted) with permission from Citation [347]. Copyright (2011) American Chemical Society.*

Table 3 (goes here): *Recent progress on CO_2 capture*

Hierarchically structured porous N-doped carbon structures synthesized with deep eutectic solvents have allowed for the incorporation of relatively high nitrogen concentrations despite relatively high synthesis temperatures. For example, N content of 8-12 at% and 5 at% were reported for 600°C and 800°C synthesis temperatures, respectively. The best CO_2

uptake was obtained for the sample treated at 800°C (3.29 mmol/g at 25 C and 1 atm). Lower uptake for the sample treated at 600°C was attributed to lower micropore surface area. Authors estimated the isosteric heat values, which decreased with the amount of adsorbed CO_2, and concluded that the materials exhibited two coexisting mechanisms for CO_2 absorption: one occurring on nitrogen sites and the other on undoped carbon sites.

Sevilla et al. have reported CO_2 adsorption uptake of 3.9 mmol $CO_2 \cdot g^{-1}$ (at 25°C and 1 atm) in a microporous carbon derived from polypyrrole and activated using KOH agent. The carbon exhibited narrow microporosity and a high concentration of nitrogen groups (~10 wt%)[348]. In addition to a high CO_2 adsorption rate, the authors highlighted the excellent selectivity and regeneration properties of their material. Good selectivity, stability and CO_2 capacities were similarly reported for nanostructured templated carbons synthesized using acetonitrile and post treated with ammonia [348]. These materials exhibited a range of BET surface areas (1361-3840 m^2/g) and possessed slightly lower N content (~6-7 wt %) than those reported by Sevilla. The authors observed a linear relationship for CO_2 adsorption capacity vs. BET surface area within a series of undoped carbons. A linear trend was also observed for the series of N-doped carbons, but an increased slope indicated an approximate doubling in capacity for a given surface area (Figure 15) [347]. Despite dramatic differences in surface area between the N-doped (1762 m^2/g) and undoped (3840 m^2/g) samples, they both showed similar CO_2 capacities (3.2 mmol/g at 298 K and 1 atm), demonstrating 2.2 improvement related to N-doping. Moreover, optimization of the synthesis procedure allowed for the N-doped, microporous carbons to attain a BET value of 2559 m^2/g with a 4.0 mmol/g CO_2 uptake[347]. This work provides a clear demonstration that both surface area and N-doping are important factors leading to increased CO_2 capacities. The interplay between these parameters was thoroughly investigated for ordered mesoporous carbons doped with nitrogen using ammonia treatment at 650-100°C. Samples treated with ammonia at 650 and 800 ^oC produced relatively lower porosity, but higher capacities per pore. Meanwhile, the sample treated with ammonia at 1000 °C had the highest BET surface area, but the lowest capacity per pore. These results indicate that surface nitrogen functionalities produced at lower temperatures improve CO_2 adsorption, while those produced at high temperature reduce CO_2 adsorption. The authors also established that higher microporosity was beneficial, whereas mesoporosity didn't matter as much[347].

Recently, Wang et al. have studied nitrogen-doped microporous carbons derived from porous polyimine. Their first report examined nitrogen-doped materials produced by calcination at 600-800 °C under argon gas flow. The reported materials had surface areas in the range 263-366 m^2/g and nitrogen content ranging from 8.74-5.58 wt%. Interestingly, materials prepared at 800°C had the lowest surface area and the lowest nitrogen content among the calcined samples, but demonstrated the highest CO_2 capacity of 1.955 mmol/g[349]. Their second report examined nitrogen-doped materials also fabricated from polyimine, but chemically activated in KOH at temperatures from 600-750°C[350]. Nitrogen content ranged from 5.05-1.52 wt%, which was lower than the nitrogen content of the calcined materials, but surface areas were significantly improved and reached 1033-3195 m^2/g. In this case, the materials prepared at 600 and 650 C showed better performance than the materials prepared at 700 and 750 C, mainly due to their single narrower pore size and higher nitrogen content, although they had lower surface area. The highest CO_2 capacity so far reported for a N-doped porous carbon material (4.3 mmol/g at 1 atm and 298 K) was obtained via a facile one-pot evaporation induced self-assembly process, where HNO_3 was used as a nitrogen source and catalyst, promoting polymerization. The resulting material

had 4.32 wt.% nitrogen and a surface area of 1979 m^2/g[90]. Table 3 compares recent publications and their figures of merit for CO_2 capture.

4.7. Other Applications

As the field of nitrogen-modified carbon structures continues to grow, it use has expanded to a wide range of other applications. Below we provide a brief discussion on some of these less researched topics.

4.7.1. Chemical Production (H_2O_2, butyronitile, oxidized-cyclohexane)

As of 2007, the annual world production of hydrogen peroxide was about 2.5 million tons, making hydrogen peroxide number 47 on a list of the 100 most important chemicals in the world[351]. The need for efficient and inexpensive H_2O_2 production is therefore essential; however, direct reactions via H and O are dangerous. To mitigate these risks, attention has been drawn to the idea of reaction separation using an electrochemical flow reactor. With significant current research in improving ORR reaction kinetics, mechanistic analysis of the electrochemical reduction of oxygen on nitrogen modified carbon structures has led to a better understanding of electron reaction pathways. As was previously discussed in the ORR section of this review, the reduction of oxygen with hydrogen does not always proceed through the direct transfer of 4 electrons. Instead, 2 electron or combined electron pathways are typical, which lead to the formation of H_2O_2 instead of H_2O[352].

Fellinger et al. used N-doped mesoporous carbons derived from an ionic liquid to explore the effects of electrocatalytic hydrogen peroxide production. The high-resolution N1s XPS spectra showed high levels of pyridinic and quaternary nitrogen species in addition too pyrrolic and nitrogen-oxide functionalities (see Figure 1). A Koutecky-Levich plot derived from polarization curves obtained at various rotation rates during electrochemical testing clearly revealed a two-electron process[94]. Quantum calculations by Sidik et al. further validated these results, indicating that carbon radical sites formed adjacent to substitutional nitrogen dopants are essential for the reduction of O_2 to hydrogen peroxide in an acid electrolyte[353]. The authors also hypothesized that pyrrolic nitrogen might be a contributing factor in the two-electron nature of the samples; however, the true dependence of the structure on the reactivity remains unclear and further investigations are needed. Photometric determination of a flow reactor using N-doped carbon as the catalyst was able to produce H_2O_2 at .241 Wh/g, corresponding to >65% efficiency. The true utility of this approach lies in its flexibility, relatively low cost, and the ability to synthesize H_2O_2 "on-demand" in specific locations without the need for transport and storage[353].

For similar reasons, the hydrogenation of nitrilic-based species bear industrial interest because the commercial production of amines has a wide range of industrial applications including the fabrication of fungicides, chelating agents, surfactants and fine chemicals. Using nickel supported on nitrogen-doped carbon nanospheres Nieto-Marquez et al. investigated the hydrogenation of butyronitrile [354]. They hypothesized that nitrogen doping strongly affects the electronic properties of the nickel support, facilitating hydrogenation and enhanced metal sintering through electron surface enrichment.

Within the last year, Cao et al. have explored the aerobic oxidation of cyclohexane (CyH) through a myriad of functionalizations (N,P,B)[51]. Using CVD of aniline-NH_3, N-CNT's were fabricated with ~4 at% N, mostly in the form of pyridinic and substitutional nitrogen defects. N-modified structures had the best mass normalized activity for the oxidation of cyclohexane in the liquid phase with molecular oxygen as the oxidant. Electron transfer

between graphene sheets and the reactive radicals was determined to play an important role in the oxidation. The current industrial process for the oxidation of CyH is only about 4% efficient and uses unrecyclable catalysts[355]. Creating an improved and reusable method for this oxidation process would be extremely important for the modern chemical industry, because oxidized CyH is used in the synthesis of adipic acid and caprolactam, which are then used to create various nylon polymers.

Taken together, these recent studies on peroxide, butyronitile, and oxidized-cyclohexane synthesis using nitrogen-functionalized carbon catalysts suggests that the nitrogen modification approach can play an important role in improving the catalytic processes needed to form a variety of important chemicals.

4.7.2. Photocatalysis

Due to environmental concerns arising from global energy demands, problems such as pollution and fossil fuel depletion have inspired the search for ways to convert waste and pollutants into environmentally friendly by-products. To this end, Photocatalysis is touted as a future 'green technology' for the degradation of pollutants, purification of various chemicals (including water), as well as water splitting to form hydrogen. It has been reported that nanoparticles, such as Pt, Au, Ag, ZnO, CdS, TiO_2, CeO_2, and MnO_2, incorporated with structured carbon supports can demonstrate enhanced activity for various catalytic applications including fuel cells, capacitors, photocatalytic degradation, and photovoltaic devices. However, only a few studies have examined the photocatalytic properties of such catalysts (particularly the semiconducting catalysts) on N-doped modified carbon nanocomposites [356,357].

Support systems like N-modified graphene can significantly promote charge transfer from semiconductor nanoparticles (like CdS or ZnSe) due to an electron density shift caused by a change in sp^2 to sp^3 bonding configuration[358,359]. This shift can also accelerate the transfer of electrons between the reactants and the electrode, thereby creating a possible intermediate pathway for chemical transformations during the reaction.

Recently, Min et al. reported on the photoactivity of carbon-supported TiO_2 catalysts, demonstrating a significant increase in activity through the use of nitrogen modified graphene supports[360]. XPS results show that hydrothermal treatment in urea produced an N-graphene structure mostly consisting of sp^2 bound graphitic nitrogen. To explore the photocatalytic properties, the degradation of benzoic acid (BA) was studied. Adding N-graphene to the TiO_2 catalyst assists the charge separation and surface affinity. It was suggested that N-graphene/ $TiO_{2-x}N_x$ exhibits improved degradation for BA because the nitrogen-doped graphene facilitates stronger interactions between the organic molecules and the carbon structure through enhanced π-π interactions, leading to longer electron lifetimes. It was shown that the graphene content must be differently optimized depending on the surface chemistry of the organic being degraded (i.e., BA vs. Methyl Orange). Impedance measurements also showed enhanced conductivity for the graphene supports modified with nitrogen, especially under solar irradiation, which can be an additional factor for the improved performance.

Jia et al. studied the photocatalytic activity of hydrogen evolution on N-graphene/CdS nanocomposites[358]. Their results clearly showed that the hydrogen evolution rate from the CdS catalyst was significantly enhanced by incorporating N-doped graphene. Adding 2 wt% of N-graphene resulted in the most significant increase in H_2 production rate, exceeding that of pure CdS by more than 5 times and generating 210 umol/h (0.2g of catalyst). The

enhancement in H_2 evolution activity was attributed to the electrical conductivity of the N-graphene. The authors suggested that the larger work function of N-graphene vs. the conduction band minimum of CdS created a thermodynamic driving force for charge transfer, thereby reducing the recombination of photogenerated electron-hole pairs.

Interestingly, a metal-free graphitic carbon nitride (g-C_3N_4) polymeric photocatalyst has also been tested for hydrogen and oxygen production. Results showed good photocatalytic performance due to a 2.7 eV bandgap straddling the electrolytic oxidation (O_2/H_2O) and reduction (H^+/H_2) potentials[361]. By combining g-C_3N_4 with graphene sheets to improve conductivity and charge carrier separation, catalytic performance was increased, resulting in a 3X increase in the H_2 evolution rate. These studies show that C-N structures can be used to create semiconducting materials with beneficial properties for energy applications and/or to enhance other semiconductors by reducing charge recombination. These materials are therefore interesting for potential direct application in photocatalysis.

4.7.3. Biosensing

Biosensors have become an important component of both scientific and commercial interest. For a typical application, a material is designed to facilitate the identification of a specific target molecule and assist in a direct electron transfer process needed to access the redox active sites. Recently, researchers have focused on nitrogen-modified carbon materials for glucose sensors, where the oxidation of glucose produces hydrogen peroxide, which is then detected by the electrode (See ORR application above).

In 2005, it was shown that electrocatalytic C-N architectures have beneficial effects on the immobilization of glucose oxidase (GO_x), leading to novel "third-generation" designs for glucose sensing[362]. More recently, a novel glucose biosensor was prepared by the immobilization of GOx on a nitrogen-doped carbon nanotube electrode[363]. The results showed that nitrogen doping accelerated the electron transfer process, leading to the direct electrochemical reaction of GOx and its cofactor (flavin adenine dinucleotide = FAD) through a two-electron redox process:

$$GO_x\ (FAD) + 2e^- + 2H^+ \rightarrow GO_x\ (FAD\text{-}H_2)$$

$$GO_x\ (FADH_2) + O_2 \rightarrow GO_x\ (FAD) + H_2O_2$$

This approach yielded sensitive amperometric biosensing for glucose levels ranging from 0.02 to 1.02mM with a detection limit of 0.01mM (signal to noise ratio of 3), demonstrating high affinity and excellent selectivity. In a similar approach, Xu et al. designed N-CNT-based electrochemical biosensors and obtained good analytical results with an even more sensitive detection limit, but a smaller linear detection range (from 2-140 μM) [50].

Wang et al. fabricated an analogous glucose sensor using N-graphene rather than N-CNTs[39]. Their results showed that the GOx redox peak current was greatly improved on N-doped graphene compared to pristine graphene, which was attributed to the enhanced electron transfer efficiency attained by nitrogen doping. Their biosensor shows glucose detection at concentrations ranging from 0.01 to 0.5 mM in the presence of other molecules. This was also confirmed by a study on nitrogen-doped pyrolytic carbon films using cyclic voltammetry with a ferri/ferro-cyanide redox probe[364]. Results showed significantly enhanced electron transfer kinetics for the nitrogen-doped pyrolytic carbon films as compared with unmodified carbon films. EIS measurements confirmed that the N-PyC films yielded lower resistance to charge transfer.

Recently, Goran et al. demonstrated CVD-fabricated N-CNT's containing 7.4at% N that displayed a detection limit of 24 μM with a linear range of 6.5 mM. It was suggested that the N-CNT's outperformed unmodified CNT's due to a more positive ORR onset potential[365]. There have been several studies exploring similar effects for nitrogen modified carbons applied to other biosensing applications including ascorbic acid[366], dopamine[366], uric acid[366], proteins[367], and thioridazine[368]. Collectively, the results strongly indicate that N-modified carbons show great promise for the construction of highly selective and efficient, third-generation enzyme biosensors that possess less cytotoxicity and better biophilicity[369].

5. Outlook and Conclusions

In this work we have discussed a wide breadth of recent findings in nitrogen modified carbon architectures, ranging from materials synthesis to theory to applications. The review of current literature indicates that nitrogen doping is beneficial in many areas, as it allows for the tailoring and tuning of carbon materials for various applications of interest.

Recent cost-effective and creative strategies for the synthesis of a variety of N-doped carbon materials have yielded promising results; continued research in this field is focused on creating inexpensive, high surface area materials with high N contents. In general, synthesis/treatment approaches that lead to high nitrogen content tend to favor low surface areas, while procedures that enhance surface area tend to decrease nitrogen content. Unfortunately, for many applications, including hydrogen storage, CO adsorption, and supercapacitors, both high nitrogen content and high surface area are essential for improved performance. This fact makes it clear that there is a significant need for further innovations in synthesis of materials that contain high nitrogen concentration in addition to high surface area and developed porosity.

Among the potential N-doped materials systems, N-doped graphene possesses particularly intriguing intrinsic properties. The future utility of this material will greatly depend on the ability to design new fabrication methods, specifically those that create well-dispersed 1 to 2 graphene layer materials rather than multi-layer clumps. Templated carbon structures also show promise, as they combine the benefits of functionalization and nanoconfinement. Novel concepts and strategies toward synthesis of N-doped materials will create a positive ripple effect through out the community as they can be directed to a variety of important applications.

The application of carbon nitride like films onto high surface area materials is an interesting area of increasing interest. Creative strategies and applications of such "core-shell" materials will likely become a more widely studied area of research. These types of materials have already show excelent performance and durability in areas such as supercapacitors, hydrogen adsorption, and photocatalytic applications and we expect it see their utility continue to increase.

For many applications, nitrogen functionalized carbon materials are interesting because the nitrogen sites improve performance by influencing important properties such as catalytic activity, sorption, conductivity, and the general interactions between components. Of the three most dominant nitrogen functionalities (graphitic, pyridinic and pyrrolic), pyridinic and graphitic nitrogen are the most frequently reported as beneficial. While nitrogen has been proven to be an import player in many applications, the observed beneficial effects vary depending on the type of N-doped materials. Furthermore, studies of N-doped carbon

materials for certain applications have sometimes shown contradictory results. Therefore, continued progress in mechanistic understanding is necessary.

Possibly the most beneficial property of nitrogen, as it has been demonstrated across a wide range of applications, is its ability to stabilize catalytically active metal sites. Additionally, when used as a catalyst support, a general increase in nitrogen content leads to improvement in nucleation, dispersion and stability of metal nanoparticles. For example, it has been well documented both theoretically and experimentally that clustered nitrogen defects have a greater stabilizing effect than single N defects. In addition, it has been demonstrated that stabilization can be achieved by the incorporation of nitrogen either beneath or around nanoparticles. DFT studies have also provided insight into the effect nitrogen has on various systems. These results provide mechanistic explanations for the modified electronic properties, catalytic activity, reaction mechanisms and improved stability observed in N-doped carbon materials when used as catalytic supports. Further investigations combining theoretical and experimental work are critically needed to add further depth to our understanding of N-doped systems and the functionalities most important for specific applications.

By combining the insights derived from disparate applications, we hope that the data reviewed herein will assist future studies and inspire new uses for N-modified carbon materials. The research reviewed in this article illustrates the great interest associated with nitrogen-modified carbons for applications in sustainability, energy storage, energy production, and catalysis. While great strides have been made in the last 5 years, future progress is essential to ensure cost effective, sustainable materials that can outperform current, commercially available technology. The next five years are therefore sure to be even more exciting!

Acknowledgements

This work was supported by the Army Research Office under grant #W911NF-09-1-0528

References:

1. K. Kinoshita, *Carbon: electrochemical and physicochemical properties*, John Wiley Sons,New York, NY, 1AD.
2. S. Maldonado, S. Morin, and K. J. Stevenson, *Carbon N. Y.*, 2006, **44**, 1429–1437.
3. D. Jana, C.-L. Sun, L.-C. Chen, and K.-H. Chen, *Prog. Mater. Sci.*, 2013, **58**, 565–635.
4. S. Maldonado and K. J. Stevenson, *J. Phys. Chem. B*, 2005, **109**, 4707–16.
5. P. Ayala, R. Arenal, M. Rümmeli, a. Rubio, and T. Pichler, *Carbon N. Y.*, 2010, **48**, 575–586.
6. M. Cohen, *Phys. Rev. B*, 1985, **32**.
7. D. Teter and R. Hemley, *Science (80-.).*, 1996, **271**, 1–3.
8. a Y. Liu and M. L. Cohen, *Science*, 1989, **245**, 841–2.
9. K. S. Novoselov, a K. Geim, S. V Morozov, D. Jiang, Y. Zhang, S. V Dubonos, I. V Grigorieva, and a a Firsov, *Science*, 2004, **306**, 666–9.
10. H. Wang, T. Maiyalagan, and X. Wang, *ACS Catal.*, 2012, **2**, 781–794.
11. D. Wei, Y. Liu, Y. Wang, H. Zhang, L. Huang, and G. Yu, *Nano Lett.*, 2009, **9**, 1752–8.
12. D. Chen, L. Tang, and J. Li, *Chem. Soc. Rev.*, 2010, **39**, 3157–80.
13. S.-K. Lee, J.-H. Kim, M.-G. Jeong, M.-J. Song, and D.-S. Lim, *Nanotechnology*, 2010, **21**, 505302.
14. A. Lherbier, X. Blase, Y.-M. Niquet, F. Triozon, and S. Roche, *Phys. Rev. Lett.*, 2008, **101**, 036808.
15. Z. Luo, S. Lim, Z. Tian, J. Shang, L. Lai, B. MacDonald, C. Fu, Z. Shen, T. Yu, and J. Lin, *J. Mater. Chem.*, 2011, **21**, 8038.

16. L. Qu, Y. Liu, J.-B. Baek, and L. Dai, *ACS Nano*, 2010, **4**, 1321–6.
17. A. Leela, M. Reddy, A. Srivastava, S. R. Gowda, H. Gullapalli, M. Dubey, and P. M. Ajayan, 2010, **4**, 6337–6342.
18. Z. Jin, J. Yao, C. Kittrell, and J. M. Tour, 2011, 4112–4117.
19. Y.-F. Lu, S.-T. Lo, J.-C. Lin, W. Zhang, J.-Y. Lu, F.-H. Liu, C.-M. Tseng, Y.-H. Lee, C.-T. Liang, and L.-J. Li, *ACS Nano*, 2013, **7**, 6522–32.
20. X. Wang, X. Cao, L. Bourgeois, H. Guan, S. Chen, Y. Zhong, D.-M. Tang, H. Li, T. Zhai, L. Li, Y. Bando, and D. Golberg, *Adv. Funct. Mater.*, 2012, **22**, 2682–2690.
21. B. Xiong, Y. Zhou, Y. Zhao, J. Wang, X. Chen, R. O'Hayre, and Z. Shao, *Carbon N. Y.*, 2013, **52**, 181–192.
22. C. H. Choi, S. H. Park, M. W. Chung, and S. I. Woo, *Carbon N. Y.*, 2013, **55**, 98–107.
23. D. Deng, X. Pan, L. Yu, Y. Cui, Y. Jiang, J. Qi, W. Li, Q. Fu, X. Ma, Q. Xue, G. Sun, and X. Bao, 2011, 1188–1193.
24. L. S. Panchakarla, K. S. Subrahmanyam, S. K. Saha, A. Govindaraj, H. R. Krishnamurthy, U. V. Waghmare, and C. N. R. Rao, *Adv. Mater.*, 2009, **560012**, NA–NA.
25. L. S. Panchakarla, a. Govindaraj, and C. N. R. Rao, *Inorganica Chim. Acta*, 2010, **363**, 4163–4174.
26. B. P. Vinayan and S. Ramaprabhu, *J. Mater. Chem. A*, 2013, **1**, 3865.
27. X. Wang, X. Li, L. Zhang, Y. Yoon, P. K. Weber, H. Wang, J. Guo, and H. Dai, *Science*, 2009, **324**, 768–71.
28. B. Guo, Q. Liu, E. Chen, H. Zhu, L. Fang, and J. R. Gong, *Nano Lett.*, 2010, 4975–4980.
29. D. Geng, Y. Chen, Y. Chen, Y. Li, R. Li, X. Sun, S. Ye, and S. Knights, *Energy Environ. Sci.*, 2011, **4**, 760.
30. Y. Li, J. Wang, X. Li, D. Geng, M. N. Banis, R. Li, and X. Sun, *Electrochem. commun.*, 2012, **18**, 12–15.
31. X. Li, H. Wang, J. T. Robinson, H. Sanchez, G. Diankov, and H. Dai, *J. Am. Chem. Soc.*, 2009, **131**, 15939–44.
32. L.-S. Zhang, X.-Q. Liang, W.-G. Song, and Z.-Y. Wu, *Phys. Chem. Chem. Phys.*, 2010, **12**, 12055–9.
33. Y. Zhao, Y. Zhou, B. Xiong, J. Wang, X. Chen, R. O'Hayre, and Z. Shao, *J. Solid State Electrochem.*, 2012, **17**, 1089–1098.
34. Z. Sheng, L. Shao, J. Chen, and W. Bao, *ACS …*, 2011, 4350–4358.
35. G. Yang, Y. Li, R. K. Rana, and J.-J. Zhu, *J. Mater. Chem. A*, 2013, **1**, 1754.
36. D. Long, W. Li, L. Ling, J. Miyawaki, I. Mochida, and S.-H. Yoon, *Langmuir*, 2010, **26**, 16096–102.
37. D.-W. Wang, I. R. Gentle, and G. Q. (Max) Lu, *Electrochem. commun.*, 2010, **12**, 1423–1427.
38. R. Imran Jafri, N. Rajalakshmi, and S. Ramaprabhu, *J. Mater. Chem.*, 2010, **20**, 7114.
39. Y. Wang, Y. Shao, D. Matson, J. Li, and Y. Lin, *ACS Nano*, 2010, **4**.
40. Y. Shao, S. Zhang, M. H. Engelhard, G. Li, G. Shao, Y. Wang, J. Liu, I. a. Aksay, and Y. Lin, *J. Mater. Chem.*, 2010, **20**, 7491.
41. H. M. Jeong, J. W. Lee, W. H. Shin, Y. J. Choi, H. J. Shin, J. K. Kang, and J. W. Choi, *Nano Lett.*, 2011, **11**, 2472–7.
42. Y.-C. Lin, C.-Y. Lin, and P.-W. Chiu, *Appl. Phys. Lett.*, 2010, **96**, 133110.
43. S. H. Rhim, Y. Qi, Y. Liu, M. Weinert, and L. Li, *Appl. Phys. Lett.*, 2012, **100**, 233119.
44. V. B. Parambhath, R. Nagar, and S. Ramaprabhu, *Langmuir*, 2012, **28**, 7826–33.
45. S. Pylypenko, K. Wood, and A. Serov, 10000.
46. U. Bangert, a. Bleloch, M. Gass, a. Seepujak, and J. van den Berg, *Phys. Rev. B*, 2010, **81**, 1–11.
47. R. Sen, B. C. Satishkumar, a. Govindaraj, K. R. Harikumar, M. K. Renganathan, and C. N. R. Rao, *J. Mater. Chem.*, 1997, **7**, 2335–2337.
48. L. C. Chen, C. Y. Wen, C. H. Liang, W. K. Hong, K. J. Chen, H. C. Cheng, C. S. Shen, C. T. Wu, and K. H. Chen, *Adv. Funct. Mater.*, 2002, **12**, 687–692.
49. T. Thomas, R. J. Mascarenhas, B. E. K. Swamy, P. Martis, Z. Mekhalif, and B. S. Sherigara, *Colloids Surf. B. Biointerfaces*, 2013, **110**, 458–65.
50. X. Xu, S. Jiang, Z. Hu, and S. Liu, *ACS Nano*, 2010, **4**, 4292–8.
51. Y. Cao, H. Yu, J. Tan, F. Peng, H. Wang, J. Li, W. Zheng, and N.-B. Wong, *Carbon N. Y.*, 2013, **57**, 433–442.

52. J. D. Wiggins-Camacho and K. J. Stevenson, *J. Phys. Chem. C*, 2011, **115**, 20002–20010.
53. J. D. Wiggins-Camacho and K. J. Stevenson, *J. Phys. Chem. C*, 2009, **113**, 19082–19090.
54. Z. Wang, R. Jia, J. Zheng, J. Zhao, L. Li, J. Song, and Z. Zhu, *ACS Nano*, 2011, **5**, 1677–84.
55. K. Ghosh, M. Kumar, T. Maruyama, and Y. Ando, *Carbon N. Y.*, 2010, **48**, 191–200.
56. W.-C. Fang, *Nanoscale Res. Lett.*, 2009, **5**, 68–73.
57. H. Liu, Y. Zhang, R. Li, X. Sun, S. Désilets, H. Abou-Rachid, M. Jaidann, and L.-S. Lussier, *Carbon N. Y.*, 2010, **48**, 1498–1507.
58. S. Kundu, W. Xia, W. Busser, M. Becker, D. A. Schmidt, M. Havenith, and M. Muhler, *Phys. Chem. Chem. Phys.*, 2010, **12**, 4351–9.
59. T. C. Nagaiah, S. Kundu, M. Bron, M. Muhler, and W. Schuhmann, *Electrochem. commun.*, 2010, **12**, 338–341.
60. V. G. Ramu, A. Bordoloi, T. C. Nagaiah, W. Schuhmann, M. Muhler, and C. Cabrele, *Appl. Catal. A Gen.*, 2012, **431-432**, 88–94.
61. K. Gong, F. Du, Z. Xia, M. Durstock, and L. Dai, *Science (80-.).*, 2009, **323**.
62. X. Tuaev, J. P. Paraknowitsch, R. Illgen, A. Thomas, and P. Strasser, *Phys. Chem. Chem. Phys.*, 2012, **14**, 6444–7.
63. C.-H. Hsu and P.-L. Kuo, *J. Power Sources*, 2012, **198**, 83–89.
64. G. Xu, B. Ding, P. Nie, L. Shen, J. Wang, and X. Zhang, *Chemistry*, 2013, **19**, 12306–12.
65. M. I. Ionescu, Y. Zhang, R. Li, H. Abou-Rachid, and X. Sun, *Appl. Surf. Sci.*, 2012, **258**, 4563–4568.
66. J. Liu, Y. Zhang, M. I. Ionescu, R. Li, and X. Sun, *Appl. Surf. Sci.*, 2011, **257**, 7837–7844.
67. A. Morozan, P. Jégou, M. Pinault, S. Campidelli, B. Jousselme, and S. Palacin, *ChemSusChem*, 2012, **5**, 647–51.
68. Y. Chen, J. Wang, H. Liu, R. Li, X. Sun, S. Ye, and S. Knights, *Electrochem. commun.*, 2009, **11**, 2071–2076.
69. B. An, S. Xu, L. Li, J. Tao, F. Huang, and X. Geng, *J. Mater. Chem. A*, 2013, **1**, 7222.
70. E. J. Biddinger, D. Deak, and U. S. Ozkan, *Top. Catal.*, 2009, **52**, 1566–1574.
71. G. Wu, K. L. More, C. M. Johnston, and P. Zelenay, *Science*, 2011, **332**, 443–7.
72. M. Lefèvre, E. Proietti, F. Jaouen, and J.-P. Dodelet, *Science*, 2009, **324**, 71–4.
73. M. G. Plaza, C. Pevida, B. Arias, J. Fermoso, M. D. Casal, C. F. Martín, F. Rubiera, and J. J. Pis, *Fuel*, 2009, **88**, 2442–2447.
74. M. G. Plaza, C. Pevida, B. Arias, J. Fermoso, F. Rubiera, and J. J. Pis, *Energy Procedia*, 2009, **1**, 1107–1113.
75. S. Pylypenko, A. Borisevich, K. L. More, A. R. Corpuz, T. Holme, A. a. Dameron, T. S. Olson, H. N. Dinh, T. Gennett, and R. O'Hayre, *Energy Environ. Sci.*, 2013.
76. A. R. Corpuz, K. N. Wood, S. Pylypenko, A. a. Dameron, P. Joghee, T. S. Olson, G. Bender, H. N. Dinh, T. Gennett, R. M. Richards, and R. O'Hayre, *J. Power Sources*, 2014, **248**, 296–306.
77. T.-Y. Ma, L. Liu, and Z.-Y. Yuan, *Chem. Soc. Rev.*, 2013, **42**, 3977.
78. M. S. Shafeeyan, W. M. A. W. Daud, A. Houshmand, and A. Shamiri, *J. Anal. Appl. Pyrolysis*, 2010, **89**, 143–151.
79. W. Shen and W. Fan, *J. Mater. Chem. A*, 2013, **1**, 999.
80. D. Hulicova-Jurcakova, M. Kodama, S. Shiraishi, H. Hatori, Z. H. Zhu, and G. Q. Lu, *Adv. Funct. Mater.*, 2009, **19**, 1800–1809.
81. J. P. Paraknowitsch, A. Thomas, and M. Antonietti, *J. Mater. Chem.*, 2010, **20**, 6746.
82. S. Giraudet, Z. Zhu, X. Yao, and G. Lu, *J. Phys. Chem. C*, 2010, **114**, 8639–8645.
83. G.-P. Hao, W.-C. Li, D. Qian, and A.-H. Lu, *Adv. Mater.*, 2010, **22**, 853–7.
84. F. Su, C. K. Poh, J. S. Chen, G. Xu, D. Wang, Q. Li, J. Lin, and X. W. Lou, *Energy Environ. Sci.*, 2011, **4**, 717.
85. L. L. Zhang and X. S. Zhao, *Chem. Soc. Rev.*, 2009, **38**, 2520–31.
86. C. Jin, T. C. Nagaiah, W. Xia, B. Spliethoff, S. Wang, M. Bron, W. Schuhmann, and M. Muhler, *Nanoscale*, 2010, **2**, 981–7.
87. A. K. Mishra and S. Ramaprabhu, *J. Mater. Chem.*, 2012, **22**, 3708.
88. R. Silva, D. Voiry, M. Chhowalla, and T. Asefa, *J. Am. Chem. Soc.*, 2013, **135**, 7823–6.
89. Z. Rozlívková, M. Trchová, M. Exnerová, and J. Stejskal, *Synth. Met.*, 2011, **161**, 1122–1129.
90. X. Ma, M. Cao, and C. Hu, *J. Mater. Chem. A*, 2013, **1**, 913.

91. W. Yang, T.-P. Fellinger, and M. Antonietti, *J. Am. Chem. Soc.*, 2011, **133**, 206–9.
92. J. S. Lee, X. Wang, H. Luo, G. a Baker, and S. Dai, *J. Am. Chem. Soc.*, 2009, **131**, 4596–7.
93. B. Qiu, C. Pan, W. Qian, Y. Peng, L. Qiu, and F. Yan, *J. Mater. Chem. A*, 2013, **1**, 6373.
94. T.-P. Fellinger, F. Hasché, P. Strasser, and M. Antonietti, *J. Am. Chem. Soc.*, 2012, **134**, 4072–5.
95. B. Xu, D. Zheng, M. Jia, G. Cao, and Y. Yang, *Electrochim. Acta*, 2013, **98**, 176–182.
96. X. Wang and S. Dai, *Angew. Chem. Int. Ed. Engl.*, 2010, **49**, 6664–8.
97. C. Pan, L. Qiu, Y. Peng, and F. Yan, *J. Mater. Chem.*, 2012, **22**, 13578.
98. X. Duan, D. Li, H. Zhang, J. Ma, and W. Zheng, *Chemistry*, 2013, **19**, 7231–42.
99. D.-C. Guo, J. Mi, G.-P. Hao, W. Dong, G. Xiong, W.-C. Li, and A.-H. Lu, *Energy Environ. Sci.*, 2013, **6**, 652.
100. N. Fechler, T.-P. Fellinger, and M. Antonietti, *Adv. Mater.*, 2013, **25**, 75–9.
101. T.-P. Fellinger, D. S. Su, M. Engenhorst, D. Gautam, R. Schlögl, and M. Antonietti, *J. Mater. Chem.*, 2012, **22**, 23996.
102. L. Qie, W.-M. Chen, Z.-H. Wang, Q.-G. Shao, X. Li, L.-X. Yuan, X.-L. Hu, W.-X. Zhang, and Y.-H. Huang, *Adv. Mater.*, 2012, **24**, 2047–50.
103. L. Zhao, N. Baccile, S. Gross, Y. Zhang, W. Wei, Y. Sun, M. Antonietti, and M.-M. Titirici, *Carbon N. Y.*, 2010, **48**, 3778–3787.
104. A. Thomas, F. Goettmann, and M. Antonietti, *Chem. Mater.*, 2008, **20**, 738–755.
105. M.-M. Titirici, A. Thomas, and M. Antonietti, *J. Mater. Chem.*, 2007, **17**, 3412.
106. R. J. White, M. Antonietti, and M.-M. Titirici, *J. Mater. Chem.*, 2009, **19**, 8645.
107. L. Zhao, R. Crombez, F. P. Caballero, M. Antonietti, J. Texter, and M.-M. Titirici, *Polymer (Guildf).*, 2010, **51**, 4540–4546.
108. M.-M. Titirici and M. Antonietti, *Chem. Soc. Rev.*, 2010, **39**, 103–16.
109. B. Xu, S. Hou, G. Cao, F. Wu, and Y. Yang, *J. Mater. Chem.*, 2012, **22**, 19088.
110. Y. Wang, X. Wang, and M. Antonietti, *Angew. Chem. Int. Ed. Engl.*, 2012, **51**, 68–89.
111. Y. Zhang and M. Antonietti, *Chem. Asian J.*, 2010, **5**, 1307–11.
112. A. Thomas, A. Fischer, F. Goettmann, M. Antonietti, J.-O. Müller, R. Schlögl, and J. M. Carlsson, *J. Mater. Chem.*, 2008, **18**, 4893.
113. F. Goettmann, A. Fischer, M. Antonietti, and A. Thomas, *Angew. Chemie*, 2006, **118**, 4579–4583.
114. S. Giraudet and Z. Zhu, *Carbon N. Y.*, 2011, **49**, 398–405.
115. J. Zhang, F. Guo, and X. Wang, *Adv. Funct. Mater.*, 2013, **23**, 3008–3014.
116. K. K. R. Datta, V. V Balasubramanian, K. Ariga, T. Mori, and A. Vinu, *Chemistry*, 2011, **17**, 3390–7.
117. Y. Ham, K. Maeda, D. Cha, K. Takanabe, and K. Domen, *Chem. Asian J.*, 2013, **8**, 218–24.
118. M. J. Bojdys, N. Severin, J. P. Rabe, A. I. Cooper, A. Thomas, and M. Antonietti, *Macromol. Rapid Commun.*, 2013, **34**, 850–4.
119. M. J. Bojdys, J.-O. Müller, M. Antonietti, and A. Thomas, *Chemistry*, 2008, **14**, 8177–82.
120. S. Pylypenko, A. Queen, T. S. Olson, A. Dameron, K. O'Neill, K. C. Neyerlin, B. Pivovar, H. N. Dinh, D. S. Ginley, T. Gennett, and R. O'Hayre, *J. Phys. Chem. C*, 2011, **115**, 13667–13675.
121. S. Pylypenko, A. Queen, T. S. Olson, A. Dameron, K. O'Neill, K. C. Neyerlin, B. Pivovar, H. N. Dinh, D. S. Ginley, T. Gennett, and R. O'Hayre, *J. Phys. Chem. C*, 2011, **115**, 13676–13684.
122. K. N. Wood, S. Pylypenko, T. S. Olson, A. a Dameron, K. O'Neill, S. T. Christensen, H. N. Dinh, T. Gennett, and R. O'Hayre, *ACS Appl. Mater. Interfaces*, 2012, **4**, 6728–34.
123. E. F. Holby and C. D. Taylor, *Appl. Phys. Lett.*, 2012, **101**, 064102.
124. G. Wu, M. Nelson, S. Ma, H. Meng, G. Cui, and P. K. Shen, *Carbon N. Y.*, 2011, **49**, 3972–3982.
125. F. Gao, G.-L. Zhao, S. Yang, and J. J. Spivey, *J. Am. Chem. Soc.*, 2012.
126. N. Roy, R. Sengupta, and A. K. Bhowmick, *Prog. Polym. Sci.*, 2012, **37**, 781–819.
127. K. Sakaushi and G. Nickerl, *Angew. Chemie …*, 2012, 7850–7854.
128. L. Hao, B. Luo, X. Li, M. Jin, Y. Fang, Z. Tang, Y. Jia, M. Liang, A. Thomas, J. Yang, and L. Zhi, *Energy Environ. Sci.*, 2012, **5**, 9747.
129. D. Bélanger and J. Pinson, *Chem. Soc. Rev.*, 2011, **40**, 3995–4048.
130. A. Grondein and D. Bélanger, *Carbon N. Y.*, 2012, **50**, 4335–4342.
131. T. Schiros, D. Nordlund, L. Pálová, D. Prezzi, L. Zhao, K. S. Kim, U. Wurstbauer, C. Gutiérrez, D. Delongchamp, C. Jaye, D. Fischer, H. Ogasawara, L. G. M. Pettersson, D. R. Reichman, P. Kim, M. S. Hybertsen, and A. N. Pasupathy, *Nano Lett.*, 2012, **12**, 4025–31.

132. C. L. Muhich, J. Y. Westcott, T. C. Morris, A. W. Weimer, and C. B. Musgrave, *J. Phys. Chem. C*, 2013, **117**, 10523–10535.
133. L. Zhao, R. He, K. T. Rim, T. Schiros, K. S. Kim, H. Zhou, C. Gutiérrez, S. P. Chockalingam, C. J. Arguello, L. Pálová, D. Nordlund, M. S. Hybertsen, D. R. Reichman, T. F. Heinz, P. Kim, A. Pinczuk, G. W. Flynn, and A. N. Pasupathy, *Science*, 2011, **333**, 999–1003.
134. M. Mananghaya, E. Rodulfo, G. N. Santos, A. R. Villagracia, and A. N. Ladines, *J. Nanomater.*, 2012, **2012**, 1–14.
135. M. N. Groves, a. S. W. Chan, C. Malardier-Jugroot, and M. Jugroot, *Chem. Phys. Lett.*, 2009, **481**, 214–219.
136. S.-F. Huang, K. Terakura, T. Ozaki, T. Ikeda, M. Boero, M. Oshima, J. Ozaki, and S. Miyata, *Phys. Rev. B*, 2009, **80**, 235410.
137. L. Yu, X. Pan, X. Cao, P. Hu, and X. Bao, *J. Catal.*, 2011, **282**, 183–190.
138. Y. Zhou, T. Holme, J. Berry, T. R. Ohno, D. Ginley, and R. O'Hayre, *J. Phys. Chem. C*, 2010, **114**, 506–515.
139. S. Ni, Z. Li, and J. Yang, *Nanoscale*, 2012, **4**, 1184–9.
140. C. H. San and C. W. Hong, *J. Electrochem. Soc.*, 2012, **159**, K116.
141. X. Bao, X. Nie, D. Deak, E. J. Biddinger, W. Luo, A. Asthagiri, U. S. Ozkan, and C. M. Hadad, *Top. Catal.*, 2013, **56**, 1623–1633.
142. H. J. Yan, B. Xu, S. Q. Shi, and C. Y. Ouyang, *J. Appl. Phys.*, 2012, **112**, 104316.
143. X. Kong and Q. Chen, *Phys. Chem. Chem. Phys.*, 2013, **15**, 12982–7.
144. Y.-X. Yu, *Phys. Chem. Chem. Phys.*, 2013, **15**, 16819–27.
145. Z. M. Ao, a D. Hernández-Nieves, F. M. Peeters, and S. Li, *Phys. Chem. Chem. Phys.*, 2012, **14**, 1463–7.
146. G. Koh, Y.-W. Zhang, and H. Pan, *Int. J. Hydrogen Energy*, 2012, **37**, 4170–4178.
147. S. Lee, M. Lee, H. Choi, D. S. Yoo, and Y.-C. Chung, *Int. J. Hydrogen Energy*, 2013, **38**, 4611–4617.
148. J. G. Zhou and Q. L. Williams, *J. Nano Res.*, 2011, **15**, 29–40.
149. J. Zhao, Y. Ding, X. Wang, Q. Cai, and X. Wang, *Diam. Relat. Mater.*, 2011, **20**, 36–41.
150. L. Zhang, J. Niu, L. Dai, and Z. Xia, *Langmuir*, 2012, **28**, 7542–50.
151. G. Luo, L. Liu, J. Zhang, G. Li, B. Wang, and J. Zhao, *ACS Appl. Mater. Interfaces*, 2013, **5**, 11184–93.
152. C. Q. Qu, L. Qiao, C. Wang, S. S. Yu, Q. Jiang, and W. T. Zheng, *Phys. Lett. A*, 2010, **374**, 782–787.
153. Y. Zhou, R. Pasquarelli, T. Holme, J. Berry, D. Ginley, and R. O'Hayre, *J. Mater. Chem.*, 2009, **19**, 7830.
154. L. Zhang and Z. Xia, *J. Phys. Chem. C*, 2011, **115**, 11170–11176.
155. J. Zhang, Z. Wang, and Z. Zhu, *J. Mol. Model.*, 2013, 5515–5521.
156. S. Kattel, P. Atanassov, and B. Kiefer, *J. Phys. Chem. C*, 2012, **116**, 17378–17383.
157. S. Kattel, P. Atanassov, and B. Kiefer, *Phys. Chem. Chem. Phys.*, 2013, **15**, 148–53.
158. A. Titov, P. Zapol, P. Kra, D. Liu, H. Iddir, K. Baishya, and L. A. Curtiss, 2009, 21629–21634.
159. D. H. Lee, W. J. Lee, W. J. Lee, S. O. Kim, and Y.-H. Kim, *Phys. Rev. Lett.*, 2011, **106**, 175502.
160. R. Chen, H. Li, D. Chu, and G. Wang, *J. Phys. Chem. C*, 2009, **113**, 20689–20697.
161. H. He, Y. Lei, C. Xiao, D. Chu, R. Chen, and G. Wang, *J. Phys. Chem. C*, 2012, **116**, 16038–16046.
162. S. Kattel and G. Wang, *J. Mater. Chem. A*, 2013, **1**, 10790.
163. K. Artyushkova, B. Kiefer, B. Halevi, a Knop-Gericke, R. Schlogl, and P. Atanassov, *Chem. Commun. (Camb).*, 2013, **49**, 2539–41.
164. C. Ma, X. Shao, and D. Cao, *J. Mater. Chem.*, 2012, **22**, 8911.
165. Y. Guo, J. He, T. Wang, H. Xue, Y. Hu, G. Li, J. Tang, and X. Sun, *J. Power Sources*, 2011, **196**, 9299–9307.
166. Z. Lei, L. An, L. Dang, M. Zhao, J. Shi, S. Bai, and Y. Cao, *Microporous Mesoporous Mater.*, 2009, **119**, 30–38.
167. Z. Lei, M. Zhao, L. Dang, L. An, M. Lu, A.-Y. Lo, N. Yu, and S.-B. Liu, *J. Mater. Chem.*, 2009, **19**, 5985.

168. F. Su, Z. Tian, C. K. Poh, Z. Wang, S. H. Lim, Z. Liu, and J. Lin, *Chem. Mater.*, 2010, **22**, 832–839.
169. Z. Liu, F. Su, X. Zhang, and S. W. Tay, 2011, 3824–3830.
170. T. S. Olson, A. A. Dameron, K. Wood, S. Pylpenko, K. E. Hurst, S. Christensen, J. B. Bult, D. S. Ginley, R. O'Hayre, and H. Dinh, *J. Electrochem. Soc.*, 2013, **160**, F389–F394.
171. A. R. Corpuz, T. T. S. Olson, P. Joghee, S. Pylypenko, A. A. A. a. Dameron, H. N. H. N. Dinh, K. J. K. J. O'Neill, K. E. K. E. Hurst, G. Bender, T. Gennett, B. S. B. S. Pivovar, R. M. R. M. Richards, and R. P. R. P. O'Hayre, *J. Power Sources*, 2012, **217**, 142–151.
172. P. Joghee, S. Pylypenko, K. Wood, A. Corpuz, G. Bender, H. N. Dinh, and R. O'Hayre, *J. Power Sources*, 2014, **245**, 37–47.
173. K. N. Wood, S. T. Christensen, S. Pylypenko, T. S. Olson, A. A. Dameron, K. E. Hurst, H. N. Dinh, T. Gennett, and R. O'Hayre, *MRS Commun.*, 2012, **2**, 85–89.
174. J. Chang, X. Sun, L. Feng, W. Xing, X. Qin, and G. Shao, *J. Power Sources*, 2013, **239**, 94–102.
175. R. Chetty, S. Kundu, W. Xia, M. Bron, W. Schuhmann, V. Chirila, W. Brandl, T. Reinecke, and M. Muhler, *Electrochim. Acta*, 2009, **54**, 4208–4215.
176. K. N. Wood, S. Pylypenko, T. S. Olson, A. A. Dameron, K. O'Neill, S. T. Christensen, H. N. Dinh, T. Gennett, and R. O'Hayre, *ACS Appl. Mater. Interfaces*, 2012, **4**, 6728–6734.
177. A. R. Corpuz, K. N. Wood, S. Pylypenko, A. A. Dameron, P. Joghee, T. S. Olson, G. Bender, H. N. Dinh, T. Gennett, and R. M. Richards, *J. Power Sources*, 2014, **248**, 296–306.
178. P. Joghee, S. Pylypenko, T. Olson, A. A. Dameron, A. R. Corpuz, H. N. N. Dinh, K. Wood, K. J. O'Neill, K. E. Hurst, G. Bender, T. Gennett, B. S. Pivovar, and R. P. O'Hayre, *J. Electrochem. Soc.*, 2012, **159**, F768–F778.
179. Y. Zhou, K. Neyerlin, T. S. Olson, S. Pylypenko, J. Bult, H. N. Dinh, T. Gennett, Z. Shao, and R. O'Hayre, *Energy Environ. Sci.*, 2010, **3**, 1437.
180. S. Suthirakun, T. Sarakonsri, S. Aukkaravittayapun, and T. Vilaithong, 2009, **10**, 502–506.
181. Y. Chen, J. Wang, H. Liu, R. Li, X. Sun, S. Ye, and S. Knights, *Electrochem. commun.*, 2009, **11**, 2071–2076.
182. D. C. Higgins, D. Meza, and Z. Chen, 2010, 21982–21988.
183. R. I. Jafri, N. Rajalakshmi, and S. Ramaprabhu, *J. Power Sources*, 2010, **195**, 8080–8083.
184. M. S. Saha, R. Li, X. Sun, and S. Ye, *Electrochem. commun.*, 2009, **11**, 438–441.
185. Y. Liu, Z. Jin, J. Wang, R. Cui, H. Sun, F. Peng, L. Wei, Z. Wang, X. Liang, L. Peng, and Y. Li, *Adv. Funct. Mater.*, 2011, **21**, 986–992.
186. S.-H. Liu, M.-T. Wu, Y.-H. Lai, C.-C. Chiang, N. Yu, and S.-B. Liu, *J. Mater. Chem.*, 2011, **21**, 12489.
187. X. Li, S. Park, and B. N. Popov, *J. Power Sources*, 2010, **195**, 445–452.
188. B. P. Vinayan, R. Nagar, N. Rajalakshmi, and S. Ramaprabhu, *Adv. Funct. Mater.*, 2012, **22**, 3519–3526.
189. F. Jaouen, E. Proietti, M. Lefèvre, R. Chenitz, J.-P. Dodelet, G. Wu, H. T. Chung, C. M. Johnston, and P. Zelenay, *Energy Environ. Sci.*, 2011, **4**, 114.
190. Z. Chen, D. Higgins, A. Yu, L. Zhang, and J. Zhang, *Energy Environ. Sci.*, 2011, **4**, 3167.
191. G. Wu and P. Zelenay, *Acc. Chem. Res.*, 2013, **46**, 1878–89.
192. N. a. Karim and S. K. Kamarudin, *Appl. Energy*, 2013, **103**, 212–220.
193. M. Ferrandon, A. J. Kropf, D. J. Myers, K. Artyushkova, U. Kramm, P. Bogdanoff, G. Wu, C. M. Johnston, and P. Zelenay, *J. Phys. Chem. C*, 2012, **116**, 16001–16013.
194. G. Wu, C. M. Johnston, N. H. Mack, K. Artyushkova, M. Ferrandon, M. Nelson, J. S. Lezama-Pacheco, S. D. Conradson, K. L. More, D. J. Myers, and P. Zelenay, *J. Mater. Chem.*, 2011, **21**, 11392.
195. N. Ramaswamy and U. Tylus, *… Am. Chem. …*, 2013.
196. H. Byon and J. Suntivich, *Phys. Chem. …*, 2011, 11392–11405.
197. K. Niu, B. Yang, J. Cui, J. Jin, X. Fu, Q. Zhao, and J. Zhang, *J. Power Sources*, 2013, **243**, 65–71.
198. J. Y. Cheon, T. Kim, Y. Choi, H. Y. Jeong, M. G. Kim, Y. J. Sa, J. Kim, Z. Lee, T.-H. Yang, K. Kwon, O. Terasaki, G.-G. Park, R. R. Adzic, and S. H. Joo, *Sci. Rep.*, 2013, **3**, 2715.
199. J. Herranz, F. Jaouen, M. Lefèvre, U. I. Kramm, E. Proietti, J.-P. Dodelet, P. Bogdanoff, S. Fiechter, I. Abs-Wurmbach, P. Bertrand, T. M. Arruda, and S. Mukerjee, *J. Phys. Chem. C. Nanomater. Interfaces*, 2011, **115**, 16087–16097.

200. U. Kramm, J. Herranz, and N. Larouche, *Phys. Chem. …*, 2012, **14**, 11673–11688.
201. C. Walter, K. Kummer, D. Vyalikh, V. Bruser, and K.-D. Weltmann, *J. Electrochem. Soc.*, 2013, **160**, F1088–F1095.
202. T. S. Olson, S. Pylypenko, J. E. Fulghum, and P. Atanassov, *J. Electrochem. Soc.*, 2010, **157**, B54.
203. T. Olson and S. Pylypenko, *J. …*, 2010, 5049–5059.
204. T. S. Olson, S. Pylypenko, S. Kattel, P. Atanassov, and B. Kiefer, *J. Phys. Chem. C*, 2010, **114**, 15190–15195.
205. F. Jaouen, J. Herranz, M. Lefèvre, J.-P. Dodelet, U. I. Kramm, I. Herrmann, P. Bogdanoff, J. Maruyama, T. Nagaoka, A. Garsuch, J. R. Dahn, T. Olson, S. Pylypenko, P. Atanassov, and E. a Ustinov, *ACS Appl. Mater. Interfaces*, 2009, **1**, 1623–39.
206. F. Charreteur, F. Jaouen, and J.-P. Dodelet, *Electrochim. Acta*, 2009, **54**, 6622–6630.
207. H. Meng, N. Larouche, M. Lefèvre, F. Jaouen, B. Stansfield, and J.-P. Dodelet, *Electrochim. Acta*, 2010, **55**, 6450–6461.
208. H. T. Chung, C. M. Johnston, K. Artyushkova, M. Ferrandon, D. J. Myers, and P. Zelenay, *Electrochem. commun.*, 2010, **12**, 1792–1795.
209. G. Wu, K. L. More, P. Xu, H.-L. Wang, M. Ferrandon, A. J. Kropf, D. J. Myers, S. Ma, C. M. Johnston, and P. Zelenay, *Chem. Commun. (Camb).*, 2013, **49**, 3291–3.
210. H. Xiao, Z.-G. Shao, G. Zhang, Y. Gao, W. Lu, and B. Yi, *Carbon N. Y.*, 2013, **57**, 443–451.
211. R. Kothandaraman, V. Nallathambi, K. Artyushkova, and S. C. Barton, *Appl. Catal. B Environ.*, 2009, **92**, 209–216.
212. N. Leonard, V. Nallathambi, and S. C. Barton, *J. Electrochem. Soc.*, 2013, **160**, F788–F792.
213. R. L. Arechederra, K. Artyushkova, P. Atanassov, and S. D. Minteer, *ACS Appl. Mater. Interfaces*, 2010, **2**, 3295–302.
214. A. Serov, M. H. Robson, K. Artyushkova, and P. Atanassov, *Appl. Catal. B Environ.*, 2012, **127**, 300–306.
215. M. H. Robson, A. Serov, K. Artyushkova, and P. Atanassov, *Electrochim. Acta*, 2013, **90**, 656–665.
216. A. Serov, M. H. Robson, M. Smolnik, and P. Atanassov, *Electrochim. Acta*, 2012, **80**, 213–218.
217. A. Serov, M. H. Robson, B. Halevi, K. Artyushkova, and P. Atanassov, *Electrochem. commun.*, 2012, **22**, 53–56.
218. H. Meng, F. Jaouen, E. Proietti, M. Lefèvre, and J.-P. Dodelet, *Electrochem. commun.*, 2009, **11**, 1986–1989.
219. S. Brocato, A. Serov, and P. Atanassov, *Electrochim. Acta*, 2013, **87**, 361–365.
220. H. R. Byon, J. Suntivich, and Y. Shao-Horn, *Chem. Mater.*, 2011, **23**, 3421–3428.
221. S. Jiang, C. Zhu, and S. Dong, *J. Mater. Chem. A*, 2013, **1**, 3593.
222. K. Parvez, S. Yang, Y. Hernandez, A. Winter, A. Turchanin, X. Feng, and K. Müllen, *ACS Nano*, 2012, **6**, 9541–50.
223. Y. Liang, Y. Li, H. Wang, J. Zhou, J. Wang, T. Regier, and H. Dai, *Nat. Mater.*, 2011, **10**, 780–6.
224. Y. Liang, H. Wang, P. Diao, W. Chang, G. Hong, Y. Li, M. Gong, L. Xie, J. Zhou, J. Wang, T. Z. Regier, F. Wei, and H. Dai, *J. Am. Chem. Soc.*, 2012, **134**, 15849–57.
225. Q. He, Q. Li, and S. Khene, *J. …*, 2013.
226. H. T. Chung, J. H. Won, and P. Zelenay, *Nat. Commun.*, 2013, **4**, 1922.
227. J. Duan, Y. Zheng, S. Chen, Y. Tang, M. Jaroniec, and S. Qiao, *Chem. Commun. (Camb).*, 2013, **49**, 7705–7.
228. Y. Zhang, K. Fugane, T. Mori, L. Niu, and J. Ye, *J. Mater. Chem.*, 2012, **22**, 6575.
229. Y. Liang, H. Wang, J. Zhou, Y. Li, J. Wang, T. Regier, and H. Dai, *J. Am. Chem. Soc.*, 2012, **134**, 3517–23.
230. M. D. Sánchez, P. Chen, T. Reinecke, M. Muhler, and W. Xia, *ChemCatChem*, 2012, **4**, 1997–2004.
231. M. Chisaka, T. Iijima, and A. Tomita, *J. …*, 2010, 1701–1706.
232. A. Zahoor, M. Christy, Y. J. Hwang, Y. R. Lim, P. Kim, and K. S. Nahm, *Appl. Catal. B Environ.*, 2014, **147**, 633–641.
233. P. Pachfule, V. M. Dhavale, S. Kandambeth, S. Kurungot, and R. Banerjee, *Chemistry*, 2013, **19**, 974–80.
234. J. Ozaki, S. Tanifuji, A. Furuichi, and K. Yabutsuka, *Electrochim. Acta*, 2010, **55**, 1864–1871.

235. S. Lyth, Y. Nabae, and N. Islam, … *Electrochem. …*, 2011, 194–201.
236. Y. Ma, L. Sun, W. Huang, L. Zhang, J. Zhao, Q. Fan, and W. Huang, *J. Phys. Chem. C*, 2011, **115**, 24592–24597.
237. Y. Li, W. Zhou, H. Wang, L. Xie, Y. Liang, F. Wei, J.-C. Idrobo, S. J. Pennycook, and H. Dai, *Nat. Nanotechnol.*, 2012, **7**, 394–400.
238. N. Alexeyeva, E. Shulga, V. Kisand, I. Kink, and K. Tammeveski, *J. Electroanal. Chem.*, 2010, **648**, 169–175.
239. K. Gong, F. Du, Z. Xia, M. Durstock, and L. Dai, *Science (80-.).*, 2009, **323**.
240. S. Wang, E. Iyyamperumal, A. Roy, Y. Xue, D. Yu, and L. Dai, *Angew. Chem. Int. Ed. Engl.*, 2011, **50**, 11756–60.
241. H. Li, H. Liu, Z. Jong, W. Qu, D. Geng, X. Sun, and H. Wang, *Int. J. Hydrogen Energy*, 2011, **36**, 2258–2265.
242. D. Geng, H. Liu, Y. Chen, R. Li, X. Sun, S. Ye, and S. Knights, *J. Power Sources*, 2011, **196**, 1795–1801.
243. J. P. McClure, J. D. Thornton, R. Jiang, D. Chu, J. J. Cuomo, and P. S. Fedkiw, *J. Electrochem. Soc.*, 2012, **159**, F733–F742.
244. W. Xia, J. Masa, M. Bron, W. Schuhmann, and M. Muhler, *Electrochem. commun.*, 2011, **13**, 593–596.
245. T. C. Nagaiah, A. Bordoloi, M. D. Sánchez, M. Muhler, and W. Schuhmann, *ChemSusChem*, 2012, **5**, 637–41.
246. D. C. Higgins, J. Wu, W. Li, and Z. Chen, *Electrochim. Acta*, 2012, **59**, 8–13.
247. G. Liu, X. Li, P. Ganesan, and B. N. Popov, *Electrochim. Acta*, 2010, **55**, 2853–2858.
248. Z. Chen, D. Higgins, and Z. Chen, *Carbon N. Y.*, 2010, **48**, 3057–3065.
249. D. Higgins, Z. Chen, and Z. Chen, *Electrochim. Acta*, 2011, **56**, 1570–1575.
250. Z. Chen, D. Higgins, H. Tao, R. S. Hsu, and Z. Chen, *J. Phys. Chem. C*, 2009, **113**, 21008–21013.
251. Z. Chen, D. Higgins, and Z. Chen, *Electrochim. Acta*, 2010, **55**, 4799–4804.
252. A. Zhao, J. Masa, M. Muhler, W. Schuhmann, and W. Xia, *Electrochim. Acta*, 2013, **98**, 139–145.
253. D. Singh, I. I. Soykal, J. Tian, D. von Deak, J. King, J. T. Miller, and U. S. Ozkan, *J. Catal.*, 2013, **304**, 100–111.
254. E. J. Biddinger and U. S. Ozkan, *J. Phys. Chem. C*, 2010, **114**, 15306–15314.
255. J. Masa, A. Zhao, W. Xia, Z. Sun, B. Mei, M. Muhler, and W. Schuhmann, *Electrochem. commun.*, 2013, 34, 113–116.
256. J. Vazquez-Arenas, D. Higgins, Z. Chen, M. Fowler, and Z. Chen, *J. Power Sources*, 2012, **205**, 215–221.
257. L. Feng, Y. Yan, Y. Chen, and L. Wang, *Energy Environ. Sci.*, 2011, **4**, 1892.
258. D. C. Mirodatos, D. Y. Schuurman, D. D. Duprez, D. F. Luck, D. von Deak, D. Singh, J. C. King, and U. S. Ozkan, *Appl. Catal. B Environ.*, 2012, **113**, 126–133.
259. Z. Mo, R. Zheng, H. Peng, H. Liang, and S. Liao, *J. Power Sources*, 2014, **245**, 801–807.
260. H. Niwa, K. Horiba, Y. Harada, M. Oshima, T. Ikeda, K. Terakura, J. Ozaki, and S. Miyata, *J. Power Sources*, 2009, **187**, 93–97.
261. Z. Lin, G. H. Waller, Y. Liu, M. Liu, and C. Wong, *Nano Energy*, 2013, **2**, 241–248.
262. Z. Lin, G. H. Waller, Y. Liu, M. Liu, and C. Wong, *Carbon N. Y.*, 2013, **53**, 130–136.
263. Z.-J. Lu, M.-W. Xu, S.-J. Bao, K. Tan, H. Chai, C.-J. Cai, C.-C. Ji, and Q. Zhang, *J. Mater. Sci.*, 2013, **48**, 8101–8107.
264. C. Zhang, R. Hao, H. Liao, and Y. Hou, *Nano Energy*, 2013, **2**, 88–97.
265. J. Yan, H. Meng, F. Xie, X. Yuan, W. Yu, W. Lin, W. Ouyang, and D. Yuan, *J. Power Sources*, 2014, **245**, 772–778.
266. N. Brun, S. a. Wohlgemuth, P. Osiceanu, and M. M. Titirici, *Green Chem.*, 2013, **15**, 2514.
267. C.-Z. Guo, C.-G. Chen, and Z.-L. Luo, *J. Power Sources*, 2014, **245**, 841–845.
268. L. Lai, J. R. Potts, D. Zhan, L. Wang, C. K. Poh, C. Tang, H. Gong, Z. Shen, J. Lin, and R. S. Ruoff, *Energy Environ. Sci.*, 2012, **5**, 7936.
269. X. Lin, X. Lu, T. Huang, Z. Liu, and A. Yu, *J. Power Sources*, 2013, **242**, 855–859.
270. D. Higgins, Z. Chen, D. U. Lee, and Z. Chen, *J. Mater. Chem. A*, 2013, **1**, 2639.
271. S. Zhu, Z. Chen, B. Li, D. Higgins, H. Wang, H. Li, and Z. Chen, *Electrochim. Acta*, 2011, **56**, 5080–5084.

272. G. S. Park, J.-S. Lee, S. T. Kim, S. Park, and J. Cho, *J. Power Sources*, 2013, **243**, 267–273.
273. G. Wu, N. Mack, W. Gao, S. Ma, and R. Zhong, *ACS …*, 2012, 9764–9776.
274. H. W. Park, D. U. Lee, Y. Liu, J. Wu, L. F. Nazar, and Z. Chen, *J. Electrochem. Soc.*, 2013, **160**, A2244–A2250.
275. P. Kichambare, J. Kumar, S. Rodrigues, and B. Kumar, *J. Power Sources*, 2011, **196**, 3310–3316.
276. P. Kichambare, S. Rodrigues, and J. Kumar, *ACS Appl. Mater. Interfaces*, 2012, **4**, 49–52.
277. H. Nie, H. Zhang, Y. Zhang, T. Liu, J. Li, and Q. Lai, *Nanoscale*, 2013, **5**, 8484–7.
278. K. Zhang, L. Zhang, X. Chen, X. He, X. Wang, S. Dong, L. Gu, Z. Liu, C. Huang, and G. Cui, *ACS Appl. Mater. Interfaces*, 2013, **5**, 3677–82.
279. H. W. Park, D. U. Lee, L. F. Nazar, and Z. Chen, *J. Electrochem. Soc.*, 2012, **160**, A344–A350.
280. H. Wang, Z. Wu, F. Meng, D. Ma, X. Huang, L. Wang, and X. Zhang, *ChemSusChem*, 2013, **6**, 56–60.
281. A. L. M. Reddy, A. Srivastava, S. R. Gowda, H. Gullapalli, M. Dubey, and P. M. Ajayan, *ACS Nano*, 2010, **4**, 6337–42.
282. X. Li, D. Geng, Y. Zhang, X. Meng, R. Li, and X. Sun, *Electrochem. commun.*, 2011, **13**, 822–825.
283. Z.-S. Wu, W. Ren, L. Xu, F. Li, and H.-M. Cheng, *ACS Nano*, 2011, **5**, 5463–71.
284. C. He, R. Wang, H. Fu, and P. K. Shen, *J. Mater. Chem. A*, 2013, **1**, 14586.
285. D. Cai, S. Wang, P. Lian, X. Zhu, D. Li, W. Yang, and H. Wang, *Electrochim. Acta*, 2013, **90**, 492–497.
286. X. Zhou, L.-J. Wan, and Y.-G. Guo, *Adv. Mater.*, 2013, **25**, 2152–7.
287. M. Du, C. Xu, J. Sun, and L. Gao, *Electrochim. Acta*, 2012, **80**, 302–307.
288. Y. Chang, J. Li, B. Wang, H. Luo, H. He, Q. Song, and L. Zhi, *J. Mater. Chem. A*, 2013, **1**, 14658.
289. D. Li, D. Shi, Z. Liu, H. Liu, and Z. Guo, *J. Nanoparticle Res.*, 2013, **15**, 1674.
290. D. Cai, D. Li, S. Wang, X. Zhu, W. Yang, S. Zhang, and H. Wang, *J. Alloys Compd.*, 2013, **561**, 54–58.
291. K. Zhang, P. Han, L. Gu, L. Zhang, Z. Liu, Q. Kong, C. Zhang, S. Dong, Z. Zhang, J. Yao, H. Xu, G. Cui, and L. Chen, *ACS Appl. Mater. Interfaces*, 2012, **4**, 658–64.
292. N. Mahmood, C. Zhang, and Y. Hou, *Small*, 2013, **9**, 1321–8.
293. X. Li, J. Liu, Y. Zhang, Y. Li, H. Liu, X. Meng, J. Yang, D. Geng, D. Wang, R. Li, and X. Sun, *J. Power Sources*, 2012, **197**, 238–245.
294. L. G. Bulusheva, a. V. Okotrub, a. G. Kurenya, H. Zhang, H. Zhang, X. Chen, and H. Song, *Carbon N. Y.*, 2011, **49**, 4013–4023.
295. W. Ren, D. Li, H. Liu, R. Mi, Y. Zhang, and L. Dong, *Electrochim. Acta*, 2013, **105**, 75–82.
296. Z. Wang, X. Xiong, L. Qie, and Y. Huang, *Electrochim. Acta*, 2013, **106**, 320–326.
297. Z. Li, Z. Xu, X. Tan, H. Wang, C. M. B. Holt, T. Stephenson, B. C. Olsen, and D. Mitlin, *Energy Environ. Sci.*, 2013, **6**, 871.
298. P. Han, Y. Yue, L. Zhang, H. Xu, Z. Liu, K. Zhang, C. Zhang, S. Dong, W. Ma, and G. Cui, *Carbon N. Y.*, 2011, **50**, 1355–1362.
299. C. Hu, Y. Xiao, Y. Zhao, N. Chen, Z. Zhang, M. Cao, and L. Qu, *Nanoscale*, 2013, **5**, 2726–33.
300. Z. Ding, L. Zhao, L. Suo, Y. Jiao, S. Meng, Y.-S. Hu, Z. Wang, and L. Chen, *Phys. Chem. Chem. Phys.*, 2011, **13**, 15127–33.
301. H. Li, L. Shen, X. Zhang, J. Wang, P. Nie, Q. Che, and B. Ding, *J. Power Sources*, 2013, **221**, 122–127.
302. S. Yoon, C. Liao, X.-G. Sun, C. a. Bridges, R. R. Unocic, J. Nanda, S. Dai, and M. P. Paranthaman, *J. Mater. Chem.*, 2012, **22**, 4611.
303. D. J. Lee, M.-H. Ryou, J.-N. Lee, B. G. Kim, Y. M. Lee, H.-W. Kim, B.-S. Kong, J.-K. Park, and J. W. Choi, *Electrochem. commun.*, 2013, **34**, 98–101.
304. L. Tan, C. Cao, H. Yang, B. Wang, and L. Li, *Mater. Lett.*, 2013, **109**, 195–198.
305. G. Fang, S. Kaneko, W. Liu, B. Xia, H. Sun, R. Zhang, J. Zheng, and D. Li, *Appl. Surf. Sci.*, 2013, **283**, 963–967.
306. Y. Shao, X. Wang, M. Engelhard, C. Wang, S. Dai, J. Liu, Z. Yang, and Y. Lin, *J. Power Sources*, 2010, **195**, 4375–4379.
307. S. Wang, X. Zhao, T. Cochell, and A. Manthiram, *J. Phys. Chem. Lett.*, 2012, **3**, 2164–2167.
308. H. Lee and H. Kim, *J. Appl. Electrochem.*, 2013, **43**, 553–557.

309. F. Sun, J. Wang, H. Chen, W. Li, W. Qiao, D. Long, and L. Ling, *ACS Appl. Mater. Interfaces*, 2013, **5**, 5630–8.
310. F. Sun, J. Wang, D. Long, W. Qiao, L. Ling, C. Lv, and R. Cai, *J. Mater. Chem. A*, 2013, **1**, 13283.
311. J. Jiang, Q. Gao, K. Xia, and J. Hu, *Microporous Mesoporous Mater.*, 2009, **118**, 28–34.
312. S. L. Candelaria, B. B. Garcia, D. Liu, and G. Cao, *J. Mater. Chem.*, 2012, **22**, 9884.
313. X. Yang, D. Wu, X. Chen, and R. Fu, *J. Phys. Chem. C*, 2010, **114**, 8581–8586.
314. L. Lai, L. Wang, H. Yang, N. G. Sahoo, Q. X. Tam, J. Liu, C. K. Poh, S. H. Lim, Z. Shen, and J. Lin, *Nano Energy*, 2012, **1**, 723–731.
315. H. Guo and Q. Gao, *J. Power Sources*, 2009, **186**, 551–556.
316. W. Kim, M. Y. Kang, J. B. Joo, N. D. Kim, I. K. Song, P. Kim, J. R. Yoon, and J. Yi, *J. Power Sources*, 2010, **195**, 2125–2129.
317. Y. J. Kim, I. Y. Jang, K. C. Park, Y. C. Jung, T. Oka, S. Iinou, Y. Komori, T. Kozutsumi, T. Hashiba, Y. A. Kim, and M. Endo, *Electrochim. Acta*, 2010, **55**, 5624–5628.
318. Z. Li, L. Zhang, B. S. Amirkhiz, X. Tan, Z. Xu, H. Wang, B. C. Olsen, C. M. B. Holt, and D. Mitlin, *Adv. Energy Mater.*, 2012, **2**, 431–437.
319. D. Hulicova-Jurcakova, M. Seredych, G. Q. Lu, and T. J. Bandosz, *Adv. Funct. Mater.*, 2009, **19**, 438–447.
320. C.-T. Hsieh, H. Teng, W.-Y. Chen, and Y.-S. Cheng, *Carbon N. Y.*, 2010, **48**, 4219–4229.
321. L. Lai, H. Yang, L. Wang, B. K. Teh, J. Zhong, H. Chou, L. Chen, W. Chen, Z. Shen, R. S. Ruoff, and J. Lin, *ACS Nano*, 2012, **6**, 5941–51.
322. A. K. Mishra and S. Ramaprabhu, *J. Phys. Chem. C*, 2011, **115**, 14006–14013.
323. Z. Wen, X. Wang, S. Mao, Z. Bo, H. Kim, S. Cui, G. Lu, X. Feng, and J. Chen, *Adv. Mater.*, 2012, **24**, 5610–6.
324. E. J. Ra, E. Raymundo-Piñero, Y. H. Lee, and F. Béguin, *Carbon N. Y.*, 2009, **47**, 2984–2992.
325. J. P. Paraknowitsch, J. Zhang, D. Su, A. Thomas, and M. Antonietti, *Adv. Mater.*, 2010, **22**, 87–92.
326. X. Y. Chen, C. Chen, Z. J. Zhang, and D. H. Xie, *J. Mater. Chem. A*, 2013, **1**, 10903.
327. H. Wang, Q. Gao, and J. Hu, *Microporous Mesoporous Mater.*, 2010, **131**, 89–96.
328. Z.-S. Wu, A. Winter, L. Chen, Y. Sun, A. Turchanin, X. Feng, and K. Müllen, *Adv. Mater.*, 2012, **24**, 5130–5.
329. H. Konno, T. Ito, M. Ushiro, K. Fushimi, and K. Azumi, *J. Power Sources*, 2010, **195**, 1739–1746.
330. T. Tomko, R. Rajagopalan, P. Aksoy, and H. C. Foley, *Electrochim. Acta*, 2011, **56**, 5369–5375.
331. C. Wang, Y. Zhou, L. Sun, P. Wan, X. Zhang, and J. Qiu, *J. Power Sources*, 2013, **239**, 81–88.
332. J. Burress, M. Kraus, M. Beckner, R. Cepel, G. Suppes, C. Wexler, and P. Pfeifer, *Nanotechnology*, 2009, **20**, 204026.
333. J. Jiang, Q. Gao, Z. Zheng, K. Xia, and J. Hu, *Int. J. Hydrogen Energy*, 2010, **35**, 210–216.
334. B. P. Vinayan, R. Nagar, and S. Ramaprabhu, *J. Mater. Chem. A*, 2013, **1**, 11192.
335. B. P. Vinayan, K. Sethupathi, and S. Ramaprabhu, *Int. J. Hydrogen Energy*, 2013, **38**, 2240–2250.
336. Z. Jin, Z. Sun, L. J. Simpson, K. J. O. Neill, P. A. Parilla, Y. Li, N. P. Stadie, C. C. Ahn, C. Kittrell, and J. M. Tour, 2010, 15246–15251.
337. R. Lu, Z. Meng, E. Kan, F. Li, D. Rao, Z. Lu, J. Qian, C. Xiao, H. Wu, and K. Deng, *Phys. Chem. Chem. Phys.*, 2013, **15**, 666–70.
338. Z. M. Ao and F. M. Peeters, *J. Phys. Chem. C*, 2010, **114**, 14503–14509.
339. L. H. Kumar, C. V. Rao, and B. Viswanathan, *J. Mater. Chem. A*, 2013, **1**, 3355.
340. M. S. L. Hudson, H. Raghubanshi, D. Pukazhselvan, and O. N. Srivastava, *Int. J. Hydrogen Energy*, 2012, **37**, 2750–2755.
341. P. Berseth, A. Harter, and R. Zidan, *Nano …*, 2009.
342. M. Ismail, Y. Zhao, X. B. Yu, a. Ranjbar, and S. X. Dou, *Int. J. Hydrogen Energy*, 2011, **36**, 3593–3599.
343. R. D. Stephens, A. F. Gross, S. L. Van Atta, J. J. Vajo, and F. E. Pinkerton, *Nanotechnology*, 2009, **20**, 204018.
344. S. Choi, J. H. Drese, and C. W. Jones, *ChemSusChem*, 2009, **2**, 796–854.
345. L. Zhao, Z. Bacsik, N. Hedin, W. Wei, Y. Sun, M. Antonietti, and M.-M. Titirici, *ChemSusChem*, 2010, **3**, 840–5.
346. J. a. Thote, K. S. Iyer, R. Chatti, N. K. Labhsetwar, R. B. Biniwale, and S. S. Rayalu, *Carbon N. Y.*, 2010, **48**, 396–402.

347. L. Wang and R. Yang, *J. Phys. Chem. C*, 2011, 1099–1106.
348. M. Sevilla, P. Valle-Vigón, and A. B. Fuertes, *Adv. Funct. Mater.*, 2011, **21**, 2781–2787.
349. J. Wang, I. Senkovska, M. Oschatz, M. R. Lohe, L. Borchardt, A. Heerwig, Q. Liu, and S. Kaskel, *ACS Appl. Mater. Interfaces*, 2013, **5**, 3160–7.
350. J. Wang, I. Senkovska, M. Oschatz, M. R. Lohe, L. Borchardt, A. Heerwig, Q. Liu, and S. Kaskel, *J. Mater. Chem. A*, 2013, **1**, 10951.
351. R. Myers, *The 100 most important chemical compounds: a reference guide*, Greenwood Press, 88 Post Road West, Westport, CT 06881, 1st edn., 2007.
352. A. Morozan, B. Jousselme, and S. Palacin, *Energy Environ. Sci.*, 2011, **4**, 1238.
353. R. a Sidik, A. B. Anderson, N. P. Subramanian, S. P. Kumaraguru, and B. N. Popov, *J. Phys. Chem. B*, 2006, **110**, 1787–93.
354. A. Nieto-Márquez, D. Toledano, P. Sánchez, A. Romero, and J. L. Valverde, *J. Catal.*, 2010, **269**, 242–251.
355. J. Kochi and R. Sheldon, 1981, 1981.
356. G. Palmisano, E. García-López, G. Marcì, V. Loddo, S. Yurdakal, V. Augugliaro, and L. Palmisano, *Chem. Commun. (Camb).*, 2010, **46**, 7074–89.
357. N. Zhang, Y. Zhang, and Y.-J. Xu, *Nanoscale*, 2012, **4**, 5792–813.
358. L. Jia, D.-H. Wang, Y.-X. Huang, A.-W. Xu, and H.-Q. Yu, *J. Phys. Chem. C*, 2011, **115**, 11466–11473.
359. P. Chen, T. Xiao, H. Li, J. Yang, and Z. Wang, *ACS …*, 2011, 712–719.
360. Y. Min, G. He, R. Li, W. Zhao, Y. Chen, and Y. Zhang, *Sep. Purif. Technol.*, 2013, **106**, 97–104.
361. X. Wang, K. Maeda, A. Thomas, K. Takanabe, G. Xin, J. M. Carlsson, K. Domen, and M. Antonietti, *Nat. Mater.*, 2009, **8**, 76–80.
362. N. Jia, L. Liu, Q. Zhou, L. Wang, M. Yan, and Z. Jiang, *Electrochim. Acta*, 2005, **51**, 611–618.
363. S. Deng, G. Jian, J. Lei, Z. Hu, and H. Ju, *Biosens. Bioelectron.*, 2009, **25**, 373–7.
364. H. Nolan, N. McEvoy, G. P. Keeley, S. D. Callaghan, C. McGuinness, and G. S. Duesberg, *Phys. Chem. Chem. Phys.*, 2013, **15**, 18688–93.
365. J. M. Goran, S. M. Mantilla, and K. J. Stevenson, *Anal. Chem.*, 2013, **85**, 1571–81.
366. P. Gai, H. Zhang, Y. Zhang, W. Liu, G. Zhu, X. Zhang, and J. Chen, *J. Mater. Chem. B*, 2013, **1**, 2742.
367. Z. Zhang, R. Zhang, C. Li, L. Yuan, P. Li, L. Yao, and S. Liu, *Electroanalysis*, 2012, **24**, 1424–1430.
368. X. Feng, C. Wang, R. Cui, X. Yang, and W. Hou, *J. Solid State Electrochem.*, 2012, **16**, 2691–2698.
369. J. C. Carrero-Sanchez, a L. Elías, R. Mancilla, G. Arrellín, H. Terrones, J. P. Laclette, and M. Terrones, *Nano Lett.*, 2006, **6**, 1609–16.